

Waterfront 2A - Analysis Report
MCG4322



Waterfront Robot 2A

Marc-André Arsenault (8172498)

Mathieu Carroll (8089784)

Alexane Lahaie (8204533)

Joshua O'Reilly (8359885)

University of Ottawa
Department of Mechanical Engineering
November 20, 2019

Contents

List of Figures	v
List of Tables	vii
1 Project Charter	1
1.1 Mandate	1
1.2 Requirements	1
1.3 Constraints	1
1.4 Criteria	1
1.5 Parametrization Outline	1
2 Detailed Design	2
3 System Modelling	8
3.1 External Forces	9
3.1.1 Normal Forces	10
3.1.2 Friction Force - Slope around X axis	11
3.1.3 Friction Force - Slope around y axis	12
3.2 Dynamic Equation	12
3.3 Stability	13
3.4 Linkage Optimization	14
3.5 Power Consumption	17
3.5.1 Harmonic Drives Efficiency	17
3.5.2 Motor Power Consumption	18
3.5.3 Robot Power Consumption	19
3.5.4 Solar Power	19
3.5.5 Battery	20
3.5.6 Results of Power Consumption Simulation	21
4 Analysis	22
4.1 Analysis Outline	22
4.2 Limbs	22
4.2.1 Inputs and Outputs	22
4.2.2 Constants and Parameters	23
4.2.3 Assumptions and Simplifications	23

4.2.4	Material Selection	23
4.2.5	Free-Body Diagram	23
4.2.6	Stress Analysis	24
4.2.7	Critical Review	29
4.2.8	Parameterization	29
4.3	Belt, Tensioner and Pulleys	29
4.3.1	Inputs and Outputs	29
4.3.2	Constants and Parameters	30
4.3.3	Assumptions and Simplifications	30
4.3.4	Material Selection	30
4.3.5	Free-Body Diagram	31
4.3.6	Stress Analysis	31
4.3.7	Critical Review	33
4.3.8	Parameterization	34
4.4	Torsion Springs	34
4.4.1	Inputs and Outputs	34
4.4.2	Constants and Parameters	34
4.4.3	Assumptions and Simplifications	35
4.4.4	Material Selection	35
4.4.5	Free-Body Diagram	35
4.4.6	Stress Analysis	36
4.4.7	Critical Review	38
4.4.8	Parameterization	39
4.5	Shaft Analysis	39
4.5.1	Inputs and Outputs	39
4.5.2	Constants and Parameters	40
4.5.3	Assumptions and Simplifications	40
4.5.4	Material Selection	40
4.5.5	Stress Analysis and Free-Body Diagrams	41
4.5.5.1	Exterior Knee Shaft	41
4.5.5.2	Hip Control Shaft	46
4.5.5.3	Knee Control Shaft	50
4.5.5.4	Example Calculation	53
4.5.6	Critical Review	54

4.5.7	Parameterization	55
4.6	Keys	55
4.6.1	Description	55
4.6.2	Stress Analysis and Free-Body Diagrams	55
4.6.3	Critical Review	57
4.6.4	Parameterization	57
4.7	Bearings and Spacers	57
4.7.1	Inputs and Outputs	57
4.7.2	Constants and Parameters	57
4.7.3	Assumptions and Simplifications	57
4.7.4	Material Selection	58
4.7.5	Stress Analysis and Free-Body Diagrams	58
4.7.6	Critical Review	60
4.7.7	Parameterization	60
4.8	Fasteners	60
4.8.1	Inputs and Outputs	60
4.8.2	Constants and Parameters	60
4.8.3	Assumptions and Simplifications	61
4.8.4	Material Selection	61
4.8.5	Free-Body Diagram	63
4.8.6	Stress Analysis	65
4.8.7	Critical Review	69
4.8.8	Parameterization	70
4.9	Bellows	70
4.9.1	Inputs and Outputs	70
4.9.2	Constants and Parameters	71
4.9.3	Assumptions and Simplifications	71
4.9.4	Material Selection	71
4.9.5	Free-Body Diagram	71
4.9.6	Analysis	72
4.9.7	Critical Review	74
4.9.8	Parameterization	74
4.10	Hip Bracket	74
4.10.1	Inputs and Outputs	74

4.10.2	Constants, Parameters and Assumptions	75
4.10.3	Material Selection	75
4.10.4	Free-Body Diagram	75
4.10.5	Stress Analysis	76
4.10.6	Critical Review	76
4.10.7	Parameterization	76
5	Discussion and Future Work	77
6	References	78
	Appendix A Equation Derivation	80
	Appendix B Additional Analysis	80
B.1	Robot Coordinate System	80
B.2	Approximation Curved Beam	80
B.3	Limbs and Internal Stresses	81
B.4	Ball Bearings	85
B.5	Sleeve Bearing Friction	86
	Appendix C Data sheets	87
	Appendix D Code	111
D.1	Power Consumption	111
D.1.1	Power Consumption Script	111
D.1.2	Harmonic Drive Inputs Script	117
D.1.3	Motor Inputs Script	118

List of Figures

1	Side view of leg assembly in extended position	2
2	Side section of leg assembly with bellow	3
3	Top view of leg assembly	3
4	Front View of leg assembly	4
5	Hip plate alignment pin section	5
6	Foot assembly	5
7	Exterior knee shaft section	6
8	Knee control shaft section	6
9	Hip control shaft section	7
10	Isometric view of belt and pulleys with a tensioner on the belt's slack side	7
11	Isometric view of belt and pulleys with a tensioner on the belt's tight side	8
12	Slope Worst Case Scenarios: Around X (Left) and Around Y (Right)	9
13	Normal Force for all slope angles around y-axis	11
14	Torque over the foot's distance from the hip motor.	13
15	Torque at hip joint before and after adding torsion spring	13
16	Torque at knee joint before and after adding torsion spring	14
17	Stability Visualization	15
18	Linkage Optimization lengths and angles	15
19	Visualization of leg going through leg lifting and putting down motion, as well as ground height d	16
20	3D plots of range in x , y and height from ground d as functions of tibia angle α and linkage lengths r_2 and r_3	17
21	Hourly Solar Radiation Emission - Ottawa July 1st 2019 [4]	20
22	Force-Body Diagram of one leg	24
23	Force-Body Diagram for inner forces	25
24	Axial Force Diagram	27
25	Knee pulley FBD	31
26	Hip pulley FBD	32
27	Hip right-handed torsion spring FBD	36
28	Torques before (left) and after (right) the addition of torsion springs on the limbs for the worst phase	39
29	Exterior knee shaft - Friction moments	41

30	Exterior knee shaft - Side section view of pulley (bearing reaction forces not visible in view)	42
31	Exterior knee shaft - Tibia free-body diagram	43
32	Exterior knee shaft - Free-body diagram in X-Z plane	43
33	Exterior knee shaft - Free-body diagram in Y-Z plane	44
34	Exterior knee shaft - Shear force and bending moment diagrams	45
35	Hip control shaft - Friction moments	46
36	Hip control shaft - Thigh free-body diagram	47
37	Hip control shaft - Free-body diagram in X-Z plane	48
38	Hip control shaft - Free-body diagram in Y-Z plane	48
39	Hip control shaft - Shear force, bending moment and torque diagrams	49
40	Knee control shaft - Free-body diagram in X-Z plane	51
41	Knee control shaft - Free-body diagram in Y-Z plane	51
42	Knee control shaft - Shear force, bending moment and torque diagrams	52
43	Keys - Free-body diagram (cross-section of shaft)	56
44	Sleeve Bearing - Dimensional diagram	58
45	Force-Body Diagram of hip bolts	62
46	Primary and Secondary Shear Stresses in Bolts	63
47	Determining spring constant of bolt and clamping member [14]	68
48	Bellow - Dimensions and Geometry	72
49	Bellow - Finding the required inner diameter based on chassis leg hole	73
50	Hip Bracket - Bending Stress	75
51	Coordinate System for the robot	80
52	Axial Force Diagram for link AB	81
53	Shear Force Diagram for link AB	82
54	Moment Diagram for link AB	82
55	Axial Force Diagram for link BC	83
56	Shear Force Diagram for link BC	83
57	Moment Diagram for link BC	84
58	Axial Force Diagram for link CD	84
59	Shear Force Diagram for link CD	85
60	Moment Diagram for link CD	85

List of Tables

1	Assumptions Made During Robot Modelling	8
2	Calculated shaft diameters and forces at bearings	54
3	Properties of ISO Class 9.8 Bolts	62

1 Project Charter

1.1 Mandate

Group WR2A is mandated to develop a rugged device which uses a biomimetic inspired locomotion system to remove waste from waterfronts. It must be self-reliant and be resistant to exterior environments such as areas with minimal accessibility, rough weather and arduous terrain.

1.2 Requirements

The design is to be solar powered and have a biomimetic inspired locomotion system. It must operate in rain, water, high heat, and navigate terrain such as sand, mud, plants and bramble. Human intervention should only be necessary to empty the litter container. It should resist vandalism. The litter collector size will vary from 1 to 5000 cm³ and 1 to 5 kg.

1.3 Constraints

The device should not have any continuously rotating joints. Additionally, bellows must be used to waterproof joints instead of o-rings to avoid corrosion damage from salt water.

1.4 Criteria

Power consumption per kilogram (device and litter) should be minimized. The operating time should be maximized for better litter collection efficiency. The robot's capacity to navigate a variety of environments, including sand and pebble beaches, shallow water, mud and around small plants, should be maximized. The mechanical stability of the robot should be optimized as well to allow navigation of rough terrain. Finally, aesthetics should be considered as it will operate in public spaces.

1.5 Parametrization Outline

Input parameters that modify the design include the maximum litter weight, litter dimensions as per Group WR2B, desired obstacle size the robot can climb along its forward and upwards axes, and number of days the robot can operate without recharging.

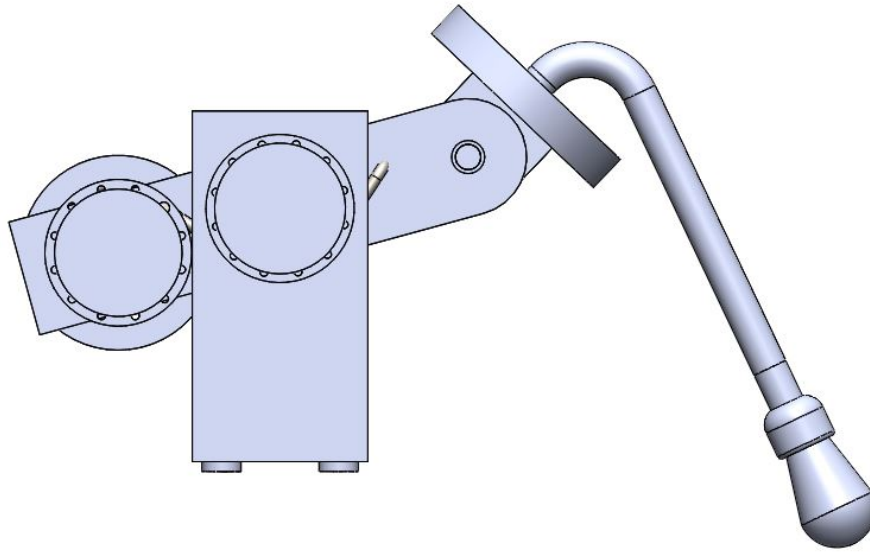


Figure 1: Side view of leg assembly in extended position

2 Detailed Design

The following figures show images of the preliminary CAD model for the legs. Note that some small features may be missing, and some were added on the pictures for clarity. There are also a few interfering parts that will need to be adjusted. Figure 1 shows the leg in an extended position, which is taken as the worse case scenario for the torques applied on the legs.

Figure 2 shows a side section view of the leg, with the bellow. Each leg now only has one bellow as the space between the two joints (knee and hip) is too small to accommodate two separate bellows. The side of the bellow with the largest diameter is going to be attached to the chassis. The smaller diameter side is attached to a circular part into which the tibia tube is press fit.

Figure 3 gives a view of the assembly of the leg with the motors and harmonic drives. It also shows the torsion springs that were added to provide backdriving torque for when the robot is not moving. Note that the torsion springs on the hip control shaft should be holding on to the hip bracket as well as the hip plate. Their configuration will be changed to allow for that. Circular plates (spring supports) were added on each side of the pulley on the knee control shaft to allow for the attachment of the torsion springs. Figure 4 gives another view of the assembly.

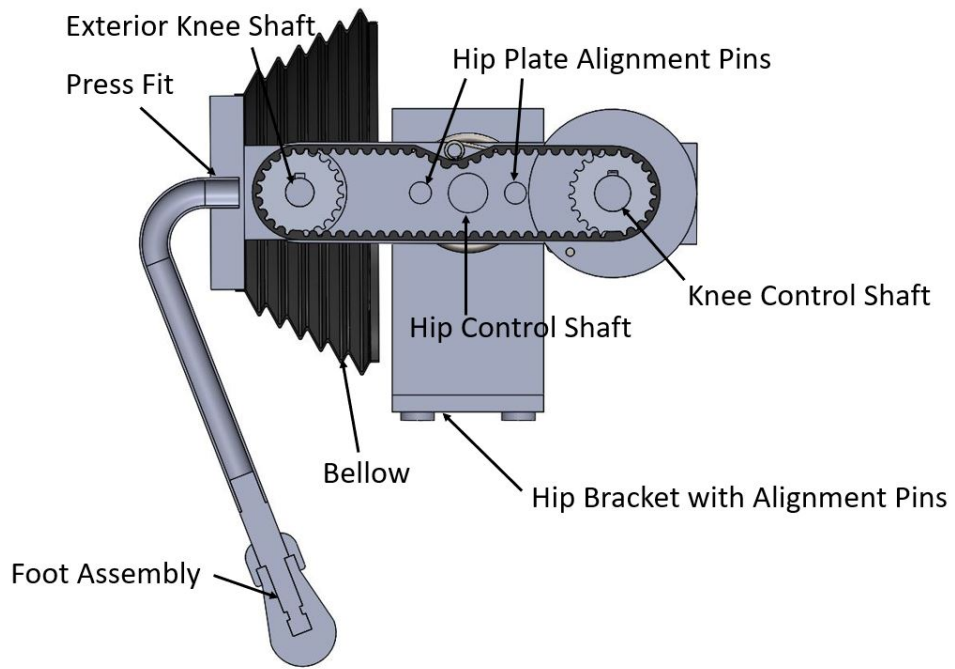


Figure 2: Side section of leg assembly with bellow

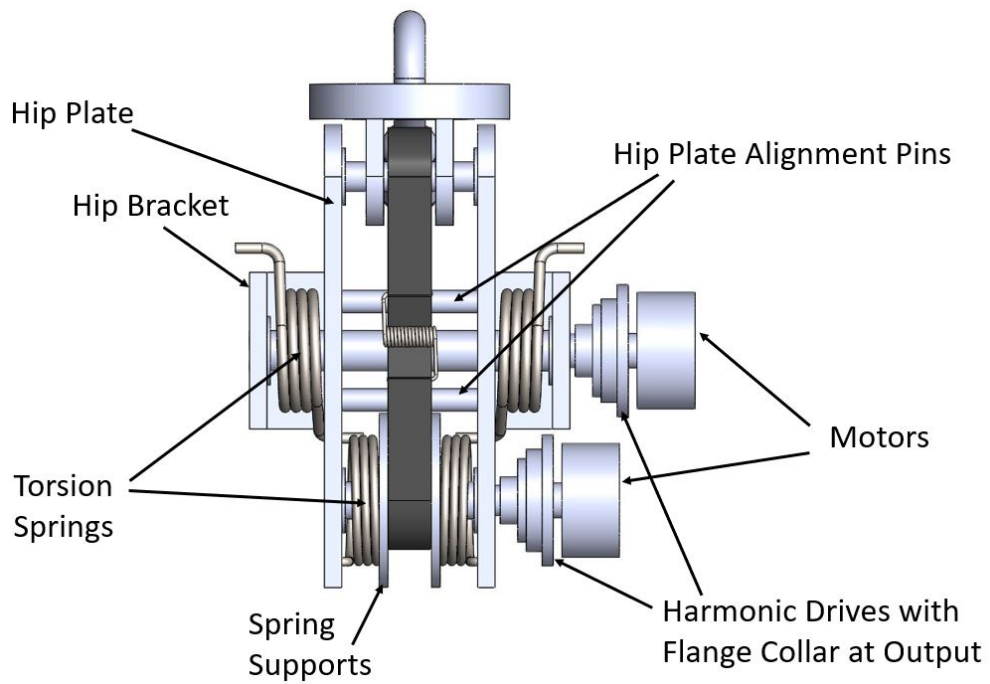


Figure 3: Top view of leg assembly

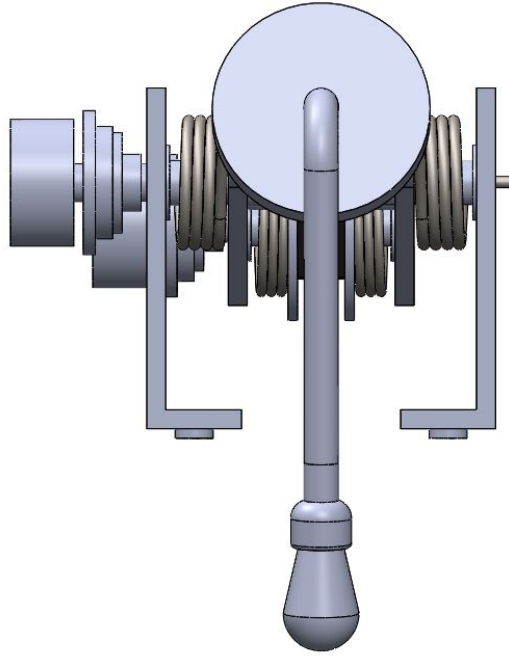


Figure 4: Front View of leg assembly

As seen in the previous figures, the thigh member no longer consists of a tube. Instead, the machined hip and knee plates were joined and now consist of the thigh. Pins in between the two plates were added for alignment and sturdiness. A cross-section of a pin is shown in Figure 5.

An updated version of the foot assembly is shown in Figure 6. The solid tube is going to be threaded to allow the compression cap to screw onto the silicone sock (the thread is drawn over the picture for now as it is not yet implemented in the CAD).

Cross-sections of all three shafts along their axis are shown in Figures 7, 8 and 9. Note that spacers and keys were added over the pictures as those features have not yet been implemented in CAD. Fasteners have not been included yet. For the knee shaft, there should be no clearance between the pulley and the tibia connection, and they are to be connected with fasteners. Note also that the torsion springs on the knee control shaft have some interference with neighbouring parts, which will be fixed.

The timing belt's tensioner has been drawn in two possible configurations. The first scenario presented on Figure 10 is when the slack side of the belt is the top which occurs when the knee is holding the robots weight or when the tibia is moving downward. The other scenario illustrated on Figure 11 represents what would happen if the belt were to overtighten and cancel the effects of the torsion spring.

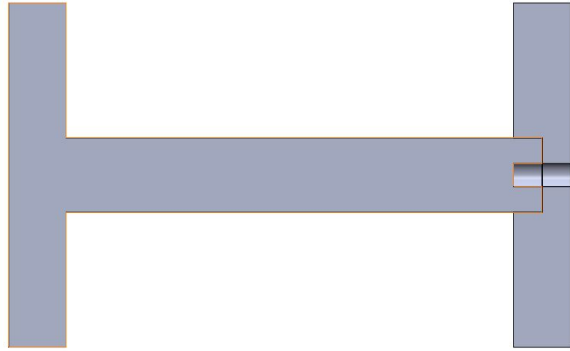


Figure 5: Hip plate alignment pin section

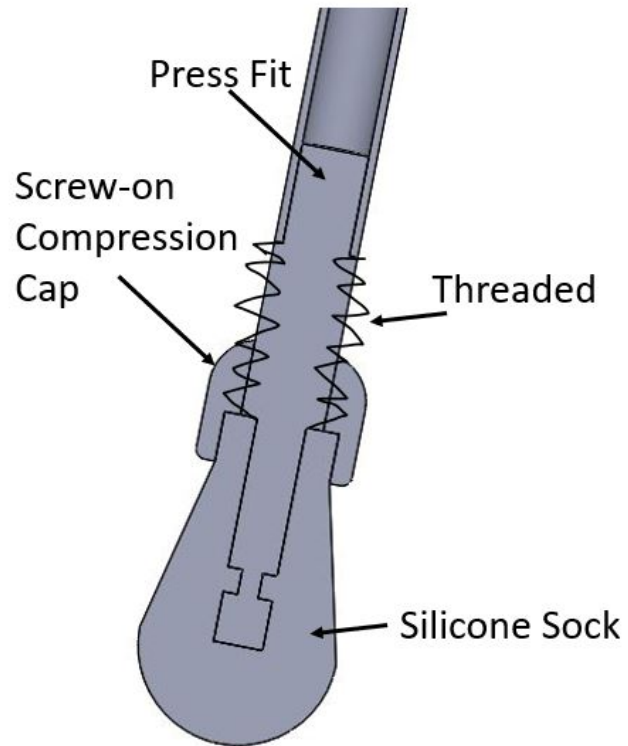


Figure 6: Foot assembly

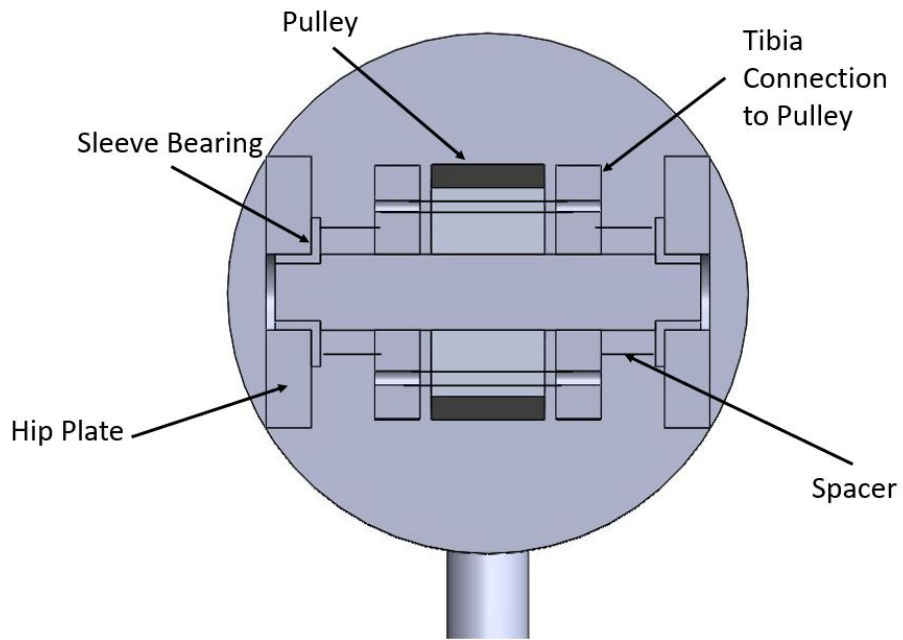


Figure 7: Exterior knee shaft section

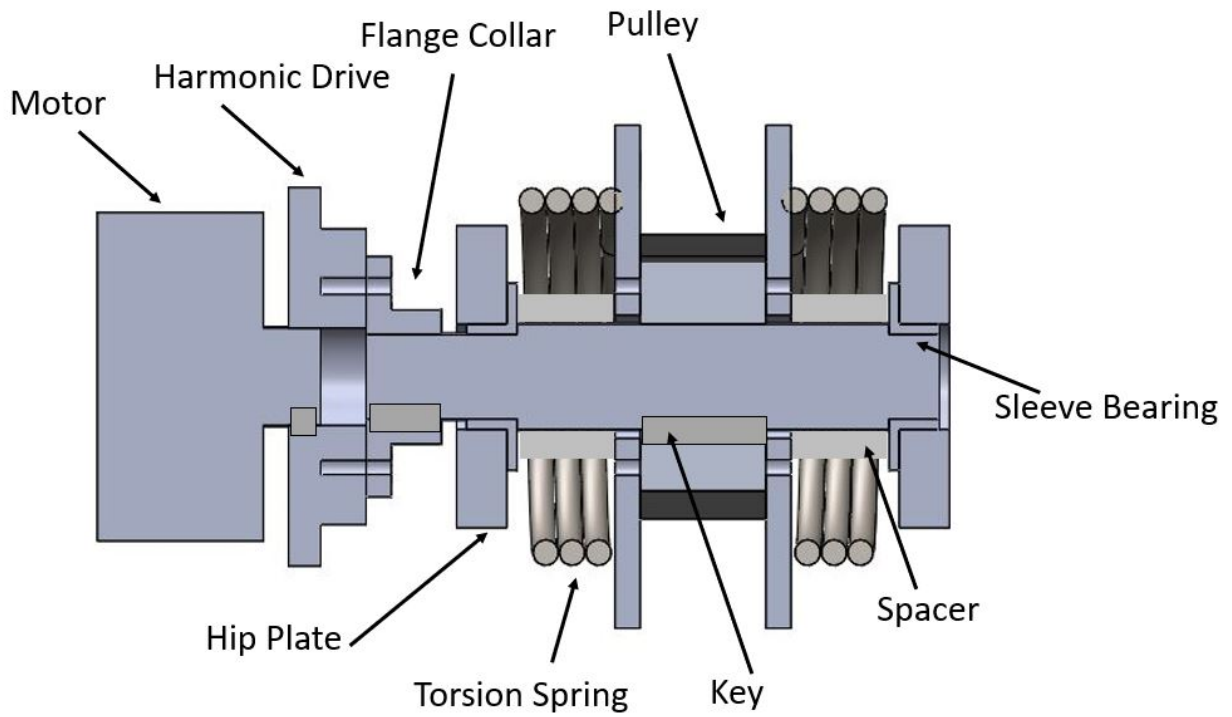


Figure 8: Knee control shaft section

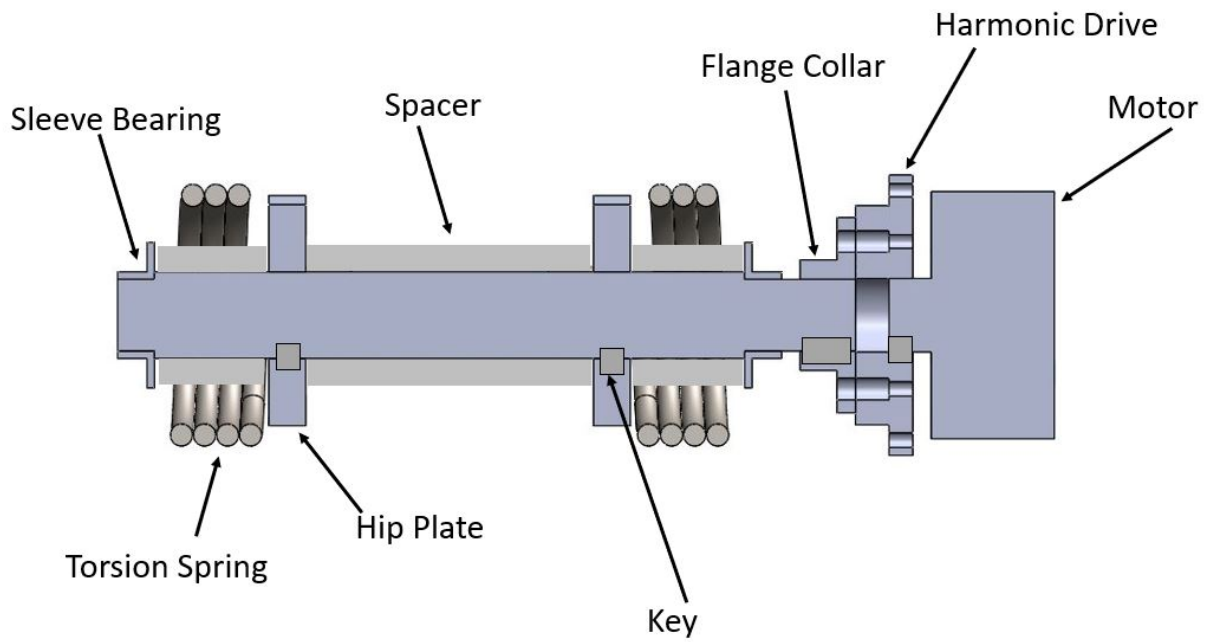


Figure 9: Hip control shaft section

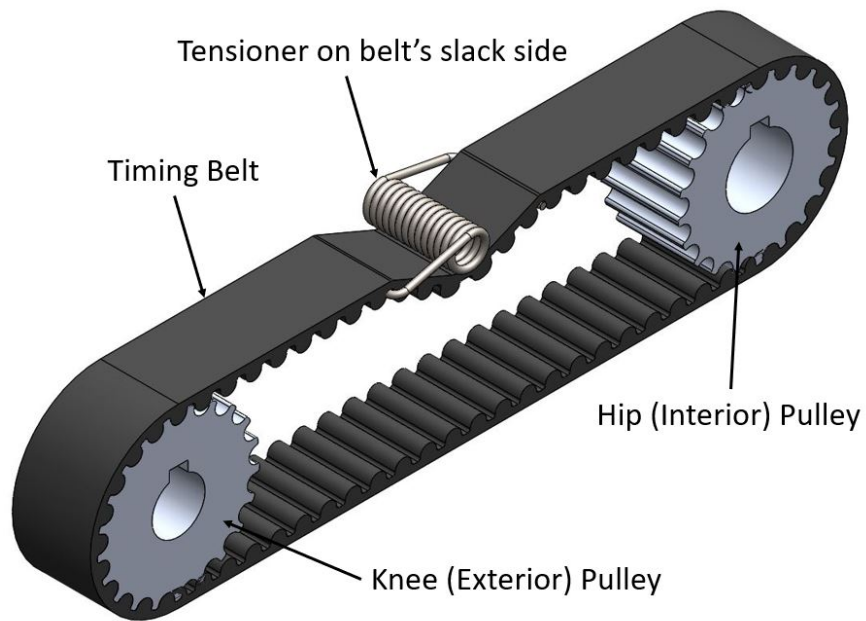


Figure 10: Isometric view of belt and pulleys with a tensioner on the belt's slack side

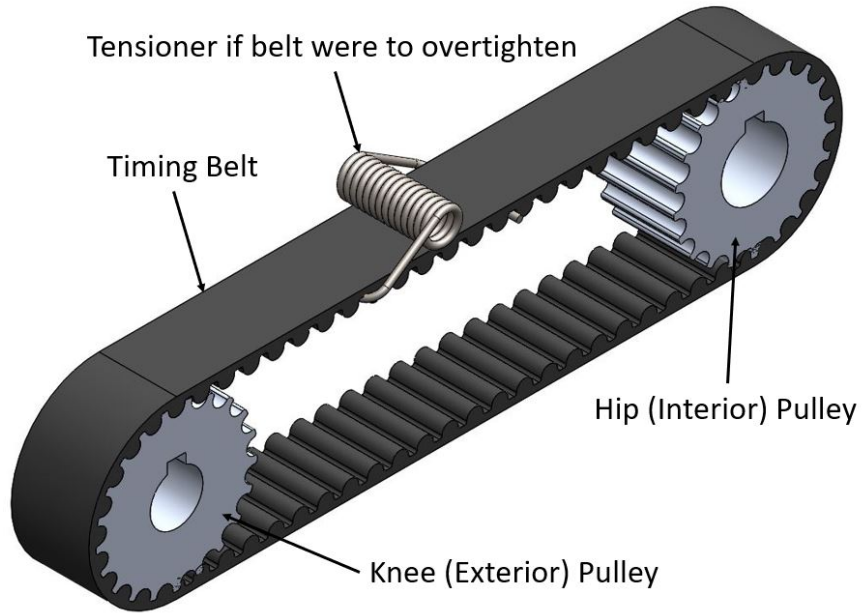


Figure 11: Isometric view of belt and pulleys with a tensioner on the belt’s tight side

3 System Modelling

Table 1 contains assumptions and approximations about the working conditions and applied loads.

Table 1: Assumptions Made During Robot Modelling

Assumption Type	Assumption
Maximum slope angle	20°
Maximum wind speed	73 km/h (Ottawa, September 2018 Tornadoes)
Linkage composition	Homogeneous rigid bodies
Terrain	Sand, pebble, shallow water (under chassis), mud, small plants
Environment	Salt, dust, high heat, humidity

The maximum slope angle was found as the largest angle for which the robot is still stable.

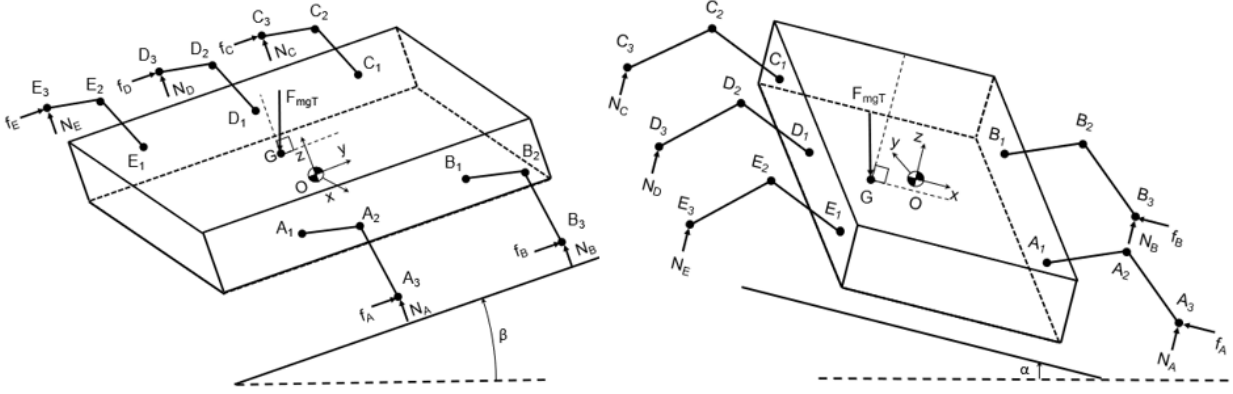


Figure 12: Slope Worst Case Scenarios: Around X (Left) and Around Y (Right)

3.1 External Forces

The defining forces are external forces applied at various locations on the limbs of the robots, mainly normal forces and friction forces which are applied at the extremities of the limbs. Different environmental scenarios encountered by the robot have an impact on the magnitude and direction of these external forces.

The robot must resist two types of soil slope, one around the x axis and the other around the y axis as shown in Figure 12.

The robot will have three legs touching the ground at all times in two different possible leg configuration: ACD and BDE, these were determined by the stability analysis found in section 4. The worst case scenario were assumed for both slope scenarios and shown in Figure 12. For a slope around the x axis, the worst case combination is ACD. For a slope around y axis, both leg combinations are worst case scenarios as long as only one leg is situated at the lower end of the slope. By analysing both scenarios, the following assumptions were made for easier calculations.

Assumptions for slope around x axis.

1. Friction force only acts on the two lowest legs
2. No slipping

Assumptions for slope around y axis.

1. Friction force only acts on the lowest leg
2. No slipping

A visual analysis of both scenarios demonstrates that the friction force will have negligible to beneficial impact on the torque of the motors. For a slope around x axis, the friction will affect the shaft and bearing calculations. For the slope around the y axis, the friction force will counter the torque created by the normal force thus being beneficial to the motor. As discussed later in Section 4.4 the robot is now equipped with springs to reduce the torque when static. Due to the spring, the friction force will now have a negative impact on the motor. However, this impact will mostly impact the energy required for the robot to standstill.

3.1.1 Normal Forces

The 2 combinations of feet touching the ground are: 1. A, C, D and 2. B, D, E. To simplify calculations and algebra, a matrix system approach was used.

For combination 1., the sum of forces and moments are given by

$$\sum F_z = 0 = N_A + N_C + N_D - F_{mgT} \quad (1)$$

$$\sum M_{A_x} = 0 = N_C r_{ca_y} + N_D r_{da_y} - F_{mgT} r_{ga_y} \quad (2)$$

$$\sum M_{C_y} = 0 = -N_A r_{ac_x} - N_D r_{dc_x} + F_{mgT} r_{gc_x} \quad (3)$$

For combination 2., the sum of forces and moments are given by

$$\sum F_z = 0 = N_B + N_D + N_E - F_{mgT} \quad (4)$$

$$\sum M_{B_x} = 0 = -N_D r_{db_y} - N_E r_{eb_y} + F_{mgT} r_{gb_y} \quad (5)$$

$$\sum M_{E_y} = 0 = -N_B r_{be_x} - N_D r_{de_x} + F_{mgT} r_{ge_x} \quad (6)$$

where the r values represent the distance between the foot and the reference point, perpendicular to the rotation axis. To calculate the distance between two points, cartesian coordinates were used, these can be found in Appendix B.1.

The following is an example with combination 1. A matrix solver is used to find reaction

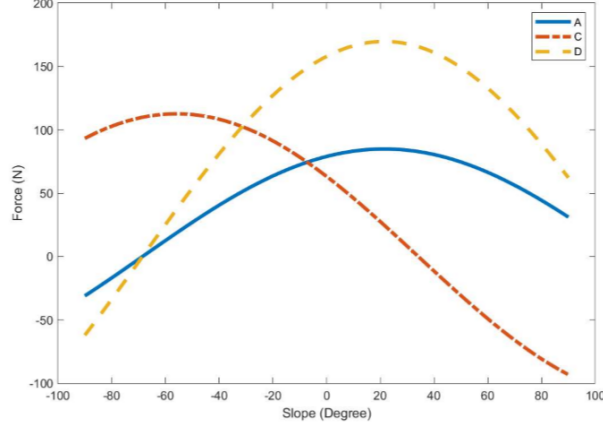


Figure 13: Normal Force for all slope angles around y-axis

values.

$$\begin{aligned}
 \begin{bmatrix} N_A \\ N_C \\ N_D \end{bmatrix} &= \begin{bmatrix} 1 & 1 & 1 \\ 0 & r_{ca_y} & r_{da_y} \\ r_{ac_x} & r_{dc_x} & 0 \end{bmatrix}^{-1} \begin{bmatrix} F_{mgT} \\ F_{mgT}r_{ga_y} \\ F_{mgT}r_{gc_x} \end{bmatrix} \\
 &= \begin{bmatrix} 1 & 1 & 1 \\ 0 & 600mm & 200mm \\ 1137mm & 0 & 0 \end{bmatrix}^{-1} \begin{bmatrix} 302N \\ 60443Nmm \\ 180118Nmm \end{bmatrix} = \begin{bmatrix} 158N \\ 79N \\ 64N \end{bmatrix} \quad (7)
 \end{aligned}$$

The equations are modified to include a slope factor as shown in Equation 8, the normal forces are found when the robot is subject to a slope. Figure 13 shows the normal force for every leg of a combination when subjected to a slope around the y-axis.

$$\begin{bmatrix} N_A \\ N_C \\ N_D \end{bmatrix} = \begin{bmatrix} 1 & 1 & 1 \\ 0 & r_{ca_y} & r_{da_y} \\ r_{ac_x} & r_{dc_x} & 0 \end{bmatrix}^{-1} \begin{bmatrix} F_{mgT} \cos Slope \\ F_{mgT}r_{ga_y} \cos Slope \\ F_{mgT}(r_{gc_x} \cos Slope - r_{gc_z} \sin Slope) \end{bmatrix} \quad (8)$$

3.1.2 Friction Force - Slope around X axis

For this type of slope, the lowest leg on each side of the robot will be subject to friction, for combination of leg ACD, Leg A and Leg D will be subject to friction. The slope of 20 degrees was determined and explained in Section 3.3.

$$\begin{aligned} \sum M_{A_z} = 0 &= -F_D r_{D \rightarrow A} + F_{mgt} \sin \beta r_{CG \rightarrow A} \\ \rightarrow F_D &= \frac{F_{mgt} \sin \beta r_{CG \rightarrow A}}{r_{D \rightarrow A}} = \frac{(299.99N) \sin(20deg)(1136mm - 596mm)}{(1136mm - 0mm)} = 48.6N \end{aligned} \quad (9)$$

$$\begin{aligned} \sum F_y = 0 &= F_A + F_D - F_{mgt} \sin \beta \\ \rightarrow F_A &= F_{mgt} \sin \beta - F_D = (299.99N) \sin(20deg) - (48.6N) = 54.01N \end{aligned} \quad (10)$$

3.1.3 Friction Force - Slope around y axis

Due to the assumptions for a slope around y axis, the friction force F_A (for the case of the leg combination ACD) is the totality of the force transferred as shown in Equation 11. The slope of 20 degrees was determined and explained in Section 3.3.

$$F_A = F_{mgt} \sin \alpha = (299.99N) \sin 20 = 102.6N \quad (11)$$

3.2 Dynamic Equation

For both the static and dynamic case where the legs are moving, the joint torques are found by developing an inertial matrix, force and gravity matrices, and combining them in the dynamic equation developed in the Robotics course, MCG4134 [1]. The final form, following derivations presented in the Modelling Report, is given by Equation 12

$$\begin{aligned} \begin{bmatrix} (m_1 + m_2)L^2 & m_2\ell L \cos(\theta - \phi) \\ m_2\ell L \cos(\theta - \phi) & m_2\ell^2 \end{bmatrix} \begin{bmatrix} \ddot{\theta} \\ \ddot{\phi} \end{bmatrix} - g \begin{bmatrix} (m_1 + m_2)L \cos \theta + m_2\ell \cos \theta \\ m_2\ell \cos \phi \end{bmatrix} \\ + N \begin{bmatrix} L \cos \theta + \ell \cos \phi \\ \ell \cos \phi \end{bmatrix} - f \begin{bmatrix} L \sin \theta + \ell \sin \phi \\ \ell \sin \phi \end{bmatrix} = \begin{bmatrix} \tau_1 \\ \tau_2 \end{bmatrix} \end{aligned} \quad (12)$$

where m_1 and m_2 are the masses of the linkages and joints (moved to the most distal point of the linkage), N is the normal force at the foot, f is the friction force at the foot (and encompasses wind, chassis acceleration, and other external forces parallel the ground), and τ_1 and τ_2 are the joint torques at the hip and knee respectively. This approach is conservative, as the actual inertial matrix would contain mass values closer to the center of the linkages.

As the foot location moves throughout a leg cycle, the torque for both knee and hip motors also fluctuate as shown in Figure 14, where the the torque is plotted over the foot's distance from the hip motor. The torque was calculated using the dynamic equation. Torsion springs

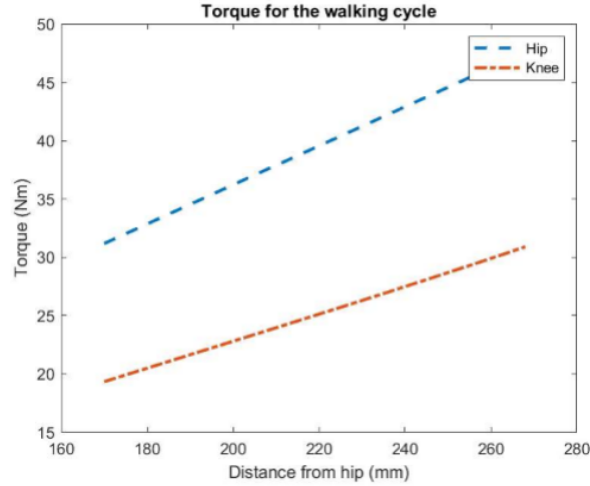


Figure 14: Torque over the foot’s distance from the hip motor.

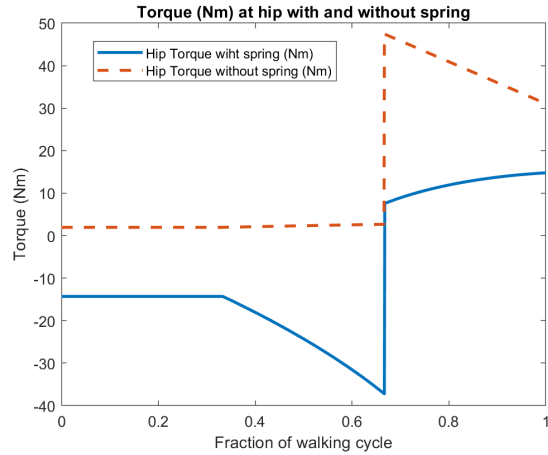


Figure 15: Torque at hip joint before and after adding torsion spring

were added later to the robot to reduce the power consumption when in an idle position; the torques before and after adding torsion springs are found in Figures 15 and 16. It can be seen that, during the last third of the cycle, the leg is on the ground and pulling the robot forward; with the torsion springs, the torque is below the backdriving torque of the Harmonic Drives, and so the motors should not consume any power.

3.3 Stability

To determine the maximum terrain operating slope, the centre of mass was determined for all three directions, x, y, and z. By connecting the feet for each combination of legs touching

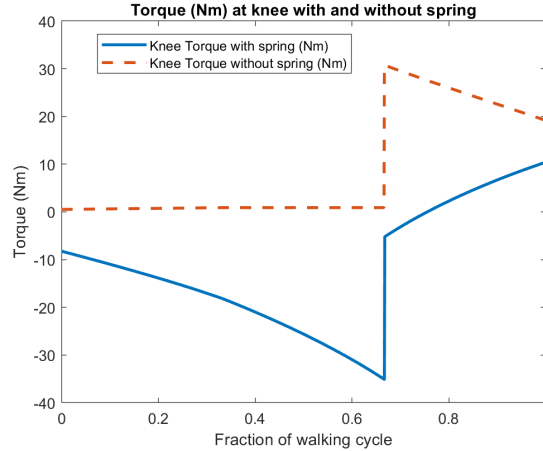


Figure 16: Torque at knee joint before and after adding torsion spring

the ground simultaneously, stability triangles are created and then used to visually determine an area of stability for both leg combination. The triangle of stability for combination ACD and BDE, the area of stability and the optimal location for the centre of mass is shown in Figure 17. For the robot to stay stable during all phases of the walking cycle, the centre of mass must remain in the area of stability. When the robot is subjected to a terrain slope, the different height of the centre of mass (in z direction) will cause the centre of mass to "move" closer to the edges of the area of stability. By using rotational matrices previously presented in the modelling report, the maximum slopes were determined. It was determined that an angle of 20 degrees and -20 degrees around the x and y axis will enable the robot to move properly in one or both slopes.

3.4 Linkage Optimization

In order to determine the relative lengths of the leg linkages, as well as the bend angle in the lower member/tibia, a simple simulation was performed. First, the range of θ is between 0° and 45° with the body reference frame, shown in Figure 18. Then, the range of ψ is between -22.5° and 22.5° relative to the thigh linkage (this ensures half of the 45° range above or below the thigh). These values were chosen while considering the limited range of bellows and optimal stability. The length of r_1 is 100mm, and combined length of r_2 and r_3 is 350mm. The relative ratio of r_1 to $r_2 + r_3$ was determined through trial and error (and would have required more sophisticated methods to determine than the one presented below).

Ranges of r_2 and α are generated, and all permutations are run through the following

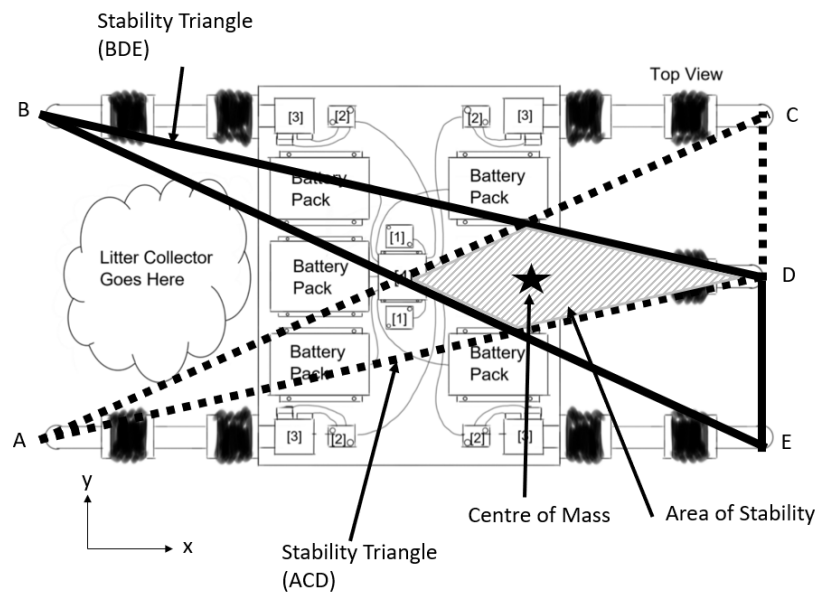


Figure 17: Stability Visualization

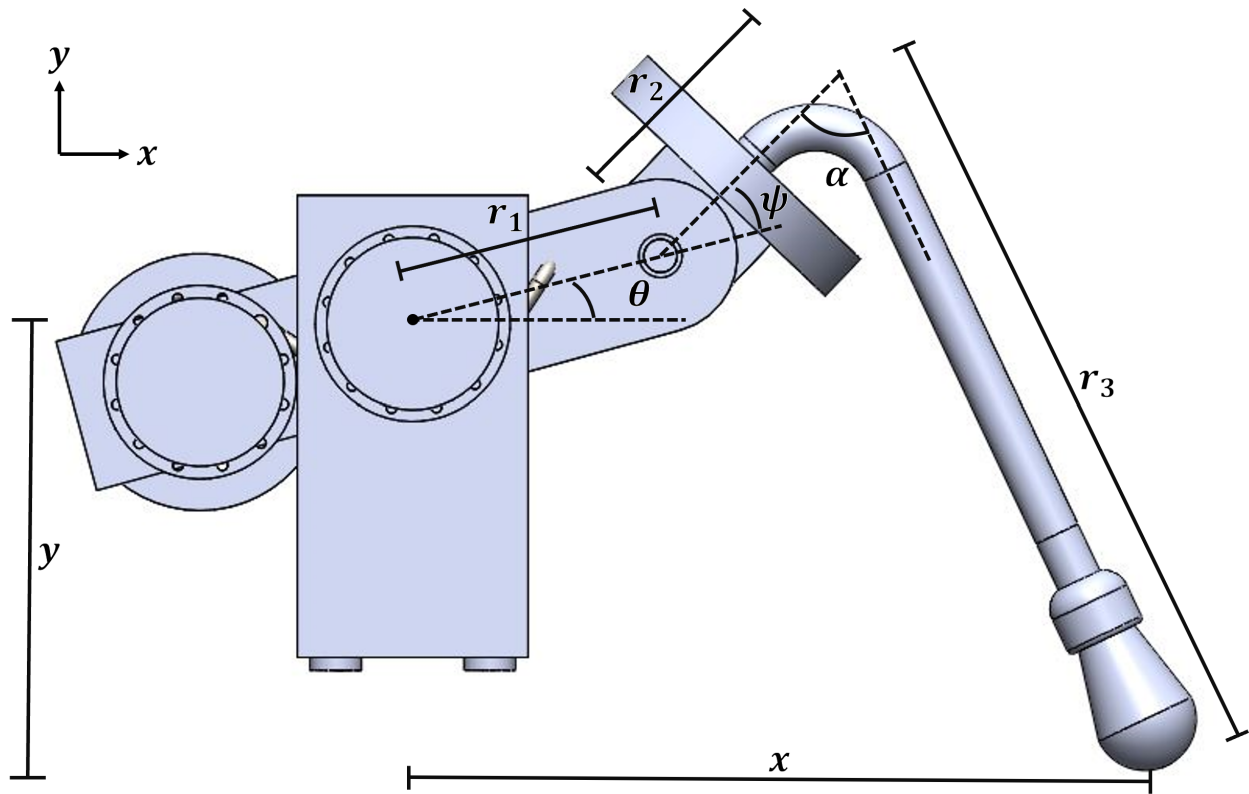


Figure 18: Linkage Optimization lengths and angles

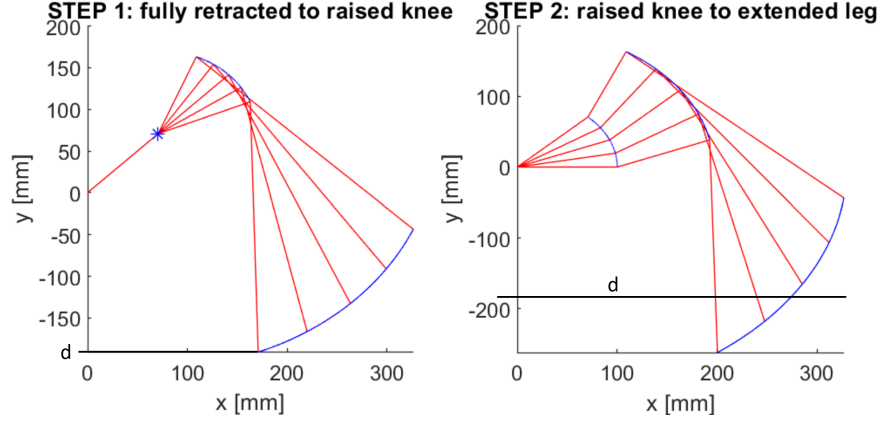


Figure 19: Visualization of leg going through leg lifting and putting down motion, as well as ground height d

steps:

1. Begin with $\theta = 45^\circ$ and $\psi = -22.5^\circ$; this position gives the "ground contact height" (d) shown in Figure 19, as well as the closest the foot can get to the body (x_{min})
2. Increase to $\psi = 22.5^\circ$. This position gives the highest the leg can reach (y_{max})
3. Decrease θ until the ground is reached, giving x_{max}

The results were then plotted in 3D, shown in Figure 20, and a configuration that gave equal $x_{range} = x_{max} - x_{min}$ and $y_{range} = y_{max} - y_{min}$ was determined visually. This method does not necessarily give the most optimal solution, as there is no guarantee that the furthest position the leg can reach in x is with $\psi = 22.5^\circ$ (once α reaches a certain angle, ϕ must be lowered to touch the ground, even with $\theta = 0$). As shown in Figure 19, the foot can technically reach further in x than the found value, just at a different height y . Additionally, setting different maximum and minimum angles for ψ may have also provided better results. The configuration giving a "square workspace" was $r_2 = 50mm$, $r_3 = 300mm$ and $\alpha = 69^\circ$, giving $x_{range} = 103mm$, $y_{range} = 103mm$, and the height of the hip joint from the ground $d = 190mm$. The length r_2 was then found to be too small for mounting the bellow; it was doubled to $100mm$, with the ranges changing to $x_{range} = 97.60mm$ and $y_{range} = 147.51mm$. During parametrization, the maximum reach in x and y will be decided by the user; the values of r_1 , r_2 , r_3 and α will scale relative the the maximum desired reach.

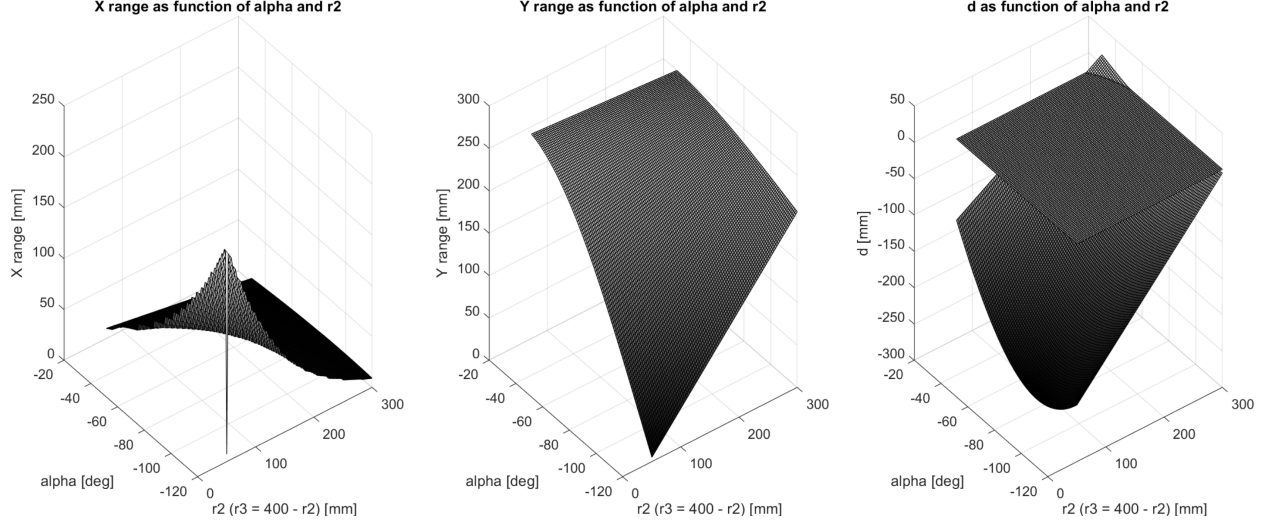


Figure 20: 3D plots of range in x , y and height from ground d as functions of tibia angle α and linkage lengths r_2 and r_3

3.5 Power Consumption

3.5.1 Harmonic Drives Efficiency

The Harmonic Drive and motor at the hip for the heaviest and largest robot were selected to demonstrate the following equations. The example uses the average output speed and half of peak torque seen by the drive. Specifications will appear as used. Harmonic Drive efficiency depends on the input rotation speed and ratio of output torque to rated torque [2]. The speed efficiency η_r was extracted from Harmonic Drive's website using Engauge Digitizer and is approximated using MATLAB's curve fit tool.

$$\begin{aligned} \eta_r &= 4.848 \times 10^{-9} (rpm_{motor})^2 - 5.879 \times 10^{-5} (rpm_{motor}) + 0.8367 \\ &= 4.848 \times 10^{-9} (237.77rpm)^2 - 5.879 \times 10^{-5} (237.77rpm) + 0.8367 = 0.823 \end{aligned} \quad (13)$$

where rpm_{motor} is the output speed of the motor in rotations per minute (RPM). Harmonic Drive only gives values of $0.69 < \eta_r < 0.81$, so the result will be limited to this range ($\eta_r = 0.81$). The torque efficiency depends on

$$\alpha = \frac{\text{load torque}}{\text{rated torque}} = \frac{18.61Nm}{37.23Nm} = 0.5 \quad (14)$$

where the rated torque is the L10 rated torque provided by Harmonic Drive. The torque efficiency is found in the same way as the speed efficiency and approximated as

$$\begin{aligned} k_e &= -1.481\alpha^4 + 4.312\alpha^3 - 5.013\alpha^2 + 3.159\alpha - 0.02076 \\ &= -1.481(0.5)^4 + 4.312(0.5)^3 - 5.013(0.5)^2 + 3.159(0.5) - 0.02076 = 0.75 \end{aligned} \quad (15)$$

Finally, the overall efficiency of the Harmonic Drive is given by

$$\eta_{HD} = \eta_r k_e = (0.823)(0.75) = 0.61 \quad (16)$$

The input torque to the Harmonic Drive (and thus output by the motor) is given by

$$T_m = \frac{T_{HD}}{\eta_{HDe}} = \frac{18.61\text{Nm}}{(0.61)(100)} = 305.63\text{mNm} = 305.63\text{Nmm} \quad (17)$$

where e is the gear ratio of the Harmonic Drive (chosen for our project to be 100).

3.5.2 Motor Power Consumption

Maxon Motor provides equations relating the power in and out of the motor, and power losses [3]. Rearranging these equations provides us with the voltage of the motor

$$\begin{aligned} U &= \frac{1}{k_s} \left(\frac{30000R_m T_m}{\pi k_T^2} + \omega_m \right) = \frac{1}{81.31 \frac{\text{rpm}}{\text{V}}} \left(\frac{30000(2.96\Omega)(305.63\text{Nmm})}{\pi(117.43 \frac{\text{Nmm}}{\text{A}})^2} + (237.77\text{rpm}) \right) \\ &= 10.6210.62\text{V} \end{aligned} \quad (18)$$

where $k_s \left[\frac{\text{RPM}}{\text{V}} \right]$ is the speed constant, $k_T \left[\frac{\text{mNm}}{\text{A}} \right]$ is the torque constant, $R_m [\Omega]$ is the motor resistance and $\omega_m = \omega_{HDe}[\text{RPM}]$ is the output speed of the motor. The motor current can be solved for using the quadratic equation with $a = R_m = 2.91\Omega$, $b = -U = -10.62\text{V}$ and $c = \frac{\pi\omega_m T_m}{30000} = \frac{\pi(237.77\text{rpm})(305.63\text{Nmm})}{30000} = 7.61$. If the motor speed is 0, then the lower result gives 0 and the larger result should be taken. Otherwise, the smaller result should be taken (for a motor running near nominal conditions, the lower result of the quadratic equation will give very close to the nominal current whereas the upper value will give an answer an order of magnitude higher). For the given instance, $I = 0.9876\text{A}$.

3.5.3 Robot Power Consumption

An inaccurate method of calculating robot power consumption is to sum the nominal current of all motors (and electronics), and treat the total current as being continuously drawn. As our design allows for springs and Harmonic Drives to take the robot's weight during rest, as well as the robot gait only moving one leg forward at a time, a more accurate method is required to allow significant battery size and robot weight reductions. A simulation was written that splits the gait into 3 phases. The steps for a front leg are:

1. The leg starts fully retracted ($\theta = 45^\circ$ and $\phi = -22.5^\circ$). Phi moves from its bottom position to its top position ($\phi = 22.5^\circ$).
2. The leg lowers by reducing θ until the foot makes contact with the ground (a position determined in 3.4)
3. The leg pulls the body forward until reaching the position from the beginning of phase 1

The steps for a rear leg are the opposite. While one leg is performing steps 1 and 2, the other 4 legs remain stationary, and while close to the body the legs consume no power. The simulation ran over each phase for each leg and summed the coulombs expended at each step based on the output speed and torque, joint angles, and Harmonic Drive and motor calculations presented in Subsections 3.5.1 and 3.5.2. The total number of coulombs was summed and divided by the simulation time to give the average amperage during walking. The code can be found in Appendix D.1. For the heaviest and largest predicted robot, with a body mass of 30kg and leg geometry taken from 20, consumes on average 5.4A. The other electronics (Raspberry Pi, NVIDIA Jetson, drivers, sensors, etc.) collectively consume 2.13A, giving a total system power draw of 7.55A. Since the batteries output at 48V for the motors, the total power consumption is

$$P = (7.55A)(48V) = 362.4W \quad (19)$$

3.5.4 Solar Power

A typical day in Ottawa during the summer will emit solar radiation similar to Figure 21. As solar radiation emission will vary greatly with weather, two days were taken into account,

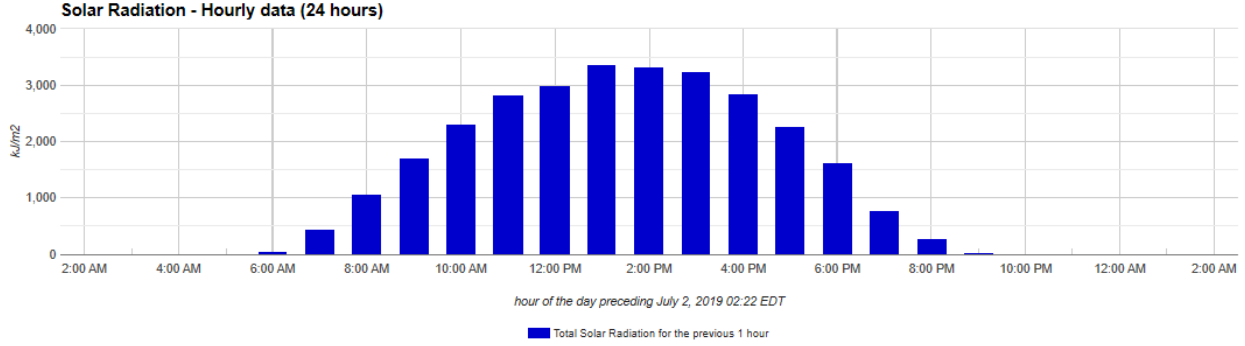


Figure 21: Hourly Solar Radiation Emission - Ottawa July 1st 2019 [4]

July 1st 2019 as shown in Figure 21 and July 17th 2019. The mean KJ/m^2 for both days was taken to calculate a more realistic solar radiation average. The average was calculated as $2111.273KJ/hm^2$.

The total watts produced is calculated using the equation below and where S is the radiation emission in KJ/hm^2 , μ is the solar panels efficiency [5] and A the area of solar panels on the robot.

$$W_{absorbed} = \frac{S\mu A}{(3600s/h)} = \frac{(2111.273 \frac{KJ}{hm^2})(0.223)(0.5m^2)}{(3600s/h)} = 65.39W \quad (20)$$

As a constraint, the robot's batteries must be completely recharged by the end of the day. Thus, the total amount of energy consumed by the robot during the day must be compensated by the solar energy absorbed. The robot requires 355 Watts of power, and according to the calculations above will absorb 65 Watts. Using the equation below, the total run time capability of the robot is calculated by:

$$R = \frac{W_{absorbed}H}{W_{consumed}} = \frac{(65.39W)(10h)}{(362.4W)} = 1.80h \quad (21)$$

where R is the total runtime in hours, H the number of hours of sun during the day. The robot can only accomplish throughout the day 1.8 hours of work time if it is to only use the energy it can absorb.

3.5.5 Battery

Cells are arranged into a battery and managed by a Battery Management System [6]. All electronics are powered from this with the necessary voltage regulators. The battery voltage

is defined as the highest voltage of any component, V_{max} , which is the motors running at 48 V. The number of battery cells running in series, N_{series} , is defined as

$$N_{series} = \frac{V_{max}}{V_{cell}} = \frac{48V}{3.6V} = \frac{48V}{3.6V} = 14 \text{ cells} \quad (22)$$

The number of cells in parallel, $N_{parallel}$, to achieve the desired run time is defined as

$$N_{parallel} = \frac{T \cdot I}{Q} = \frac{(1.8h)(7.55A)}{3.4Ah} = 4 \text{ cells} \quad (23)$$

where T is the runtime in hours, I is the total current draw of the robot and Q is the Amp-hour rating of an individual battery cell [7]. The total number of required cells is the number of series cells multiplied by the number of parallel cells.

$$N = N_{parallel} \cdot N_{series} = 4 \times 14 = 56 \quad (24)$$

3.5.6 Results of Power Consumption Simulation

Using the code given in Appendix D.1, the average current draw is found to be 7.53A. This results in four cells in parallel for 1.8 hours of battery life and 14 cells in series to match the 48V of the motor, giving a total of 56 cells. At 50g each, the combined weight of the cells is 2.8kg, far down from the approximately 238 cells needed when constantly running at nominal current (or 11.9kg) [8]. The more accurate method of calculating power consumption in Section 3.5.3 reduces the battery mass by two thirds over the naive approach.

4 Analysis

4.1 Analysis Outline

All analyzed components are found in chronological order below.

1. Limbs
2. Belt, tensioner and pulleys
3. Torsion springs
4. Shafts
5. Keys
6. Bearings and spacers
7. Fasteners
8. Bellows
9. Hip Brackets

4.2 Limbs

The robot is composed of five legs, all of which are identical in size and length. For this reason, only one leg is analyzed when subject to worst case scenario forces. However, as the robot configuration is not symmetrical for the frontal legs and rear legs, some legs will never be submitted to worst case scenario forces.

4.2.1 Inputs and Outputs

The inputs are the links length determined by optimal link length analysis, the size of internal component such as the pulley at the knee, and the normal and friction force found at the foot. This analysis does not output any parameters to other components analysis. This analysis ensures a reasonable safety factor and determines the diameter and thickness of the tibia, where possible.

4.2.2 Constants and Parameters

The lengths, angle and sizes of the limbs must be known to calculate the bending and shearing in the limbs. They are predetermined by optimal limb length analysis which establishes the legs reach and height. Some limitations exist such as the size of the pulley which restricts the minimal size of the thigh member. The normal force and friction force are found using external force analysis. For this analysis, the worst case scenario of both frictional forces and normal forces are used. The circular tube thickness is set constant at 1.6 mm due to industry standards. The targeted safety factor for this section is 2.0 due to unknown external forces such as human interactions, obstacles, drops, etc.

4.2.3 Assumptions and Simplifications

Limb weight were assumed as they cannot be calculated until the size the limbs are determined by this analysis which creates an iterative process. The weight of the foot is included in the weight of member 3 (m_3) and the weight of the knee is included in the weight of member 2 (m_2) as shown in Figure 22. The weights have been assumed to be in the centre of the member whereas the weight should technically be distributed over the whole member. In between point B and C, the member is press fitted to a mounting piece, no calculation on the press fit was performed as it was assumed a non critical failure location due to only compression forces and relatively small bending forces.

4.2.4 Material Selection

The material selected for the application of the limb is marine grade aluminum 6061-T6 for its outdoor resistance, high yield strength of about 276 MPa and low mass [9].

4.2.5 Free-Body Diagram

First, the FBD of the leg is used to determine external forces on the members. This is shown in Figure 22. External forces are the frictional forces F_f and reactive forces perpendicular to the ground F_N . A friction force at the foot in the y direction is not shown in the FBD but included in the calculation.

To properly analyse all members/links of the leg, the leg must be decomposed into its various sections. The leg is decomposed into three sections, AB which is the foot and lower tibia, BC is the higher tibia, and CD is the thigh. The decomposition enables to calculate

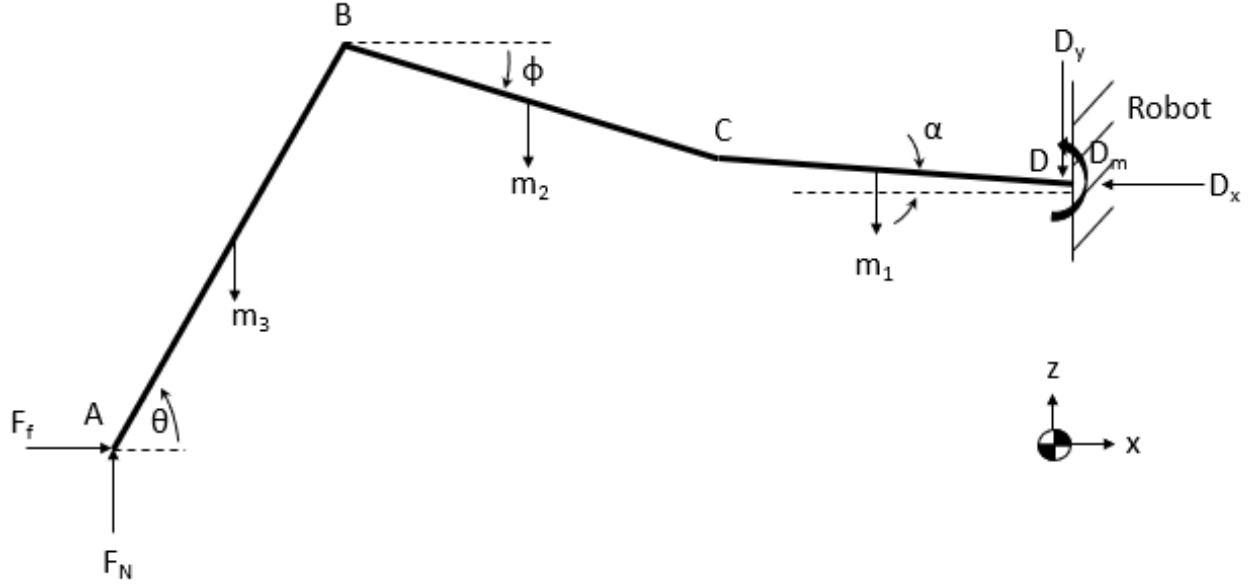


Figure 22: Force-Body Diagram of one leg

internal forces at the joint of all members as shown in Figure 23 where r_3 , r_2 , r_1 are length of the member, B_m , C_m , and D_m are moments at the joints and all other arrow are forces.

4.2.6 Stress Analysis

To calculate the stress in the members, first the axial, radial and bending forces must be determined. Using the sum of forces and moments about an axis, the joint forces $B_{x,y}$, $C_{x,y}$ and $D_{x,y}$, and moments B_M , C_M , D_M can be determined as follows.

$$\sum F_{x_{AB}} = 0 = F_f - B_x \rightarrow B_x = F_f = 10.6N \quad (25)$$

$$\begin{aligned} \sum F_{y_{AB}} = 0 = F_N - m_3g - B_y \rightarrow \\ B_y = F_N - m_3g = 160N - (0.532kg)(9.81m/s^2) = 154.8N \end{aligned} \quad (26)$$

$$\sum F_{x_{BC}} = 0 = B_x - C_x \rightarrow C_x = B_x = 10.6N \quad (27)$$

$$\begin{aligned} \sum F_{y_{BC}} = 0 = B_y - m_2g - C_y \rightarrow \\ C_y = B_y - m_2g = 154.8N - (0.836kg)(9.81m/s^2) = 146.6N \end{aligned} \quad (28)$$

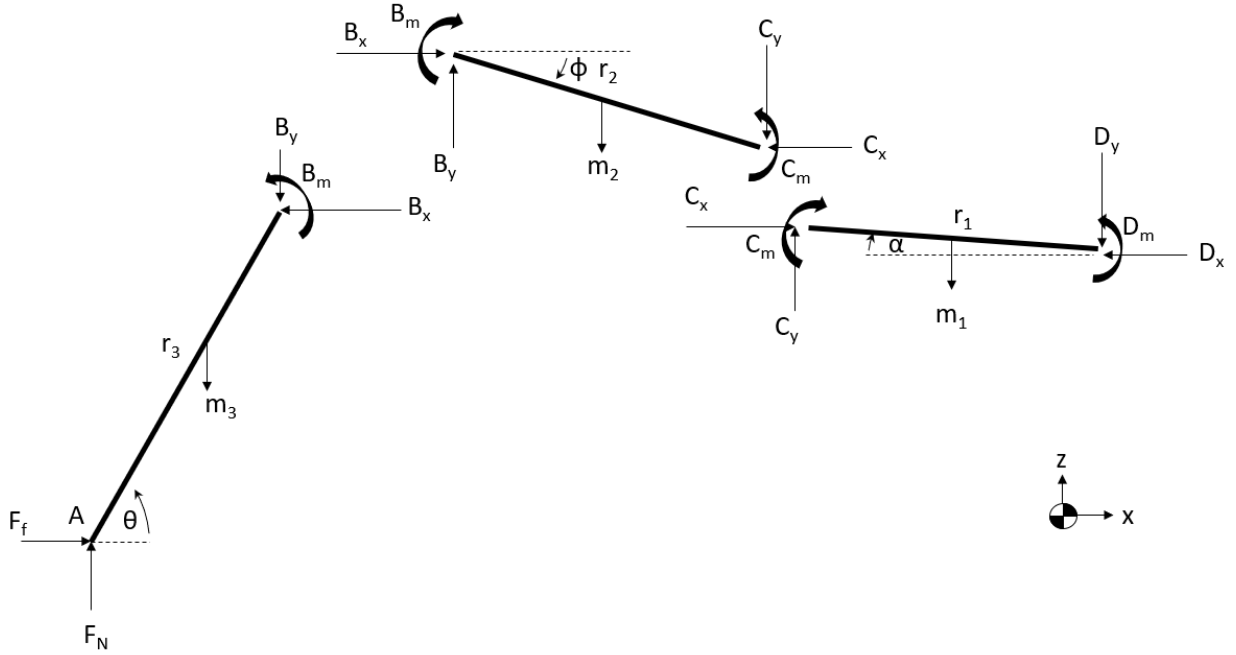


Figure 23: Force-Body Diagram for inner forces

$$\sum F_{x_{CD}} = 0 = C_x - D_x \rightarrow D_x = C_x = 10.6N \quad (29)$$

$$\begin{aligned} \sum F_{y_{CD}} = 0 &= C_y - m_1g - D_y \rightarrow \\ D_y &= C_y - m_1g = 146.6N - (0.532kg)(9.81m/s^2) = 141.4N \end{aligned} \quad (30)$$

$$\begin{aligned} \sum M_B = 0 &= -F_N r_3 \sin \theta + F_f r_3 \cos \theta + m_3 g \frac{r_3}{2} \cos \theta + B_M \rightarrow \\ B_M &= F_N r_3 \sin \theta - F_f r_3 \cos \theta - m_3 g \frac{r_3}{2} \cos \theta \\ B_M &= (160N)(300mm) \sin (71.3deg) - (10.6N)(300mm) \cos (71.3deg) - \\ &\quad (0.532kg)(9.81m/s^2) \frac{(300mm)}{2} \cos (71.3deg) \\ B_M &= 12153.4Nmm \end{aligned} \quad (31)$$

$$\begin{aligned}
\sum M_C = 0 &= -B_x r_2 \sin \phi - B_y r_2 \cos \phi + m_2 g \frac{r_2}{2} \cos \phi - B_M + C_M \rightarrow \\
C_M &= B_x r_2 \sin \phi + B_y r_2 \cos \phi - m_2 g \frac{r_2}{2} \cos \phi + B_M \\
C_M &= (10.6N)(100mm) \sin (39.8deg) + (154.8N)(100mm) \cos (39.8deg) - \\
&\quad (0.836kg)(9.81m/s^2) \frac{(100mm)}{2} \cos (39.8deg) + 12153.4Nmm \\
C_M &= 24418.6Nmm
\end{aligned} \tag{32}$$

$$\begin{aligned}
\sum M_D = 0 &= -C_x r_1 \sin \alpha - C_y r_1 \cos \alpha + m_1 g \frac{r_1}{2} \cos \alpha - C_M + D_M \rightarrow \\
D_M &= C_x r_1 \sin \alpha + C_y r_1 \cos \alpha - m_1 g \frac{r_1}{2} \cos \alpha + C_M \\
D_M &= (10.6N)(100mm) \sin (17.6deg) + (146.6N)(100mm) \cos (17.6deg) - \\
&\quad (0.5kg)(9.81m/s^2) \frac{(100mm)}{2} \cos (17.6deg) + 24418.6Nmm \\
D_M &= 38479.1
\end{aligned} \tag{33}$$

Using the internal forces convention, the axial, shear and bending forces at every point on a member/link is found using the following equations and shown in Figure 24.

Section AB:

$$\text{Axial : } -F_f \cos \theta - F_N \sin \theta \quad \text{Axial : } -F_f \cos \theta - F_N \sin \theta + m_3 g \sin \theta \tag{34}$$

$$\text{Radial : } -F_f \sin \theta + F_N \cos \theta \quad \text{Radial : } -F_f \sin \theta + F_N \cos \theta - m_3 g \cos \theta \tag{35}$$

Section BC:

$$\text{Axial : } -B_x \cos \phi + B_y \sin \phi \quad \text{Axial : } -B_x \cos \phi + B_y \sin \phi - m_2 g \cos \phi \tag{36}$$

$$\text{Radial : } B_x \sin \phi + B_y \cos \phi \quad \text{Radial : } B_x \sin \phi + B_y \cos \phi - m_2 g \sin \phi \tag{37}$$

Section CD:

$$\text{Axial : } -C_x \cos \alpha + C_y \sin \alpha \quad \text{Axial : } -C_x \cos \alpha + C_y \sin \alpha - m_1 g \cos \alpha \tag{38}$$

$$\text{Radial : } C_x \sin \alpha + C_y \cos \alpha \quad \text{Radial : } C_x \sin \alpha + C_y \cos \alpha - m_1 g \sin \alpha \tag{39}$$

As there are bending and shearing in multiple planes, the resultants of both are calculated as shown in equation 40 and 41. The numerical values are for point C which is located at 100mm in the stress diagrams shown in Figure 24. For other members, see Appendix B.3.

$$V = \sqrt{V_x^2 + V_y^2} = \sqrt{(119.5N)^2 + (54.0N)^2} = 131.1N \tag{40}$$

$$M = \sqrt{M_x^2 + M_y^2} = \sqrt{(12153.4Nmm)^2 + (16204.5Nmm)^2} = 20255.6Nmm \tag{41}$$

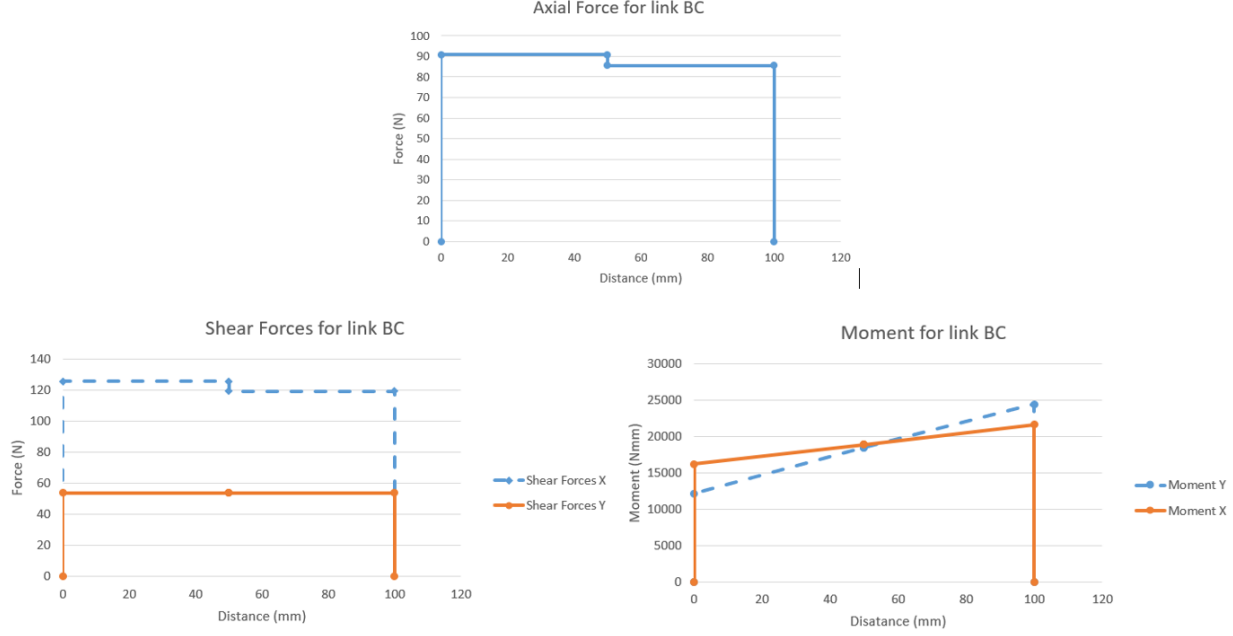


Figure 24: Axial Force Diagram

The bending can be obtained by multiplying the radial force to the distance such as $Bending = Radial \times Distance$ and can then be matched to joint values such as B_M , C_M , and D_M to confirm the calculations. The bending and shear diagrams demonstrate that between both hollow circular member AB and BC, point C will have the highest stress concentration. First the axial stress is calculate using the following equation [10]:

$$\begin{aligned} \sigma_x &= \frac{P_x}{A} + \frac{My}{I} = \frac{P_x}{\frac{\pi}{4}(D^2 - d^2)} + \frac{My}{\frac{\pi}{64}(D^4 - d^4)} \\ &= \frac{85N}{\frac{\pi}{4}((17.175mm)^2 - (14mm)^2)} + \frac{(32605Nmm)(\frac{7.175mm}{2})}{\frac{\pi}{64}((17.175mm)^4 - (14mm)^4)} = 118.5MPa \end{aligned} \quad (42)$$

The shearing stress due to radial forces in the member are calculated as shown in Equation 43, and the shearing forces created by the torsion due to frictional forces in the y direction (when on a slope) is shown in Equation 44.

$$\tau_{shear_{xy}} = \frac{2V}{A} = \frac{2(131.1N)}{\frac{\pi}{4}((17.175mm)^2 - (14mm)^2)} = 3.37MPa \quad (43)$$

$$\tau_{torsion} = \frac{T}{2r^2t} = \frac{(15128Nmm)}{2(1.59mm)(7.79mm)^2} = 24.9MPa \quad (44)$$

$$\tau_{xy} = \tau_{shear_{xy}} + \tau_{torsion} = 3.4MPa + 24.9MPa = 28.3MPa \quad (45)$$

The safety factor n of the limb to external forces is calculated by comparing the Von Mises equivalent stress σ_e and yield strength S_y of the material.

$$\sigma_e = (\sigma_x^2 + 3\tau_{xy}^2)^{(1/2)} = ((118.5MPa)^2 + 3(28.3MPa)^2)^{(1/2)} = 128.2MPa \quad (46)$$

$$n = \frac{S_y}{\sigma_e} = \frac{250MPa}{128.2MPa} = 2.0 \quad (47)$$

Another critical location on the member is the curved section of the beam which is at point B. As the member is considered a curved beam, different set of equations are used. Equations for hollow circular cross sections for curved beams could not be found nor derived, thus the stress in the beam was approximated using a full tube cross section and a suggested approximation formula. The radius of the curvature, or the radius of inner fiber r_i was set at 8.59 mm, half of the diameter of the bar which is possible in the industry but will mostlikely require advanced tooling [11]. The radius of centroidal axis r_c , radius of neutral axis r_n and the distance from centroidal axis to neutral axis e are calculated as follow for a full circular tube where R is the radius of the tube.

$$r_c = r_i + R = 8.59mm + 8.59mm = 17.175mm \quad (48)$$

$$r_n = \frac{R^2}{2(r_c - \sqrt{r_c^2 - R^2})} = \frac{(8.59mm)^2}{2(17.175mm - \sqrt{(17.18mm)^2 - (8.59mm)^2})} = 16.02mm \quad (49)$$

$$e = r_c - r_n = 17.18mm - 16.02mm = 1.51mm \quad (50)$$

The stress in the curvature is calculated at the inner fiber radius σ_i , due to its higher tension forces than at the outer fiber. Where A is the area for the cross section of a hollow tube and not of a full tube.

$$\sigma_i = \frac{Mc_i}{Aer_i} = \frac{(20256Nmm)(7.437mm)}{\frac{\pi}{4}((17.175mm)^2 - (14mm)^2)(1.505mm)(8.59mm)} = 196.1MPa \quad (51)$$

The stress at the inner fiber of the tube is thus 196.13 MPa compared to the 72.92 MPa previously calculated at point B using straight beam formulas. The safety factor for the point B is 1.27 when subject to 196.1 MPa, however multiple assumptions were made such that the tube was hollow. If the area of a full tube is used in the above equation, a safety factor of 3.7 is achieved and if the simplification method is used a safety factor of 2.2 is achieved, see appendix B.2. Due to the approximations, the low safety factor is acceptable in this case and the parametrization will ensure the safety factor at Point C is respected at 2.0.

4.2.7 Critical Review

Multiple assumptions such as the weight of the limbs and weight location were made to simplify the calculations. The stresses at the curved locations must be calculated using more advanced tools to properly determine a safety factor. Fatigue was not considered in this analysis due to the slow speed of the robot. Calculation of the weight of a member such as the lower tibia demonstrate a weight of 0.06 kg, one tenth of the approximated weight of the tibia of 0.5 kg with negligible impact on the overall bending and shear stress of the member.

4.2.8 Parameterization

Due to exterior conditions, loads and application, marine grade metals are best used for the limbs of the robot. This material will not be parameterized and will remain constant for various sizes of robots. Due to the limitation posed by the pulley found at the knee, the thigh member's size is restricted by the belt and pulley size, and height requirements, thus the thigh size are determined by the section 4.3, these sizes will produce very high safety factors. The length of members are also determined by external analysis. The diameter and thickness of the tibia hollow tube are parametrizable, however both are dependent of the other. To attain reasonable safety factors between 1 and 2.5, the thickness will be constant to ensure the thickness does not reduce to unreasonable size. However, it is also possible that the diameter reduces to unfeasible sizes, thus diameter will be assumed constant for these situations. The bend radius of the curved section is another parametrizable factor which helps reduce internal stresses. The bend radius of the curved section is set at half of the diameter of the tube, however it was found that there is limited space on the upper tibia link causing obstruction issues between the bellow mounting piece and the tibia link, and an appropriate length size issue for the press fit of the tibia. Thus, the bend radius will be set at half of the diameter when possible, but may require to be reduced furthermore due to obstructions.

4.3 Belt, Tensioner and Pulleys

4.3.1 Inputs and Outputs

The main input for the belt design is the maximum moment generated at the knee joint $M_{max} = M_{knee} = 30.71$ Nm obtained from Figure 14 in Section 3.3. Other inputs are the length of the thigh limb (from knee shaft to hip shaft) $L_{thigh} = 100$ mm and the distance

between the hip motor shaft and the knee motor shaft $L_{hm2km} = 88$ mm which form the center distance C .

$$C = L_{thigh} + L_{hm2km} = 100 \text{ mm} + 88 \text{ mm} = 188 \text{ mm} \quad (52)$$

The outputs are the belt's tight tension T_{tight} and slack tension T_{slack} , the pulleys' pitch diameter D_{pitch} , outer overall diameter D_O including the belt, number of teeth $N_{pulley \text{ teeth}}$, the belt's length L_{belt} and number of teeth $N_{belt \text{ teeth}}$ along with other dimensions for the CAD model.

4.3.2 Constants and Parameters

The mechanical efficiency of the belt is known to be somewhere between 94% and 96% [12]. A value of $\eta_{belt} = 0.95$ was chosen for this application. The chosen belt has a constant tooth pitch p of 8 mm per tooth and a width w of 25 mm. The pulleys' number of teeth n_{teeth} is a variable parameter that will change based on the maximum torque at the knee joint, but the value chosen for the calculations is 21 teeth for both pulleys. The pitch diameter of the pulley can be calculated as follows [12]:

$$D_p = \frac{p \ n_{teeth}}{\pi} = \frac{(8 \text{ mm/tooth}) (21 \text{ teeth})}{\pi} = 53.48 \text{ mm} \quad (53)$$

4.3.3 Assumptions and Simplifications

It is assumed that both pulleys have the same diameter ($D_{hip} = D_{knee} = 53.48$ mm) since no further speed reduction is required. This also simplifies the design calculations. The impact of gravity and inertia of both pulleys and the belt were neglected due to the low velocity and acceleration of the limbs.

4.3.4 Material Selection

The chosen timing belt manufacturer, Gates Mectrol, offers urethane belts reinforced with either steel or Kevlar. Both products offered different limits when it comes to the maximum tension that can be applied on a belt. However, since the steel reinforced belts are able to take higher loads than the Kevlar ones, steel was chosen to minimize the size of both the belt and the pulleys [13]. The chosen belt, a steel reinforced HTD[®]8 urethane timing belt has a maximum allowable belt tension T_{max} of 3471 N/25 mm of belt width as shown in the Gates Mectrol Urethane Belt Catalogue on page 9 in Appendix C [13]. The manufacturer

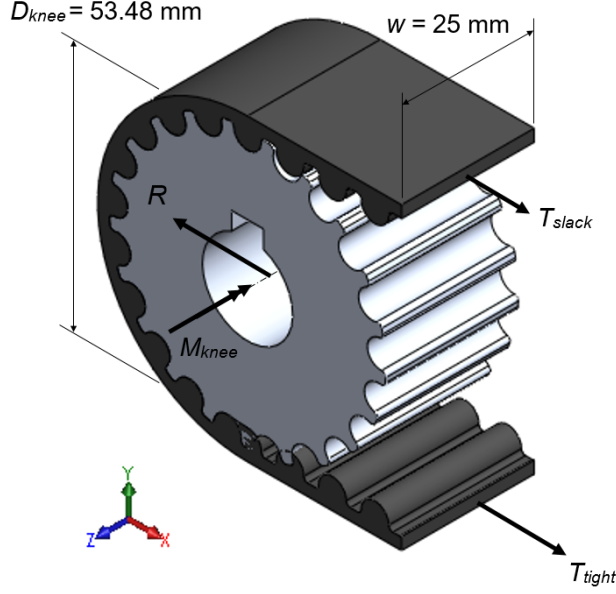


Figure 25: Knee pulley FBD

also suggests an allowable effective tension $T_{e \text{ allow}}$ of 1870 N/25 mm of belt width that is valid only if 15 teeth or more are used for meshing. This condition means that the allowable effective tension value given only applies if the the two pulleys have at least 30 teeth and therefore cannot be used for this present case.

As for the pulleys, Gates Mectrol offers aluminium, steel, and stainless steel as options for the pulley material [13]. Zinc plated steel or stainless steel flanges may also be added to the pulley to help maintain the position of the belt. The chosen material is aluminium since both pulleys are sealed from the environment, and because a reduced weight has a positive effect on the robot's general capabilities.

4.3.5 Free-Body Diagram

The free-body diagrams of both pulleys are presented in Figure 25 and Figure 26.

4.3.6 Stress Analysis

The moment taken by the driving pulley is expressed as follows [12].

$$M_{hip} = \frac{M_{knee}}{\eta_{belt}} \frac{D_{hip}}{D_{knee}} = \left(\frac{30.71 \text{ Nm}}{0.95} \right) \left(\frac{53.48 \text{ mm}}{53.48 \text{ mm}} \right) = 32.26 \text{ Nm} \quad (54)$$

Then, the effective tension of the belt T_e can be obtained from the driving torque.

$$T_e = \frac{2M_{hip}}{D_{hip}} = \frac{2(32.36 \text{ Nm})}{53.48 \text{ mm} \frac{1 \text{ m}}{1000 \text{ mm}}} = 1209 \text{ N} \quad (55)$$

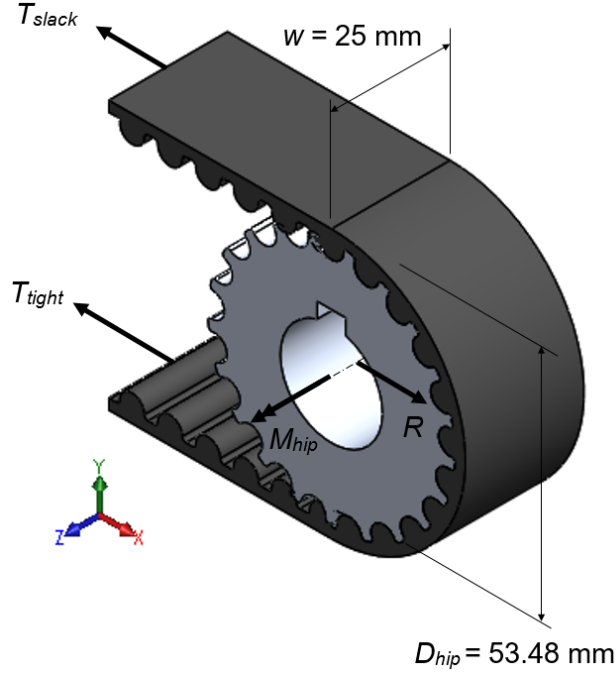


Figure 26: Hip pulley FBD

The effective tension of the belt can also be expressed by the difference between the tight tension and the slack tension and timing belts are known to perform better when the slack tension is 10% to 30% the magnitude of the effective tension [12]. 30% was chosen as a conservative approach for increasing the load on the belt.

$$T_{slack} = 0.3 T_e = (0.3) 1209 \text{ N} = 362.7 \text{ N} \quad (56)$$

Then, the tight tension can be obtained as follows.

$$T_{tight} = T_e + T_{slack} = 1209 \text{ N} + 362.7 \text{ N} = 1571.7 \text{ N} \quad (57)$$

The tight and slack tensions can be added to obtain the resultant reactive force on either shaft.

$$\sum F_x = 0 \longrightarrow R = T_{tight} + T_{slack} = 1571.7 \text{ N} + 362.7 \text{ N} = 1934.4 \text{ N} \quad (58)$$

Now, to compare the belt tensions with the manufacturer's recommendations to obtain safety factors.

$$SF = \frac{T_{max}}{T_{tight}} = \frac{3741 \text{ N}}{1571.7 \text{ N}} = 2.38 \quad (59)$$

$$SF^* = \frac{T_{e \text{ allow}}}{T_e} = \frac{1870 \text{ N}}{1209 \text{ N}} = 1.55 \quad (60)$$

However, SF^* may not mean anything since the condition of minimum 15 teeth in meshing is not respected for two pulleys with 21 teeth each.

The total length of the belt L_{belt} and the number of teeth N_{teeth} can be obtained as follows [12].

$$L_{belt} = 2C + \pi D_p = 2(188 \text{ mm}) + \pi(53.48 \text{ mm}) = 544 \text{ mm} \quad (61)$$

$$N_{teeth} = \frac{L_{belt}}{p} = \frac{544 \text{ mm}}{8 \text{ mm/tooth}} = 68 \text{ teeth} \quad (62)$$

4.3.7 Critical Review

The pulley dimensions obtained above are sufficient to reduce the belt tensions to acceptable values based on the manufacturer's recommendations. An error may have been made when the efficiency of the belt was applied: for a case where the motor is not powered, the driver pulley actually becomes the knee pulley and the motor shaft is then driven. Therefore, the torque on the motor shaft should be lower than torque on the knee pulley. However, wrongly applying the efficiency of the belt drive only makes this analysis more conservative and has no negative effects on the results. This error may be corrected for the parameterization.

The analysis of the torsion spring belt tensioner was attempted but did not yield satisfying results. No direct link could have been made between the belt tension and the properties of the torsion spring. It was then decided that the belt's total length L_{belt} would tightly fit the over the pulleys when installed by hand. Then, the installation of the torsion spring only helps ensuring that the belt tension remains in an operating range if the belt were to expand due to the temperature or due to normal life wear. The spring dimensions were chosen following a similar process as the other torsion springs in Section 4.4 but no further analysis was completed. The main spring dimensions are as follows: free angle $\beta = 270^\circ$, wire diameter $d = 2 \text{ mm}$, coil diameter $D = 10 \text{ mm}$, arm length $l = 24 \text{ mm}$, number of body turns $N_b = 14.75$ turns. The spring constant k was found to be 327.3 Nmm/rad , the maximum deflection θ_{max} is approximately 155° which yields a maximum torque M_{max} of 885.44 Nmm while respecting a safety factor of 1.03 if the belt were to perfectly straighten as shown on Figure 11 in the Detailed Design Section. If a single tensioner is not sufficient for the continuous operation of the robot, an identical torsion spring could be added on the other side of the belt to compensate for the bidirectional drive.

4.3.8 Parameterization

The idea behind the parameterization of this analysis consists of inputting the highest torque generated at the knee and the distance between the input and output shafts to obtain the pulley and belt dimensions. A loop will most likely be used to obtain an optimized value for the pulley diameter based on the tensile limits of the belt and the other belt dimensions that will remain constant. The tensioner will most likely not be parameterized due to the constant belt width and belt pitch.

4.4 Torsion Springs

4.4.1 Inputs and Outputs

Each leg's motor shafts have a pair of torsion springs to compensate for the backdrivability of the harmonic drives. The idea is to limit the torque to a value beneath the harmonic drive's backdrivable torque when it is not powered. The inputs are then the maximum torque generated at the knee $M_{knee\ max} = 32.36$ MPa and the maximum torque generated at the hip $M_{hip\ max} = 47.44$ MPa from Figure 14 in Section 3.3. Additionally, the minimum torques $M_{knee\ min} = 19.08$ Nm and $M_{hip\ min} = 31.07$ Nm are used to ensure that the minimal deflection angles of the torsion springs provide sufficient torques based on the angular positions of the limbs. The tibia span ($\theta_{tibia\ max} - \theta_{tibia\ min}$) approaches 45° while the thigh span ($\theta_{thigh\ max} - \theta_{thigh\ min}$) is only about 25° . Also, the outer diameters of the spacers ($D_{knee\ spacer} = 31.5$ mm, $D_{hips\ spacer} = 33.5$ mm) are given to ensure that all torsion springs do not interfere with the shaft spacers when deflected.

The torsion spring analysis will generate many outputs such as the various dimensions of the springs. However, the most important outputs are the spring constants k_{knee} and k_{hip} that are used to compute the resultant torques taken by both harmonic drives.

4.4.2 Constants and Parameters

The spring free angle β can vary between 90° and 360° , but a value of $\beta = 90^\circ$ was set to be a constant for the purpose of this analysis. Similarly, the number of full turns made by the spring coil was chosen to be $N_f = 3$ turns. The length arms were kept constant for both springs ($l_{1\ knee} = l_{2\ knee} = 25$ mm, $l_{1\ hip} = l_{2\ hip} = 25$ mm).

4.4.3 Assumptions and Simplifications

It is assumed that the backdriving torque of a harmonic drive corresponds to approximately 1/5 of the harmonic drive's rated torque based on the data sheets presented in Appendix C. For this purpose, it is also assumed that the rated torque of the harmonic drive coincides with the maximum torques $M_{knee\ max}$ and $M_{hip\ max}$.

$$M_{knee\ bd} \simeq \frac{M_{knee\ max}}{5} = \frac{32.36\ \text{MPa}}{5} = 6.47\ \text{MPa} \quad (63)$$

$$M_{hip\ bd} \simeq \frac{M_{hip\ max}}{5} = \frac{47.44\ \text{MPa}}{5} = 9.45\ \text{MPa} \quad (64)$$

Two torsion springs equally share the torque in such a way that the maximum and minimum torque generated by a single torsion spring can be obtained as follows.

$$M_{max\ hip\ spring} \geq \frac{1}{2}(M_{hip\ max} - M_{hip\ bd}) = \frac{1}{2} \frac{4}{5} M_{hip\ max} = \frac{4}{10} (47.44\ \text{Nm}) = 18.98\ \text{Nm} \quad (65)$$

$$M_{min\ hip\ spring} \geq \frac{1}{2}(M_{hip\ min} - M_{hip\ bd}) = \frac{1}{2}(31.07\ \text{Nm} - 9.45\ \text{MPa}) = 10.79\ \text{Nm} \quad (66)$$

4.4.4 Material Selection

The chosen material for all springs is music wire due to it being a common spring material and also due to its sufficient tensile strength for this application. The Young's Modulus E of music wire, and most carbon steels, was given as 207 GPa. The tensile strength S_{ut} was obtained with the following constants A and m , and a wire diameter d of 6 mm in the equation below [10].

$$S_{ut} = \frac{A}{d^m} = \frac{2211\ \text{MPa}\ \text{mm}^{0.145}}{(6\ \text{mm})^{0.145}} = 1705\ \text{MPa} \quad (67)$$

Then, for a music wire, the normal yield strength S_y can be obtained with the following equation [10].

$$S_y = 0.78S_{ut} = 0.78(1705\ \text{MPa}) = 1330\ \text{MPa} \quad (68)$$

4.4.5 Free-Body Diagram

The analysis presented below covers the procedure followed to obtain the spring constant of the two torsion springs mounted on the hip shaft assembly. One of the two torsion spring is right-handed and the free-body diagram is presented on Figure 27. The other spring is left-handed and is simply a mirrored version of the right-handed one.

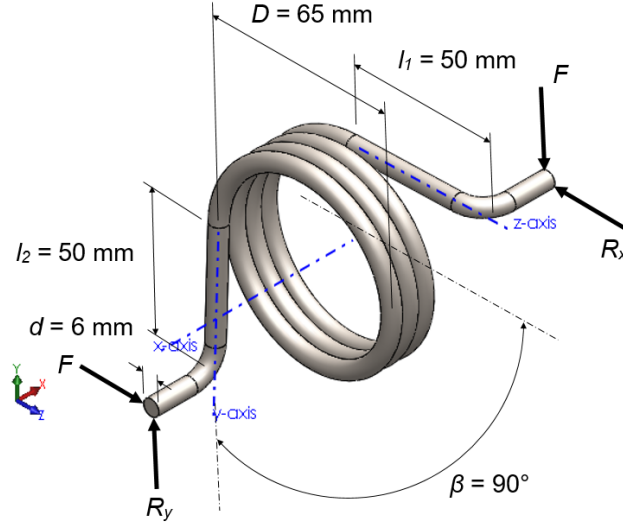


Figure 27: Hip right-handed torsion spring FBD

4.4.6 Stress Analysis

First, the maximum and minimum torque generated by the spring can be expressed as follows.

$$M_{max \text{ hip spring}} \leq k_{min} \theta_{thigh \ max} \quad M_{min \ \text{hip spring}} \leq k_{min} \theta_{thigh \ min} \quad (69)$$

Where k_{min} is the minimal spring constant necessary to reduce the harmonic drive torque below its backdrivable torque. Then, subtracting the second equation from the first isolating k_{min} produces:

$$k_{min} \geq \frac{M_{max \ \text{hip spring}} - M_{min \ \text{hip spring}}}{k \theta_{thigh \ max} - k \theta_{thigh \ min}} = \frac{18.98 \ \text{Nm} - 10.79 \ \text{Nm}}{25^\circ \frac{\pi}{180^\circ}} = 18.76 \ \text{Nm} \quad (70)$$

This signifies that the spring should be designed in such a way that $k_{min} \geq 18.76 \ \text{Nm}$. Now, to obtain the minimum and maximum spring deflections:

$$\theta_{thigh \ max} \geq \frac{M_{max \ \text{hip spring}}}{k_{min}} = \frac{18.98 \ \text{Nm}}{18.76 \ \text{Nm}} = 1.01 \ \text{rad} \frac{180^\circ}{\pi} = 57.96^\circ \quad (71)$$

$$\theta_{thigh \ min} \geq \frac{M_{min \ \text{hip spring}}}{k_{min}} = \frac{10.79 \ \text{Nm}}{18.76 \ \text{Nm}} = 0.58 \ \text{rad} \frac{180^\circ}{\pi} = 32.96^\circ \quad (72)$$

The next steps consisted of finding the spring specifications that would not only provide a valid spring constant but also limit the bending stress to the calculated yield stress. This process was done by trial and error for this report, but it will be part of the parameterization as explained in the Parameterization section.

First, based on the free angle β of the spring, a linear function was quickly obtained to compute the number of partial turns N_p .

$$N_p = -\frac{1}{360^\circ}\beta + 1 = -\frac{90^\circ}{360^\circ} + 1 = 0.25 \text{ turn} \quad (73)$$

Then, the number of body turns N_b and number of active turns N_a can be obtained. Equations 74 to 85 came from Shigley's textbook [10].

$$N_b = N_f + N_p = 3 \text{ turns} + 0.25 \text{ turn} = 3.25 \text{ turns} \quad (74)$$

$$N_a = N_b + \frac{l_1 + l_2}{3\pi D} = 3.25 \text{ turns} + \frac{50 \text{ mm} + 50 \text{ mm}}{3\pi(65 \text{ mm})} = 3.41 \text{ turns} \quad (75)$$

The shaft analysis from Section 4.5 required the length occupied by the spring over the shaft. This length can be approximated as follows by using the wire diameter d as a pitch value, and by not taking into consideration the length of the arms.

$$L_{spring} \simeq N_a d = (3.41 \text{ turns})(6 \text{ mm/turn}) = 20.48 \text{ mm} \quad (76)$$

Then, to obtain the spring constant k in torque per radian:

$$k = \frac{M}{\theta_t} = \frac{d^4 E}{64 D N_a} = \frac{(6 \text{ mm})^4 207 \times 10^3 \text{ MPa}}{64(65 \text{ mm})(3.41 \text{ turns})} = 18.89 \times 10^3 \text{ Nmm/rad} \quad (77)$$

The minimal value for k_{min} can be compared with computed value for k based of the dimensions of the spring.

$$k = 18.89 \text{ Nm/rad} > 18.76 \text{ Nm/rad} = k_{min} \quad (78)$$

Now, to verify that the spring's inner coil diameter does not interfere with the spacer, the maximum bending moment was obtained with a maximum deflection $\theta_{max} = 58^\circ$.

$$M_{max} = k(\theta_{max} - \theta) = (18.89 \times 10^3 \text{ Nmm/rad})(58^\circ \frac{\pi}{180^\circ}) = 19.13 \times 10^3 \text{ Nmm} \quad (79)$$

Then, the angular deflection of the coil body in number of turns θ'_c and the final coil diameter D' as well as the final inner diameter of the coil D'_i can be obtained as follows.

$$\theta'_c = \frac{10.8 M D N_b}{d^4 E} = \frac{10.8(19.13 \times 10^3 \text{ Nmm})(65 \text{ mm})(3.25 \text{ turns})}{(6 \text{ mm})^4 207 \times 10^3 \text{ MPa}} = 0.163 \text{ turn} \quad (80)$$

$$D' = \frac{N_b D}{N_b + \theta'_c} = \frac{(3.25 \text{ turns})(65 \text{ mm})}{3.25 \text{ turns} + 0.163 \text{ turn}} = 61.90 \text{ mm} \quad (81)$$

$$D'_i = D' - d = 61.90 \text{ mm} - 6 \text{ mm} = 55.90 \text{ mm} \quad (82)$$

For this case, the minimum inner coil diameter is well above the spacer diameter $D_{hips \text{ spacer}} = 33.5 \text{ mm}$ and therefore, both components should not interfere. The last set of steps consist of obtaining the safety factor for the spring with the previous dimensions used. First, the stress-correction factor K_i was obtained before computing the bending stress σ . Here, C is the spring index which correlates to the ratio D/d for torsion springs. Here, $C = 65 \text{ mm}/6 \text{ mm} = 10.83$ which is acceptable since it is recommended that $4 \leq C \leq 12$ [10].

$$K_i = \frac{4C^2 - C - 1}{4C(C - 1)} = \frac{4(10.83)^2 - 10.83 - 1}{4(10.83)(10.83 - 1)} = 1.07 \quad (83)$$

$$\sigma = K_i \frac{32M}{\pi d^3} = 1.07 \frac{32(19.13 \times 10^3 \text{ Nmm})}{\pi(6 \text{ mm})^3} = 968.59 \text{ MPa} \quad (84)$$

$$SF = \frac{S_y}{\sigma} = \frac{1330 \text{ MPa}}{968.59 \text{ MPa}} = 1.37 \quad (85)$$

4.4.7 Critical Review

The dimensions of the springs obtained above are reasonable considering that the spring index C of 10.83 is between the recommended range $4 \leq C \leq 12$ [10]. Also, for a music wire, the wire diameter can go up to 6.5 mm according to Shigley's textbook [10]. However, trying to find a spring with such dimensions on various manufacturers' catalogues did not yield satisfying results.

The other set of torsion springs for the knee drive that were not presented in the stress analysis above were also computed. Here are the main results: free angle $\beta = 90^\circ$, wire diameter $d = 5 \text{ mm}$, coil diameter $D = 40 \text{ mm}$, arm length $l = 25 \text{ mm}$, number of body turns $N_b = 3.25$ turns. The spring constant k was found to be 14940 Nmm/rad, the maximum deflection θ_{max} chosen as 88° which yields a maximum torque M_{max} of 26672.75 Nmm while respecting a safety factor of 1.16. Now, two graphs comparing the resulting torques that the harmonic drives have to hold before and after the addition of the spring are presented on Figure 28

One assumption that deserves to be reviewed is the backdriving torque values for the harmonic drives. In fact, multiple sources state contradicting statements. Therefore, it may be safer to limit the harmonic drives' static torques to values approaching 0 Nm by setting the spring constant k to obtain approximately the same moment as the maximum static torque.

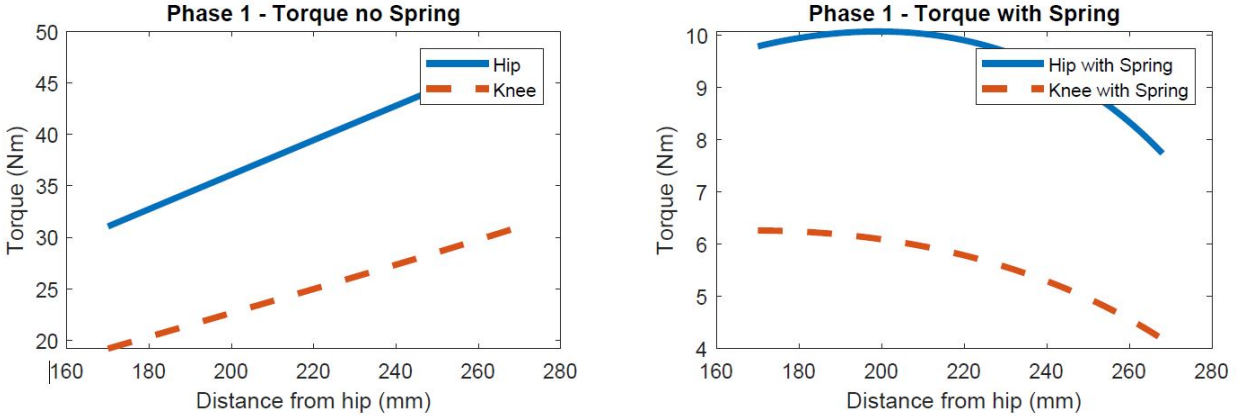


Figure 28: Torques before (left) and after (right) the addition of torsion springs on the limbs for the worst phase

4.4.8 Parameterization

One way to parameterize this portion of the analysis could be to input the maximum and minimum torques based on the worst case static analysis along with the spacer diameters and the angular span of both limbs. The backdriving torque of both harmonic drives should be proportionate to the size of the harmonic drive and a safety factor should be set constant. Then, the spring dimensions can be optimized to obtain the smallest springs possible while respecting the spacer diameters, the safety factor, and the required torque.

4.5 Shaft Analysis

4.5.1 Inputs and Outputs

There are three shafts in each robot leg: the hip control shaft and the knee control shaft, which are both inside the chassis and attached to a motor, and the exterior knee shaft, found outside the chassis. The shafts do not rotate continuously at high speeds; instead they oscillate and move at slow speeds. For this reason, a simple static force analysis was performed. The inputs include all the forces and torques applied to each shaft and the lengths of the portions of the shaft. The desired output is the diameter.

4.5.2 Constants and Parameters

A minimum safety factor of 2.5 was chosen, as the selected material is well known but some of the applied forces, namely the force applied from the leg member onto the shaft, could vary due to the terrain [14]. For example, vandalism, obstacles or shortcomings with the control system could cause slight impact forces to be felt at the shaft.

Stress concentration factors were selected for the steps and keyways on the shafts. They were chosen as per the figures provided in Juvinal [14]. For keyways, only fatigue stress concentration factors were provided, thus the static values were deduced from those values using the relations provided in the textbook.

There are many parameters affecting the shaft analysis such as its length. For the analysis, the total length was divided in multiple parts, such as the bearing thickness, pulley or hip plate thickness, torsion spring width and flange collar width. The other parameters are the various forces and torques applied to the shafts, which have been found in the modelling and in the analysis of the belt and pulleys in section 4.3.

4.5.3 Assumptions and Simplifications

The analysis of the shafts is done at the worst case scenario, where the legs are fully extended (meaning higher torques and moments). It is also assumed that we are looking at the moment where the leg is lifting itself off the ground, meaning that the shafts experience forces from the ground and also the maximum applied torque from the motor as it is fighting the spring torque.

It was assumed that forces are applied at the middle of shaft components (for example, forces at bearings or pulleys). Another simplification that was made was to apply the axial force (created by friction forces at the foot) everywhere in the shaft, as it could be applied in either direction and load any part of the shaft. It was also assumed that the force applied by the leg onto the shafts is vertical to the ground, as the largest component of the normal force is likely to be in that direction. Finally, as there are many larger forces acting on the shafts, and these are computed for worse case scenarios, the weight of the shaft assembly itself was neglected when calculating bearing forces.

4.5.4 Material Selection

The selected material for all three shafts is marine grade stainless steel 316, as it is a common material used in marine applications and is often used for pump shafts. The minimum yield

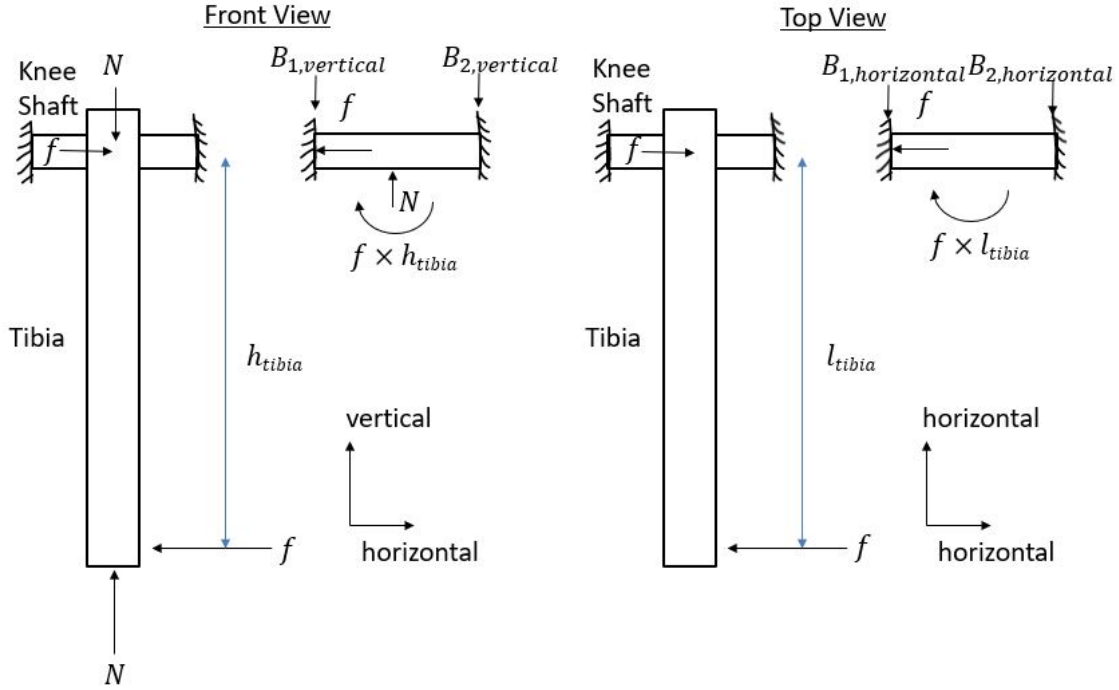


Figure 29: Exterior knee shaft - Friction moments

strength of this material is of about 205 MPa, thus we shall use a value of 240 MPa for a shaft with a cold finish [15].

4.5.5 Stress Analysis and Free-Body Diagrams

The following sections show the equations used for the static stress analysis of each shaft. A sample calculation is also provided after. It was decided not to perform a deflection and slope analysis as the shafts will be quite short and will not deflect much. A fatigue analysis was considered, however the robot will be moving quite slowly and will not have long operating hours. Thus, the complexity of this analysis was deemed unnecessary for this application.

4.5.5.1 Exterior Knee Shaft Before presenting the free-body diagram for this shaft, some of the applied forces must be looked at more closely. As a worst case scenario, the calculations were made for when the robot was on a slope, thus creating additional moments on the shaft due to the added friction force. Figure 29 shows a simplified diagram of the tibia, and how moments in two planes are created at the knee shaft.

where f is the friction force at the foot, l_{tibia} is the horizontal extended length of the tibia (parallel to the ground) and h_{tibia} is the vertical height of the tibia (perpendicular to

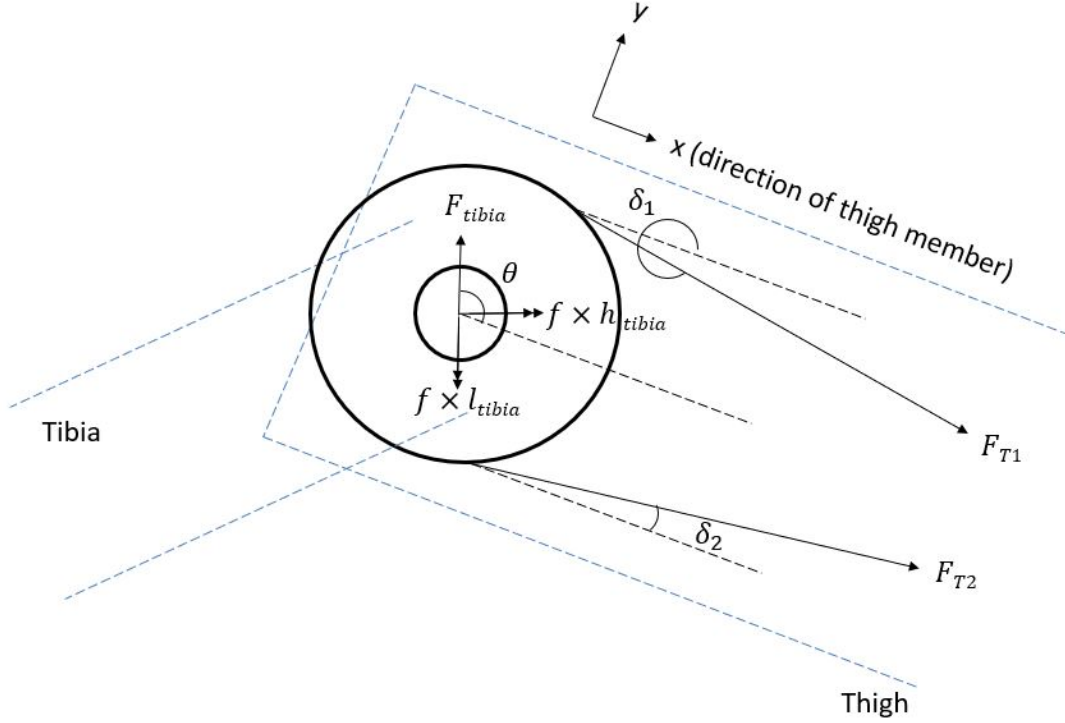


Figure 30: Exterior knee shaft - Side section view of pulley (bearing reaction forces not visible in view

the ground).

A side view of the pulley is shown in Figure 30. It shows the various angles related to the leg position and the belt. The coordinate system is chosen to have the x direction in line with the thigh. As the pulleys were chosen to be the same size (no reduction), the angles of the belt δ_1 and δ_2 are both zero. The angle θ is equal to the thigh angle plus 90 degrees.

F_{T1} and F_{T2} are the belt tension forces. The value F_{tibia} (force of leg on shaft) is found using a force balance on the tibia, as shown in Figure 31 and Equation 86, where N is the normal force on the foot and $m_{foot}g$ is the weight of the tibia lumped at the foot (as a worst case scenario for leg movement).

$$\sum F_{vertical} = 0 : F_{tibia} = N - m_{foot}g \quad (86)$$

Finally, the exterior knee shaft succumbs to the forces shown in the free-body diagrams in Figures 32 and 33.

where B_{yi} and B_{xi} are the forces at the bearings, F_{axial} is the axial force in the shaft which is equal to the friction force at the foot f , $t_{bearing}$ is the width of the bearing, L is a

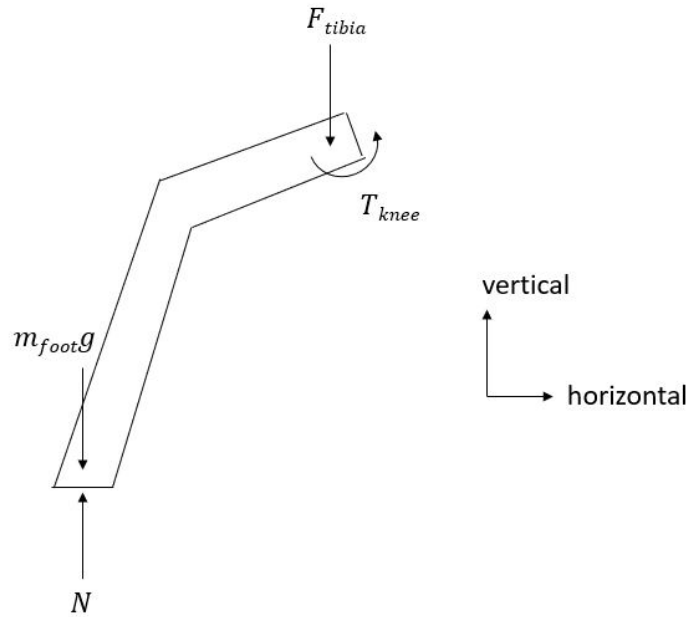


Figure 31: Exterior knee shaft - Tibia free-body diagram

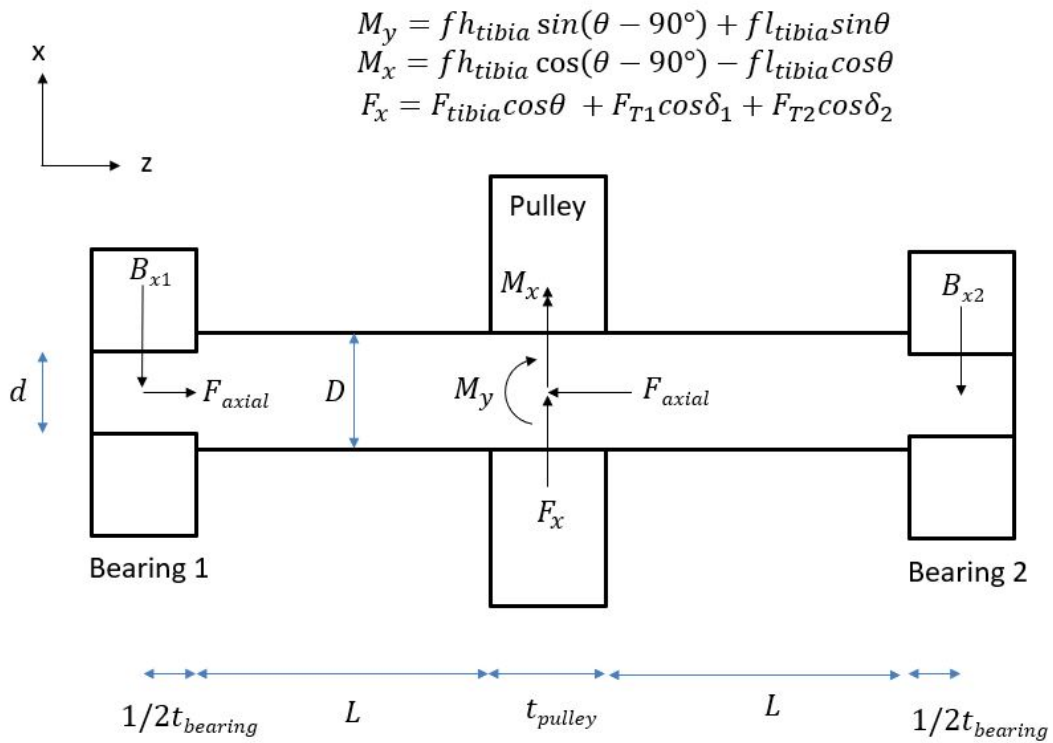


Figure 32: Exterior knee shaft - Free-body diagram in X-Z plane

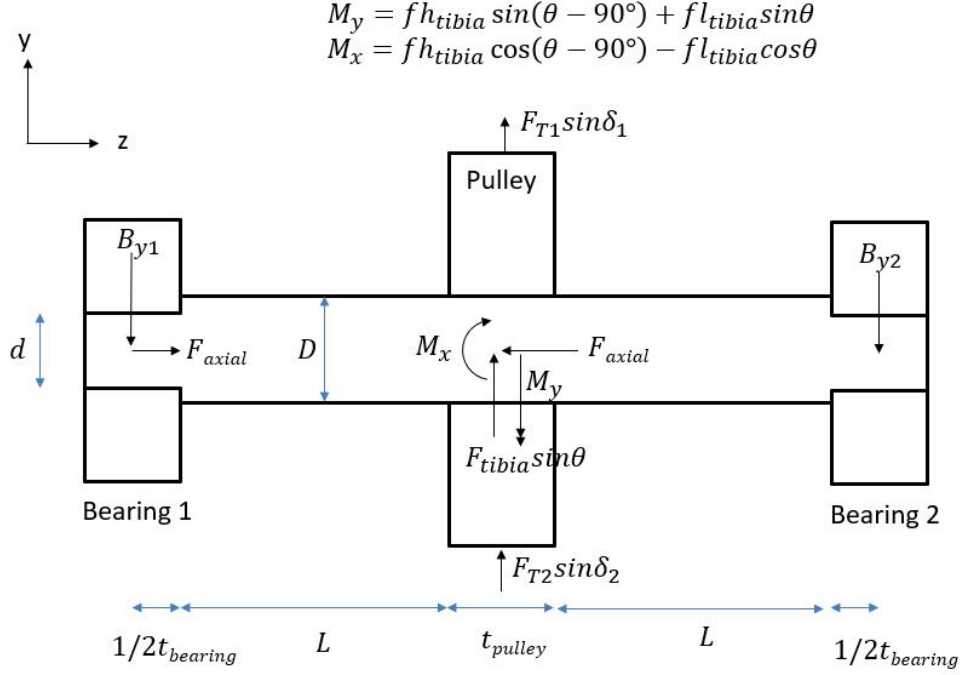


Figure 33: Exterior knee shaft - Free-body diagram in Y-Z plane

length determined by the width of the thigh and thus the spacing of the knee plates, t_{pulley} is the thickness of the pulley and d and D are the diameters of the shaft.

To start the analysis, the resulting forces applied at the bearings were calculated using sum of forces and moments.

$$\sum M_{x@Bearing1} = 0 : B_{y2} = \frac{(1/2t_{bearing} + L + 1/2t_{pulley})(F_{tibia} \sin \theta + F_{t1} \sin \delta_1 + F_{t2} \sin \delta_2) - fh_{tibia} \cos(\theta - 90^\circ) + fl_{tibia} \cos \theta}{t_{bearing} + 2L + t_{pulley}} \quad (87)$$

$$\sum M_{y@Bearing1} = 0 : B_{x2} = \frac{(1/2t_{bearing} + L + 1/2t_{pulley})(F_{tibia} \cos \theta + F_{t1} \cos \delta_1 + F_{t2} \cos \delta_2) - fh_{tibia} \sin(\theta - 90^\circ) - fl_{tibia} \sin \theta}{t_{bearing} + 2L + t_{pulley}} \quad (88)$$

$$\sum F_x = 0 : B_{x1} = F_{tibia} \cos \theta + F_{t1} \cos \delta_1 + F_{t2} \cos \delta_2 - B_{x2} \quad (89)$$

$$\sum F_y = 0 : B_{y1} = F_{tibia} \sin \theta + F_{t1} \sin \delta_1 + F_{t2} \sin \delta_2 - B_{y2} \quad (90)$$

These values were used to create shear force and bending moment diagrams over the length of the shaft. These are shown in Figure 34.

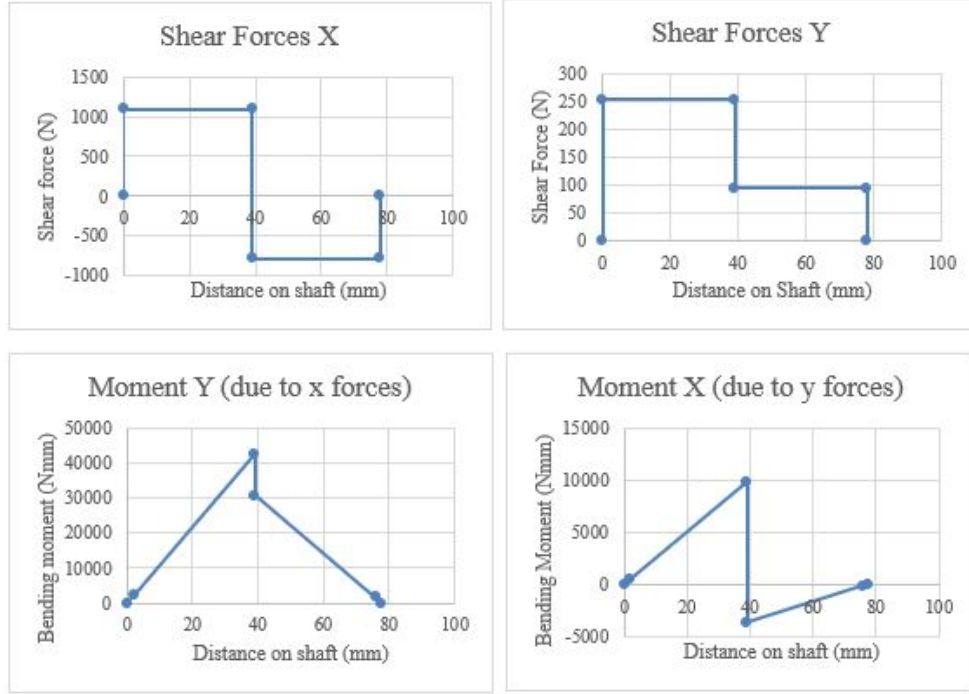


Figure 34: Exterior knee shaft - Shear force and bending moment diagrams

Critical points on the shaft were then selected and analyzed for strength. These critical points are the steps in the shaft and the maximum bending moment point located at the pulley. The forces and moments acting in perpendicular directions were added together using the following formula to find a resultant.

$$F_{total} = \sqrt{F_x^2 + F_y^2} \quad M_{total} = \sqrt{M_x^2 + M_y^2} \quad (91)$$

The bending stress, transverse shear stress and axial stress were then found using the following formulas [14]. In this case, no torsion is applied on the shaft since the pulley is not fixed to the shaft. It is the reason why transverse shear stresses are taken into account.

$$\tau_{transverse\ shear} = \frac{4}{3} \left(\frac{k_t F_{total}}{\frac{\pi d^2}{4}} \right) \quad (92)$$

$$\sigma_{bending} = \frac{32 k_t M_{total}}{\pi d^3} \quad (93)$$

$$\sigma_{axial} = \frac{k_t F_{axial}}{\frac{\pi d^2}{4}} \quad (94)$$

where k_t are the stress concentration factors for the stress mode being evaluated, at the

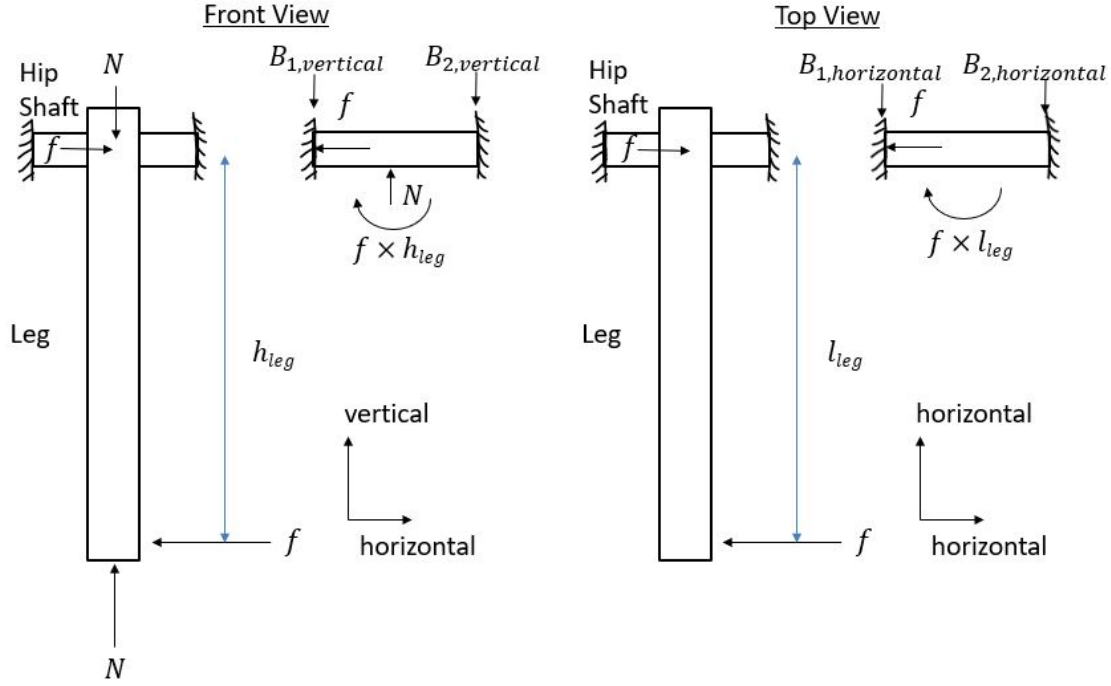


Figure 35: Hip control shaft - Friction moments

observed point on the shaft. These values were obtained from the Juvinall textbook [14]. The value for transverse shear was estimated by taking the value for torsion shear.

The equivalent stress was then calculated using the Von Mises formula [14], and this was compared to the yield strength of the chosen material to ensure the safety factor is met:

$$\sigma_{equivalent} = \sqrt{(\sigma_{bending} + \sigma_{axial})^2 + 3\tau_{transverse\ shear}^2} \quad (95)$$

$$SF = \frac{S_y}{\sigma_{equivalent}} \quad (96)$$

where $\sigma_{equivalent}$ is the equivalent Von Mises stress, S_y is the yield stress of the material and SF is the safety factor.

4.5.5.2 Hip Control Shaft The friction force created by walking on a slope would cause additional moments to be created on this shaft as well. Figure 35 shows a simplified diagram of the full leg, and how moments in two planes are created at the hip control shaft.

where f is the friction force at the foot, l_{leg} is the horizontal extended length of the leg (parallel to the ground) and h_{leg} is the vertical height of the leg (perpendicular to the ground).

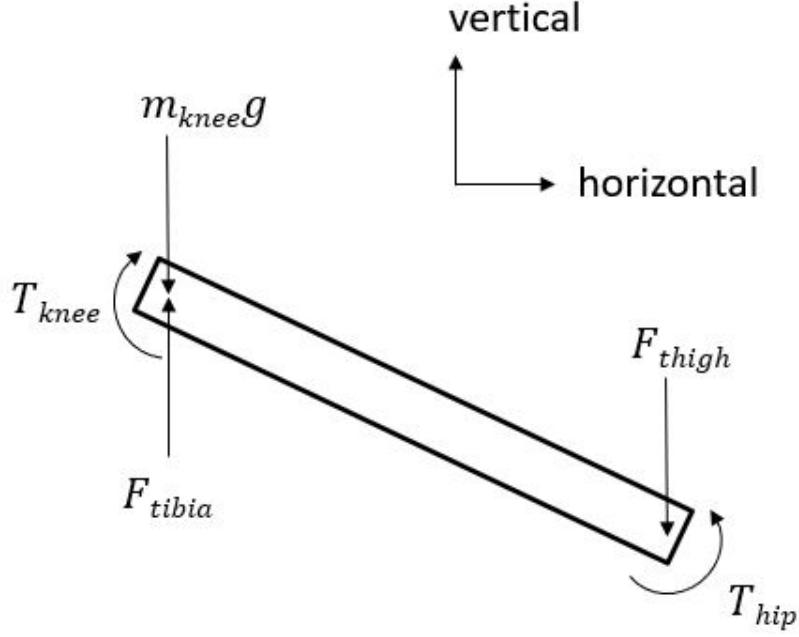


Figure 36: Hip control shaft - Thigh free-body diagram

The value of the leg force acting on the hip shaft, F_{thigh} , is found using a force balance on the thigh, as shown in Figure 36 and Equation 97, where m_{knee} is the weight of the thigh lumped at the knee (as a worst case scenario for leg movement).

$$\sum F_{vertical} = 0 : F_{thigh} = F_{tibia} - m_{knee}g \quad (97)$$

Thus, the hip control shaft succumbs to the forces shown in the free-body diagrams in Figures 37 and 38. The coordinates were chosen as x being parallel to the ground and y being vertical to the ground.

where the variables remain similar to the exterior knee shaft, however t_{hip} is the torque provided by the motor at the hip, L_1 is the width of the torsion spring which is positioned at that location on the shaft, L_2 is a length determined by the spacing of the hip plates, L_3 is the distance between bearing 2 and the middle of the flange collar attached to the harmonic drive and t_{plate} is the width of the hip plates.

Similarly to the exterior knee shaft, sum of forces and moments is used to find equations for the forces at the bearings.

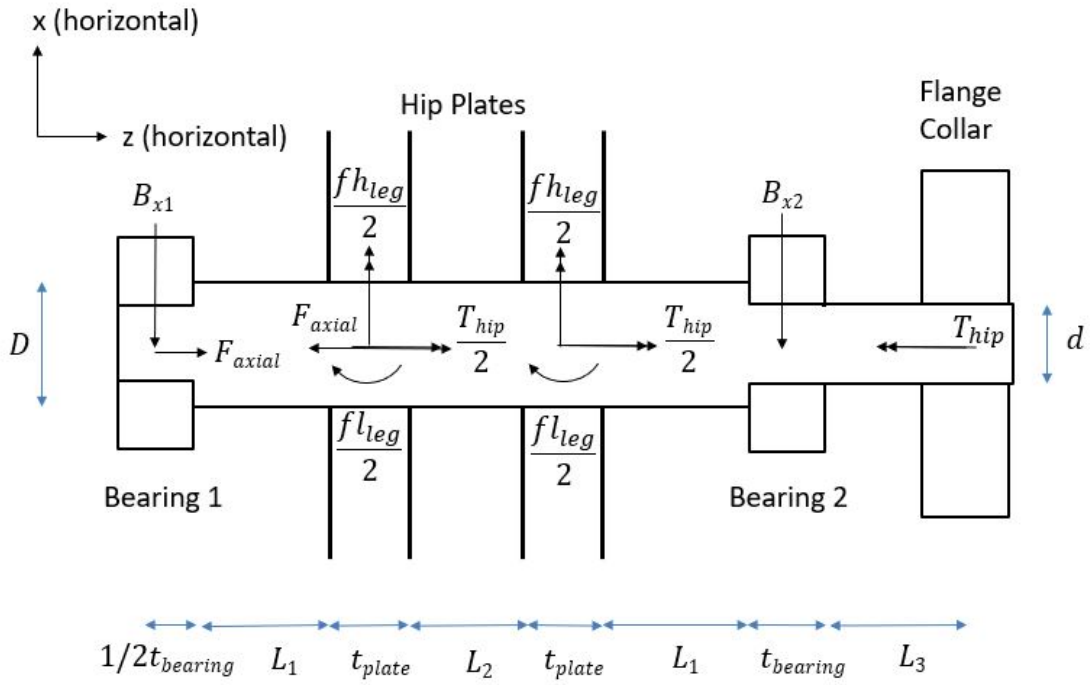


Figure 37: Hip control shaft - Free-body diagram in X-Z plane

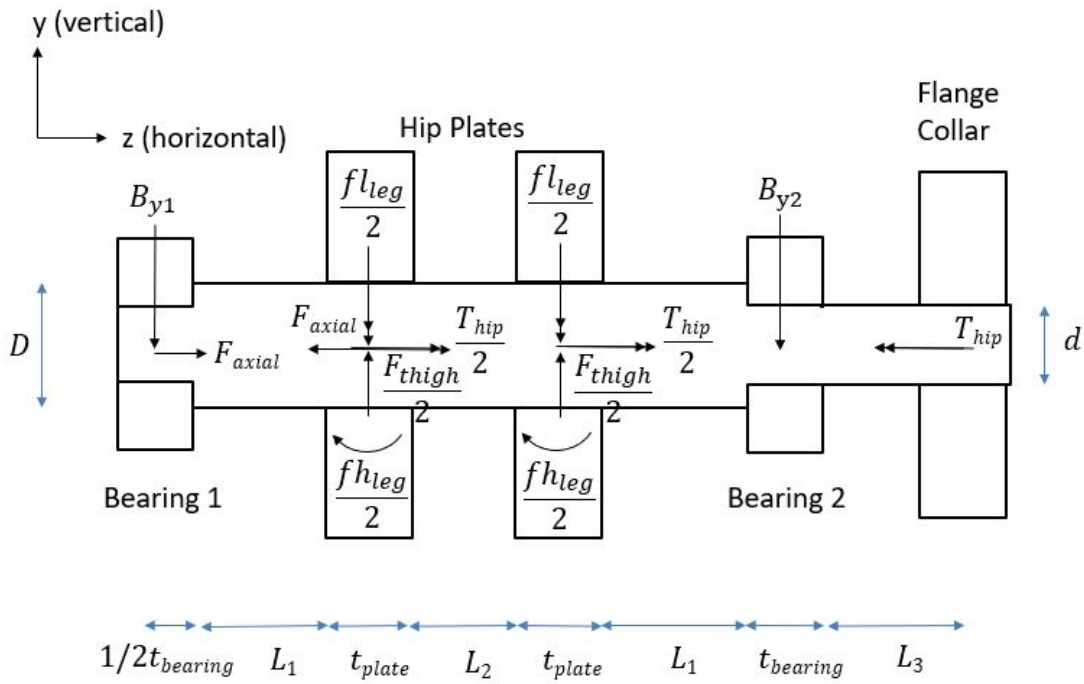


Figure 38: Hip control shaft - Free-body diagram in Y-Z plane

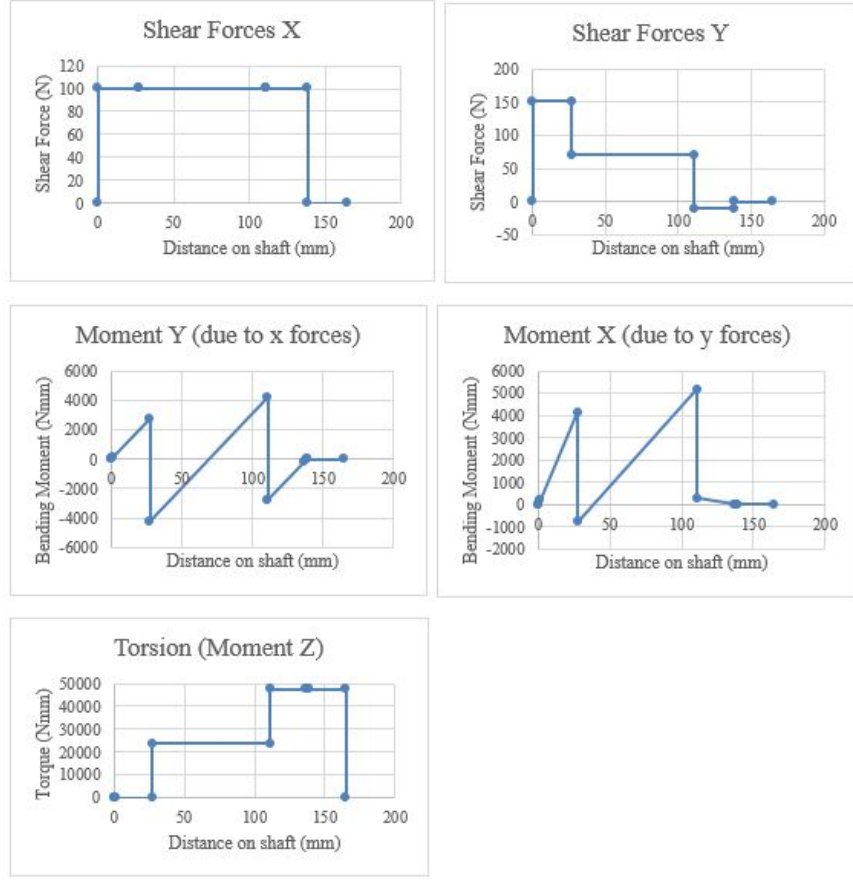


Figure 39: Hip control shaft - Shear force, bending moment and torque diagrams

$$\sum M_{x@bearing1} = 0 : B_{y2} = \frac{F_{thigh}(t_{bearing} + 2L_1 + 2t_{plate} + L_2) - fh_{leg}}{t_{bearing} + 2L_1 + 2t_{plate} + L_2} \quad (98)$$

$$\sum M_{y@bearing1} = 0 : B_{x2} = -\frac{fl_{leg}}{t_{bearing} + 2L_1 + 2t_{plate} + L_2} \quad (99)$$

$$\sum F_x = 0 : B_{x1} = -B_{x2} \quad (100)$$

$$\sum F_y = 0 : B_{y1} = F_{thigh} - B_{y2} \quad (101)$$

The shear force and bending moment diagram were then created and are shown in Figure 39. This shaft also encounters torsion as the hip plates are fixed on the shaft by keys. The torsion diagram is also shown in Figure 39. As there are two hip plates taking the torque applied by the motor, it was assumed that each took about half the torque. This should not affect the calculation of stress at the critical point, as the full torque is still used for the stress at the first plate, and will determine the diameter.

The critical points on the shaft are the two steps, as well as the keyways at both hip plates and the flanged collar (for the harmonic drive). The strength analysis was done using the same equations as for the exterior knee shaft, with the exception of the following additional torsion stress equation [14].

$$\tau_{torsion} = \frac{16k_t T}{\pi d^3} \quad (102)$$

where k_t is the stress concentration factor specific to torsion.

In this situation, the torsional shear stress is much larger than the transverse shear stress and thus the transverse shear stress was neglected. This decision is founded in the fact that the maximum torsion shear stress is at the shaft surface whereas the maximum transverse shear stress is in the middle of the shaft. They are not applied at the same point and are thus not to be considered as a summation. The Von Mises equation becomes:

$$\sigma_{equivalent} = \sqrt{(\sigma_{bending} + \sigma_{axial})^2 + 3\tau_{torsion}^2} \quad (103)$$

4.5.5.3 Knee Control Shaft This shaft does not take any force or moment from the leg. Thus, the knee control shaft succumbs to the forces shown in the free-body diagrams in Figures 40 and 41. The coordinates are the same as for the exterior knee shaft, with x in the direction of the thigh member. In this case, the angle of the belt tension forces is the same as for the exterior knee shaft, with an added 180 degrees (as they are in the opposite direction). Those forces are shown in the positive x or y direction, as they depend on the angles.

where variables are similar to the other shafts, with T_{knee} the torque provided by the motor, L_1 is the width of the torsion spring and L_3 is the distance from the bearing 2 to the middle of the flange collar.

Similarly to the other shafts, sum of forces and moments is used to find equations for the forces at the bearings.

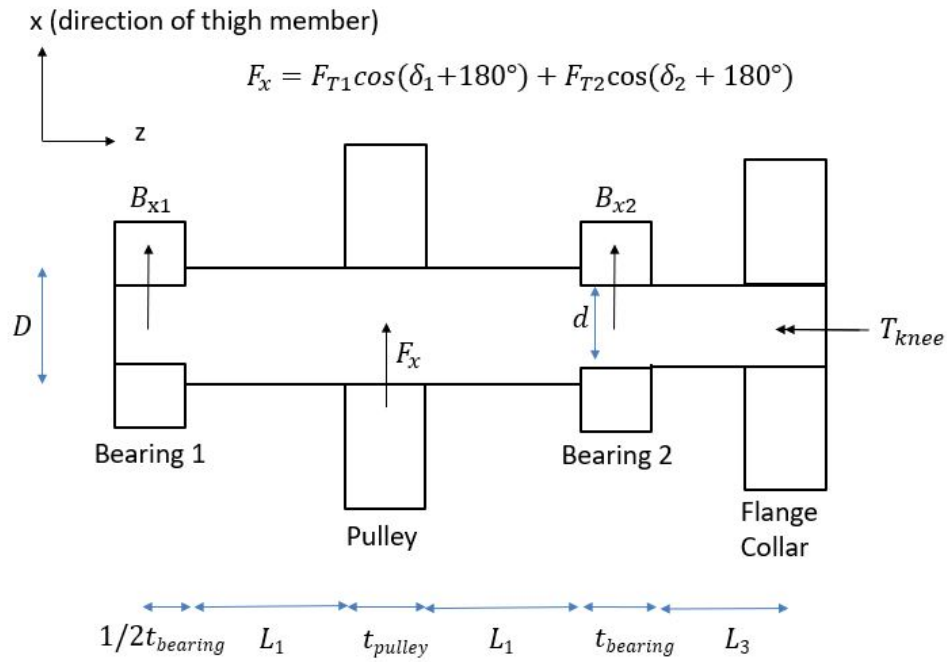


Figure 40: Knee control shaft - Free-body diagram in X-Z plane

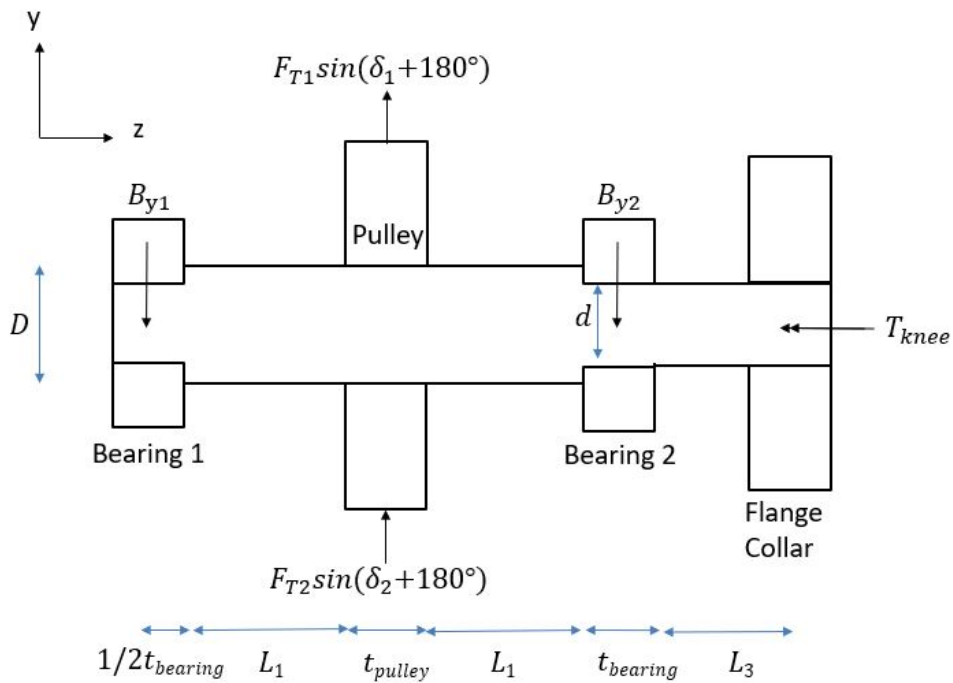


Figure 41: Knee control shaft - Free-body diagram in Y-Z plane

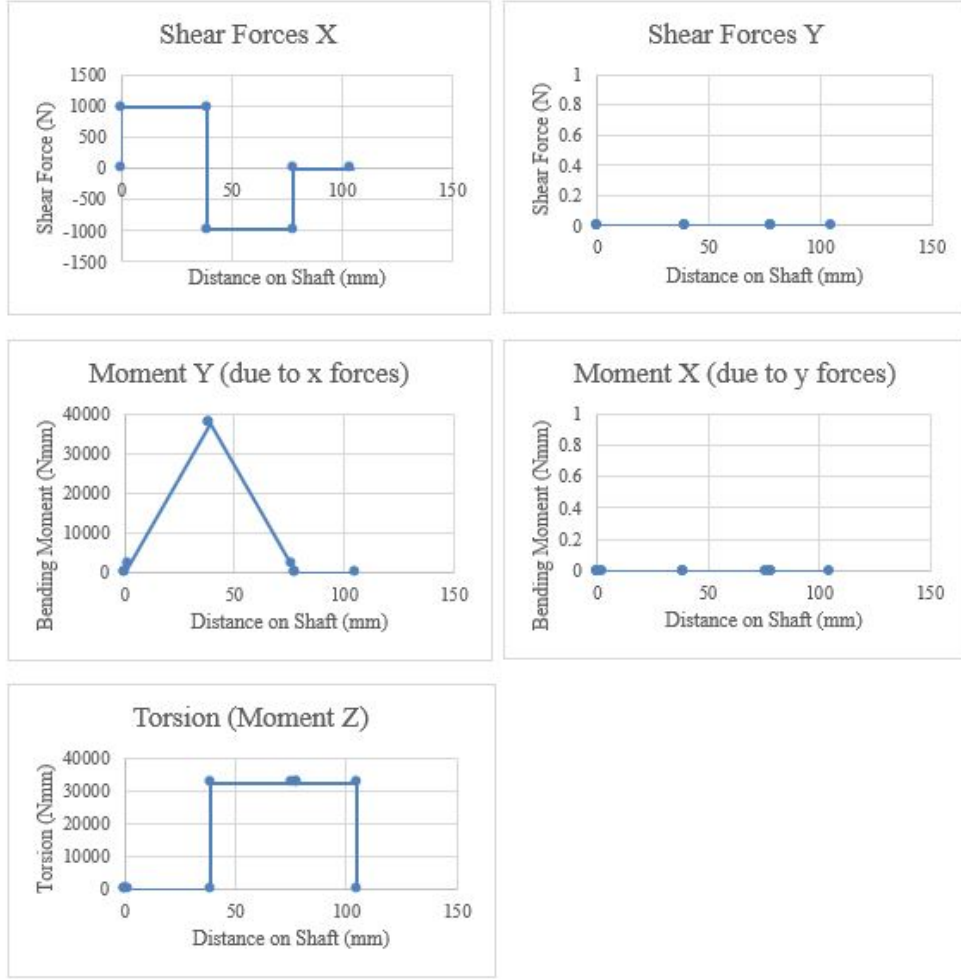


Figure 42: Knee control shaft - Shear force, bending moment and torque diagrams

$$\sum M_{x@bearing1} = 0 : B_{y2} = \frac{(1/2t_{bearing} + L_1 + 1/2t_{pulley})(F_{T1} \sin(\delta_1 + 180) + F_{T2} \sin(\delta_2 + 180))}{(t_{bearing} + 2L_1 + t_{pulley})} \quad (104)$$

$$\sum M_{y@bearing1} = 0 : B_{x2} = -\frac{(1/2t_{bearing} + L_1 + 1/2t_{pulley})(F_{T1} \cos(\delta_1 + 180) + F_{T2} \cos(\delta_2 + 180))}{(t_{bearing} + 2L_1 + t_{pulley})} \quad (105)$$

$$\sum F_x = 0 : B_{x1} = -F_{T1} \cos(\delta_1 + 180) - F_{T2} \cos(\delta_2 + 180) - B_{x2} \quad (106)$$

$$\sum F_y = 0 : B_{y1} = F_{T1} \sin(\delta_1 + 180) + F_{T2} \sin(\delta_2 + 180) - B_{y2} \quad (107)$$

The shear force, bending moment and torque diagrams were then created and are shown in Figure 42.

The critical points on the shaft are the two steps, as well as the keyway at the pulley and the flanged collar (for the harmonic drive). The strength analysis was done using the previous equations. Once again, as torsion is applied to the shaft, the transverse shear is not used in the analysis.

4.5.5.4 Example Calculation The following is a calculation to find the required shaft diameter of the hip control shaft based on the applied forces and length of the shaft. This shaft is the most critical as it succumbs to the largest torque.

First, we must find the forces acting on the bearings using Equations 98 to 101. We first find the value of $F_{thigh} = 161.6N$ using a combination of Equation 86 and 97 with the values $m_{foot} = 0.25kg$, $m_{knee} = 0.50kg$ and $N = 169N$ (maximum expected normal force, as calculated in the slope analysis Section 3.1). The friction force at the foot from the slope analysis is $f = 51.7N$ and from the leg lengths and angles we get $h_{leg} = 190.0mm$ and $l_{leg} = 268.6mm$. The other values are a bearing thickness (length) $t_{bearing} = 3mm$, a hip plate thickness of $t_{plate} = 10mm$, $L_1 = 20.8mm$ is the width of the torsion springs at the hip, $L_2 = 75.5mm$ is determined by the required length of the knee control shaft and $L_3 = 25mm$ to give space for the flange collar. Now we get the forces on the bearings:

$$\sum M_{x@Bearing1} = 0 : B_{y2} = \frac{\frac{161.6N}{2}(3mm + 2(20.8mm) + 2(10mm) + 75.5mm) - (51.7N)(190.0mm)}{3mm + 2(20.8mm) + 2(10mm) + 75.5mm} = 9.9N \quad (108)$$

$$\sum M_{y@Bearing1} = 0 : B_{x2} = -\frac{51.7N(268.6mm)}{3mm + 2(20.8mm) + 2(10mm) + 75.5mm} = -100.3N \quad (109)$$

$$\sum F_x = 0 : B_{x1} = -B_{x2} = 100.3N \quad (110)$$

$$\sum F_y = 0 : B_{y1} = 161.6N - (9.9N) = 151.8N \quad (111)$$

Note that some values are negative due to the moments created by the friction on the leg. The signs would be reversed if the friction was in the opposite direction.

The most critical point on the shaft is the step next to bearing 2, thus this is the point analysed here. From the creation of the force diagrams shown in Figure 39 we get that at its location of 136.9 mm from the middle of bearing 1, the bending moments are $M_x = 14.8N$ and $M_y = -150.4N$. The torsion is equal to $T = 47440Nmm$ and the axial force is the friction force $F_{axial} = f = 51.7N$. We use Equation 91 to get the total bending moment of $M = 151.2Nmm$. Then Equations 102, 93 and 94 can be used to find the stresses at that point. Using the Juvinall textbook [14], the concentration factors are found to be 2.0 in

bending, 2.1 in axial stress and 1.7 in torsion. A value of small diameter of $d = 19.5mm$ is assumed for now, and values of stress are verified later using the safety factor.

$$\tau_{torsion} = \frac{16(1.7)(47440Nmm)}{\pi(19.5mm)^3} = 55.4MPa \quad (112)$$

$$\sigma_{bending} = \frac{32(2.0)(151.2Nmm)}{\pi(19.5mm)^3} = 0.42MPa \quad (113)$$

$$\sigma_{axial} = \frac{2.1(51.7N)}{\frac{\pi(19.5mm)^2}{4}} = 0.36MPa \quad (114)$$

Then the Von Mises Equation 103 is used to get the equivalent stress, and the safety factor is verified. The selected diameter gives the required safety factor and is therefore considered adequate.

$$\sigma_{equivalent} = \sqrt{(0.42MPa + 0.36MPa)^2 + 3(55.4MPa)^2} = 95.9MPa \quad (115)$$

$$SF = \frac{240MPa}{95.9MPa} = 2.5 \quad (116)$$

Table 2 summarizes the bearing forces found for each shaft as well as the required diameters for each shaft.

Table 2: Calculated shaft diameters and forces at bearings

Values	Exterior Knee Shaft	Hip Control Shaft	Knee Control Shaft
B_{x1} [N]	1095.4	100.3	967.2
B_{x2} [N]	790	-100.3	967.2
B_{y1} [N]	252.6	151.8	0
B_{y2} [N]	-93.5	9.9	0
d [mm]	13	19.5	17.5
D [mm]	17	23.5	21.5

4.5.6 Critical Review

The diameters found in Table 2 are realistic for the selected material and relatively small torques and bending moments. The exterior knee shaft has the smallest values as it does not succumb to torsion. As the hip control shaft succumbs to the largest torsion, it naturally has the biggest diameters. This shaft however has the smallest bearing forces as it does not have to resist to the belt tensions like the other two shafts.

4.5.7 Parameterization

The goal of the shaft parameterization will be to take inputs such as shaft lengths (based on other component sizes), torques and forces and find the required shaft diameters for those loads. An estimated diameter will be chosen and increased until a diameter that meets the safety factor is found.

4.6 Keys

4.6.1 Description

This section gives information and calculations for the design of the keys on the shafts. The input is the applied torque and the output is the required length. For this analysis, the shaft diameters (found in the shaft analysis) are considered as a constant. The key cross-sectional dimensions are chosen as a function of the shaft diameter: the width is a quarter of the diameter and the height is a third of the diameter. These values were chosen to balance the shear and compression acting on the key [14]. A safety factor of at least 1.5 will be maintained, however it may be surpassed as the key length will be chosen to be the width of the part it is holding, for better stability. The key material is selected to be the same as the shaft (marine grade stainless steel 316), however it is not cold treated and a lower yield strength (the minimum value) of $S_y = 205MPa$ is chosen. This value is selected to ensure that the keys would fail before the parts (pulleys, flange collars and hip plates), as the key is easier to replace.

4.6.2 Stress Analysis and Free-Body Diagrams

The free-body diagram in Figure 43 can be used to illustrate the forces acting on the key.

Using the chosen cross-sectional ratios of the key (the width is a quarter of the diameter and the height is a third of the diameter), the following equations for the length of the key are found, as a function of the applied torque. The first is for the compressive force (crushing) acting on the key, and the second is for the shear of the key [14].

$$L_{required} = \frac{12T}{S_y d^2} \quad (117)$$

$$L_{required} = \frac{8T}{0.58S_y d^2} = \frac{13.79T}{S_y d^2} \quad (118)$$

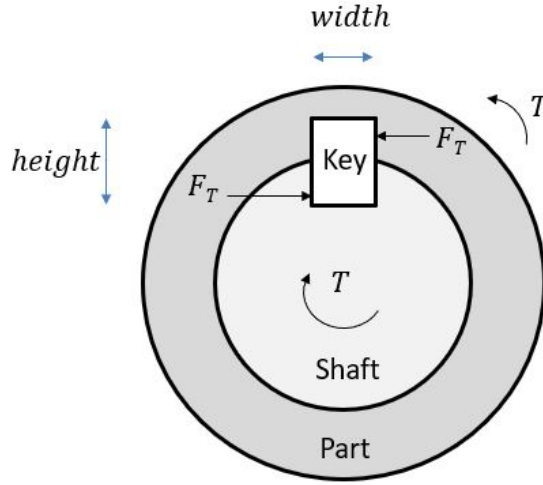


Figure 43: Keys - Free-body diagram (cross-section of shaft)

where $L_{required}$ is the required length of the key, T it the torque applied on the key, S_y is the yield strength of the key material and d is the diameter of the shaft. For the chosen geometry, the shear stress will always be slightly larger, thus Equation 118 is used. The required key length must be no larger than the part it is holding. Safety factors are calculated to ensure 1.5 is reached.

The following is an example of the key dimensions calculation for the hip plate on the hip control shaft. First, the height and width are found based on chosen diameter ratios. Then, Equation 118 is used to find the length. The applied torque is of 47440 Nmm, the shaft diameter at that point is 23.5 mm and the yield strength of the chosen material is 205 MPa.

$$height = d/3 = 23.5/3 = 7.83mm \quad (119)$$

$$width = d/4 = 23.5/4 = 5.88mm \quad (120)$$

$$L_{required} = \frac{13.79T}{S_y d^2} = \frac{13.79 \times 47440 Nmm}{205 MPa \times (23.5mm)^2} = 5.78mm \quad (121)$$

As the width of the hip plate is of 10 mm, the key length is extended to $L = 10mm$, thus we get the following safety factor:

$$SF = \frac{L}{L_{required}} = \frac{10mm}{5.78mm} = 1.73 > 1.5 \text{ Good!} \quad (122)$$

4.6.3 Critical Review

As the robot is a small application with relatively low torques, it would make sense that the size of the keys be relatively small as well. Thus, these results are representative.

4.6.4 Parameterization

This part will be parameterized by inputting the torque and shaft diameter and getting its required length. This length would then be increased to equal the width of the part it is holding, or the part itself will be made wider to ensure the key has an adequate length.

4.7 Bearings and Spacers

4.7.1 Inputs and Outputs

This section shows the analysis of the sleeve bearings (bushings) and gives specifications for the spacers on the shafts. The main input for the bearings is the shaft diameter and the radial forces at the bearings (calculated in shaft analysis). The output is the required length of the bearing. Spacers are not highly critical, but are included in this section to specify basic geometries and materials.

4.7.2 Constants and Parameters

For these analysis' the shaft diameters (found in the shaft analysis) are considered as constants. For the safety factor, the same value as the shafts (2.5) will be aimed for.

4.7.3 Assumptions and Simplifications

Friction in the sleeve bearings is neglected as its exact value was difficult to calculate and the worst case value calculated was relatively small. See the attempted calculations in Appendix B.5.

The sleeve bearings are chosen to have a constant thickness, as this does not affect their performance as per the calculations. A thickness of 2 mm was chosen based on existing sleeve bearings [16] and the fact that we will likely have very short bushings. The bearings will also have a flange to help position them in the housing and on the shafts as well as take the minor axial loads coming from the legs. As the axial loads are not very large, the size of the flange was not based on analysis and is simply based on the size of the shaft step and thickness of the spacer that will be in contact with the flange.

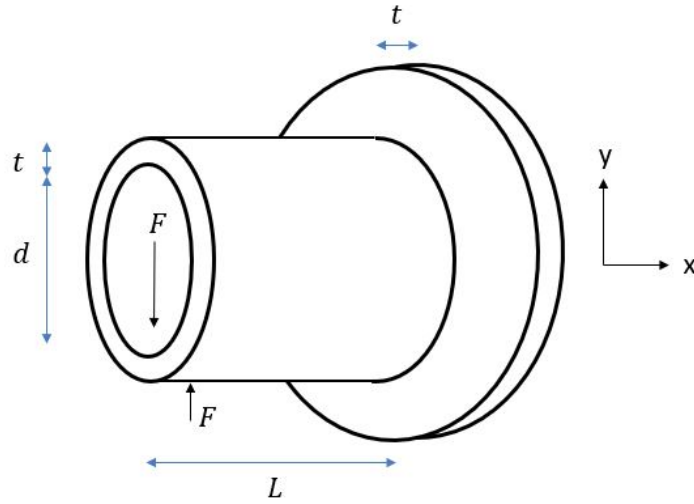


Figure 44: Sleeve Bearing - Dimensional diagram

As the spacers are not taking excessive axial loads, their thickness is chosen as 5 mm. This value is expected to be sufficient to maintain the axial position of parts, while also keeping the bushing flange at a reasonable size.

4.7.4 Material Selection

The sleeve bearings were chosen as sintered bronze bearings. The reason for this selection is that this is a common and well-known material, is corrosion resistant and is self-lubricating. The useful properties of bronze for the analysis are $P_{material} = 55MPa$ and $PV_{material} = 1.8MPa\ m/s$. A lighter material, such as plastic, might have been chosen, however these are more limited in temperature ranges and their weight difference is not considerable for a small bushing. The sleeve bearings are press fit into their respective housing, and the shaft is inserted inside with a clearance fit.

The spacers are selected to be made of polycarbonate, as it is lightweight, thermally stable, can take impact forces and is moisture resistant [17].

4.7.5 Stress Analysis and Free-Body Diagrams

The diagram in 44 shows the important dimensions of the sleeve bearing for the calculations.

where L is the sleeve bearing length, d is the inner diameter (shaft diameter for simplification) and t is the thickness of the bearing wall (constant).

The original analysis was done for roller bearings, where it was found that these were

not adequate for the static forces encountered in this application (see Appendix B.4).

Instead, the sleeve bearings (bushings) were chosen, as they can take more radial forces. The method used to determine the required length of the sleeve bearing is the pressure-velocity (PV) factor [18]. This value is a material property and is described by Equation 125. As this application uses very low velocities, the pressure (P) is also observed. This is done using Equation 123. Analysing the velocity is unnecessary for this case, as the application is close to static.

$$P = \frac{F}{dL} \quad (123)$$

$$V = \frac{\pi dn}{60 \times 10^3} \quad (124)$$

$$PV = \frac{\pi Fn}{60 \times 10^3 L} \quad (125)$$

where F is the radial force acting on the bearing in N and n is the rotational speed of the shaft in rpm. The rotational speed is assumed as the maximum value reached during a cycle. This gives a somewhat conservative estimate of the pressure-velocity factor.

The following is an example where the exterior knee shaft sleeve bearing length is found. This shaft has the highest forces on its bearings due to belt tension and forces from the leg. Equations 123 and 125 are rearranged to get the minimal required length of the bearing. To do so, the bearing material properties are used: bronze has operating limits of $P_{material} = 55MPa$ and $PV_{material} = 1.8MPa \text{ m/s}$. Other values are $d = 13.0mm$ (from shaft analysis Section 4.5.5.4), $n = 1.60rpm$ (maximum rotational speed from modelling) and $F = 1124.1N$ (the combination of the forces acting on the bearing in x and y from the shaft analysis, using Equation 91).

$$L_{required} = \frac{F}{dP_{material}} = \frac{1124.1N}{13.0mm \times 55MPa} = 1.57mm \quad (126)$$

$$L_{required} = \frac{\pi Fn}{60 \times 10^3 PV_{material}} = \frac{\pi \times 1124.1N \times 1.60rpm}{60 \times 1000 \times 1.8MPa \text{ m/s}} = 0.05mm \quad (127)$$

Thus we choose the largest value of 1.57 mm and apply the safety factor to get L . This value is quite close to the value assumed for the shaft calculations, which was 4.0 mm, thus we can round up to this value.

$$L = SF \times L_{required} = 2.5 \times 1.57mm = 3.93mm \approx 4.0mm \quad (128)$$

4.7.6 Critical Review

The bearing lengths make sense as the chosen material is quite strong for this application, meaning that only small lengths are required. The thickness of the flange (2 mm) also contributes to the length of the bearing but removes some length from the part of the sleeve bearing radially in contact with the housing. It will likely be required to choose longer bearings due to this.

4.7.7 Parameterization

The parameterization goal will be to find the required length of the bearing for the applied bearing forces, which depend highly on the weight of the robot. A value for the length of the bearing will need to be estimated for the shaft analysis in order to find bearing forces, and then the assumed length will be modified following the bearing analysis. It will be an iterative process. However, as seen in the example with the worst case scenario, the length of the bearings is already quite small. Another option would be to simply set a length that works for all situations, and keep it constant without parameterization. Otherwise, a minimum sleeve bearing length will be set to ensure stability and manufacturability of the assembly (for example, the hip shaft bearings take very low load, thus we would limit the bearing length to a minimum of 3 mm).

4.8 Fasteners

4.8.1 Inputs and Outputs

Inputs include the number of bolts n , distance P from the applied forces to the centroid, distance from the bolt to centroid r , and angles ρ and ϵ between P and x around z and y respectively (variables shown in Figure 45). The minimum acceptable bolt diameter d , member thickness t and distance from bolt to member edge ℓ are then calculated.

4.8.2 Constants and Parameters

A safety factor of 2.5 was selected. This is in accordance with the recommendations provided by Juvinall and Marshek for average materials operating in ordinary environmental conditions, subjected to loads and stresses that can be determined [14]. Since the maximum stresses have been simulated, the maximum stresses can be determined with relative accuracy, however due to the uncertainty of vandalism, a smaller safety factor was not selected;

thus 2.5 strikes a solid balance between being conservative and still flexible. A safety factor for tension is specific has been set at 2; as shown in the example below, the initial bolt tension sets the safety factor at 2.3, so the actual value will be 2.3 or smaller depending on the applied load. Bolt properties are also constant and are found in Table 3

4.8.3 Assumptions and Simplifications

The following assumptions were made while analysing the bolts at the hips:

1. Absolutely rigid members [10]
2. Ductile bolt material
3. Negligible impact loading and vibrations
4. Washers do not greatly influence the found safety factor, and are therefore not included in the analysis
5. Bolt threaded and unthreaded length can be customized and do not need to follow the formulation provided in Shigley or Juvinall
6. Fatigue loading is negligible
7. Load due to tensile moment is evenly distributed between all bolts (which would in reality become larger the further from the pivot point the bolt is)

4.8.4 Material Selection

SAE class 9.8 medium carbon bolts were pre-emptively selected as they cover a large swath of diameters (M1.6-M16), have good tensile and proof strength, and are not as expensive as higher class bolts. Environmental resistance is not paramount as all bolts are contained within the chassis or bellows, however since condensation is likely, some degree of protection against corrosion is necessary. Coarse-tooth bolts were selected. Although fine tooth bolts have higher tensile area, allowing for smaller diameter bolts, and are less likely to loosen over time, their availability in sizes below M8 seem severely limited [10] [19].

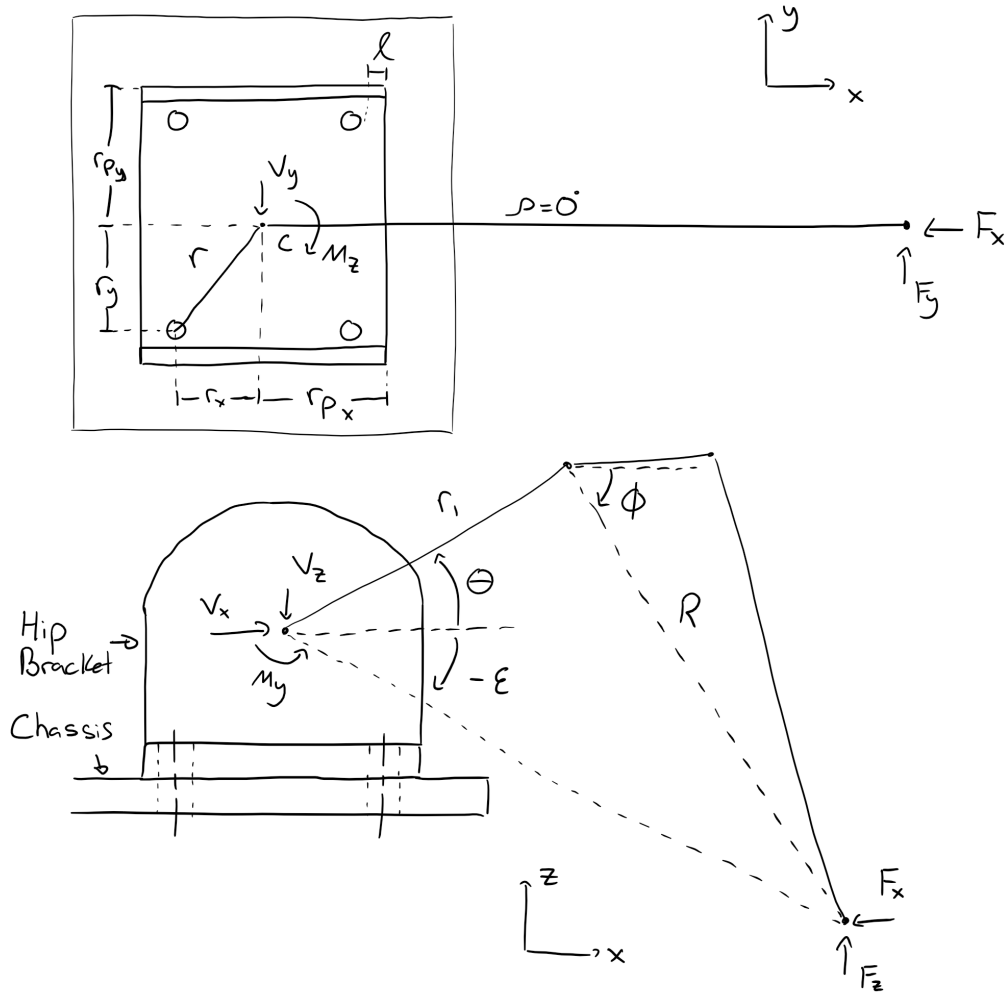


Figure 45: Force-Body Diagram of hip bolts

Table 3: Properties of ISO Class 9.8 Bolts

Property	Measure
Bolt sizes	M1.6-M16
Proof Strength S_p	650 MPa
Yield Strength S_y	720 MPa
Tensile Strength S_{ut}	900 MPa
Endurance Strength S_e	140 MPa
Fatigue Stress-Concentration Factor k_f	3.8 (Cut Threads)

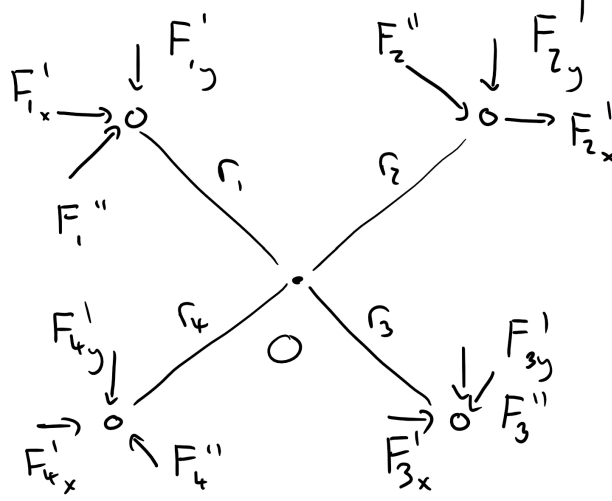


Figure 46: Primary and Secondary Shear Stresses in Bolts

4.8.5 Free-Body Diagram

The following example illustrates the stress analysis for the fasteners holding the hip plates and motor to the chassis, illustrated in Figure 45. The clamping members are assumed to be made of Aluminium 6061, with a yield strength of 276MPa [9], and a thickness of an eighth inch for each member (3.175mm), giving $g = t_1 + t_2 = 6.35\text{mm}$. The bolts are made of medium carbon steel (class 9.8), with an elastic modulus of approximately 200MPa [20]. The most extreme case for loading on a bolt is the maximum robot size (5kg of litter) with the leg fully extended, when $\theta = 17.18^\circ$, $\phi = -51.89^\circ$ (from horizontal), $r_1 = 100\text{mm}$, $R = 280.17\text{mm}$. r is assumed to be 70.71mm and r_p is assumed to be 70mm . The initial bolt diameter is estimated to be 5mm (M5). The mechanical properties of class 9.8 steel is found in Table 3. In this case, we can compute the moment arm P and angle of application ρ as

$$x = r_1 \cos \theta + R \cos \phi = 268.44\text{mm} \quad (129)$$

$$y = 0\text{mm} \quad (130)$$

$$z = r_1 \sin \theta + R \sin \phi = -190.9012\text{mm} \quad (131)$$

$$\rho = 0^\circ \quad (132)$$

$$\epsilon = \arctan\left(\frac{z}{x}\right) = -35.41^\circ \quad (133)$$

$$\begin{aligned}
P &= \sqrt{r_1^2 + R^2 - 2r_1R \cos(\phi - \theta - \pi)} \\
&= \sqrt{(100mm)^2 + (280.17mm)^2 - 2 \cdot 100 \cdot 280.17 \cos(-51.89^\circ - 17.18^\circ - \pi)} \\
&= 329.40mm
\end{aligned} \tag{134}$$

with maximum foot forces given by

$$F_x = 100N \tag{135}$$

$$F_y = 100N \tag{136}$$

$$F_z = 160N \tag{137}$$

With F_z being the normal force when on flat ground (maximum), F_x being the maximum friction force in the x direction and F_y being the maximum friction force in the y direction, while on a 20° incline. Both friction forces will never occur simultaneously, as $100N$ is the total friction amplitude and would thus be split between them, however this gives a conservative estimate. Equally, the maximum normal and friction forces will never occur simultaneously, however for the sake of being conservative both are considered here simultaneously.

The pure shear reaction forces V_x and V_y , tensile reaction force F_t and reaction moment M are.

$$V_x = F_x = 100N \tag{138}$$

$$V_y = F_y = 100N \tag{139}$$

$$F_t = F_z = 160N \tag{140}$$

$$\begin{aligned}
M_y &= (F_z \cos \epsilon - F_x \sin \epsilon)P \\
&= ((100N) \cos(0^\circ) - (100N) \sin(0^\circ))(280.17mm) \\
&= 62041Nmm
\end{aligned} \tag{141}$$

$$\begin{aligned}
M_z &= (F_y \cos \rho - F_x \sin \rho)P + T \\
&= ((160N) \cos(-35.41^\circ) - (100N) \sin(-35.41^\circ))(280.17mm) \\
&= 32940Nmm
\end{aligned} \tag{142}$$

Where T is any pure moment applied along the member (zero in this case). The centroid is located via symmetry and found to be the center of the bolts.

4.8.6 Stress Analysis

Identified failure modes include pure shear in the bolts, edge shearing of the member, crushing, tensile yielding in the bolts, and tensile yielding of the member (which will be evaluated separately in Section 4.10).

Primary shear stresses F'_{sh} and secondary shear stresses F''_{sh} are shown in Figure 46.

The primary shear stresses are given by

$$F'_{sh} = \frac{\sqrt{V_x^2 + V_y^2}}{n} = \frac{\sqrt{(100N)^2 + (100N)^2}}{4bolts} = 35.35N \quad (143)$$

where n is the number of bolts. The reaction forces required to counter M_z are given by

$$M_z = F''_{sh_1} r_1 + F''_{sh_2} r_2 + \dots + F''_{sh_n} r_n \quad (144)$$

Since $r_1 = r_2 = r_3 = r_4$, the secondary shear stress is given by [10]

$$F''_{sh} = \frac{M_z r}{nr^2} = \frac{M_z}{nr} = \frac{32940Nmm}{(4bolts)(70.71mm)} = 116.46N \quad (145)$$

Finally, the total shear force per bolt is given by

$$F_{sh} = \sqrt{F'_{sh}{}^2 + F''_{sh}{}^2} = \sqrt{(35.35N)^2 + (116.46N)^2} = 121.70N \quad (146)$$

And the shear stress

$$\tau = \frac{F_{sh}}{A_b} \quad (147)$$

where A_b is the cross-section of the bolt along the two clamping members. The safety factor is given by

$$SF_{sh} = \frac{S_{sy}}{\tau} = \frac{S_{sy} A_b}{F_{sh}} = \frac{0.58(340MPa)\pi(5mm)^2}{4(121.70N)} = 67.36 \quad (148)$$

Where S_{sy} is the shear yield strength, given by the Maximum-distortion-energy theory for ductile materials as $S_{sy} = 0.58S_y$ [14]

The stress for bearing forces varies depending on the individual member thicknesses [21]. For members of thickness $t_1 = t_2 = 3.175mm$, the bearing stresses are given by

$$\sigma = \frac{F_{sh}}{t_1 d} = \frac{121.70N}{(3.175mm)(5mm)} = 7.66MPa \quad (149)$$

where d is the nominal major diameter of the thread, t_i is the thickness of member i and F_{sh} is the shear stress held by the bolt.

The safety factors for the bolt and members are given by

$$(SF)_{cr_b} = \frac{S_{yb}}{\sigma} = \frac{200MPa}{7.66MPa} = 26.08 \quad (150)$$

$$(SF)_{cr_m} = \frac{S_{ym}}{\sigma} = \frac{276MPa}{7.66MPa} = 36.00 \quad (151)$$

With the equation inverted, the minimum required member thickness to match the safety factor is 0.2205mm. This is well below the selected thickness of 3.175mm used.

Edge shearing occurs when the member shears between a bolt and it's edge, usually characterized by a bolt being in too close proximity to the member's edge [14]. The area for edge shearing is given by

$$A_{es} = \ell_i t \quad (152)$$

where ℓ is the distance from the outside of a bolt to it's edge in the direction of the applied force and t is the thickness of the thinnest member. For example, the area for edge shearing for an applied force in x would give $A_{es_x} = \ell_x t$.

The shear force is given by F_i from Equation 146. The safety factor for edge shearing is given by

$$(SF)_{es} = \frac{0.577S_{ym}}{\tau} = \frac{0.577S_{ym}}{\frac{F_{sh}}{A_{es_x}}} = \frac{0.577S_{ym} \ell_i t}{F_{sh}} \quad (153)$$

The required distance from the edge for bolt i is thus given by isolating ℓ_i and applying the desired safety factor.

$$\ell_i = \frac{(SF)_{es} F_{sh}}{0.577S_{ym} t} = \frac{2.5(121.70N)}{0.577(276MPa)(3.175mm)} = 0.60mm \quad (154)$$

Shigley recommends placing the bolts 1.5 times the diameter away from the edge (so 7.5mm; the resulting ℓ can be increased to match this value, or retained if above this value.

The initial tension in the bolts is given by [14]

$$F_i = k_i A_t S_p = 0.7(14.175\text{mm}^2)(650\text{MPa}) = 6449.9\text{N} \quad (155)$$

where k_i is a constant between 0.7 and 1.0 (chosen here to be 1.0), A_t is the tensile strength area of the thread given in Table 10.2 of Juvinall and Marshek and curve-fitted with MATLAB's Curve Fitting Tool to $A_t = 0.7023d^2 - 2.669d + 9.963$, and S_i is the proof strength of the material, given in Table 10.5 of Juvinall and Marshek. The tightening torque is given by

$$T = 0.2F_i d = 0.2(6449.9\text{N})(5\text{mm}) = 6449.9\text{N} \quad (156)$$

where d is the nominal major diameter of the thread.

The spring constants of the bolt and member are respectively

$$A_b = \frac{\pi(5\text{mm})^2}{4} = 19.635\text{mm}^2 \quad (157)$$

$$k_b = \frac{A_b E_b}{g} = \frac{(19.635\text{mm}^2)(200\text{MPa})}{2(3.175\text{mm})} = 618.42 \frac{\text{N}}{\text{mm}} \quad (158)$$

$$A_m \approx d^2 + 0.68dg + 0.065g^2 = (5\text{mm})^2 + 0.68(5\text{mm})(6.35\text{mm}) + 0.065(6.35\text{mm})^2 = 49.21\text{mm}^2 \quad (159)$$

$$k_m = \frac{A_m E_m}{g} = \frac{(78.663\text{mm}^2)(276\text{MPa})}{2(3.175\text{mm})} = 2138.93 \frac{\text{N}}{\text{mm}} \quad (160)$$

where g is the effective length, shown in Figure 47, $A_b = A_t$, the nominal major area of the thread, and E_b and E_m are the elastic modulus of the bolt and members respectively. The clamping area A_m can be approximated for small clearance fits with Equation 159 [14].

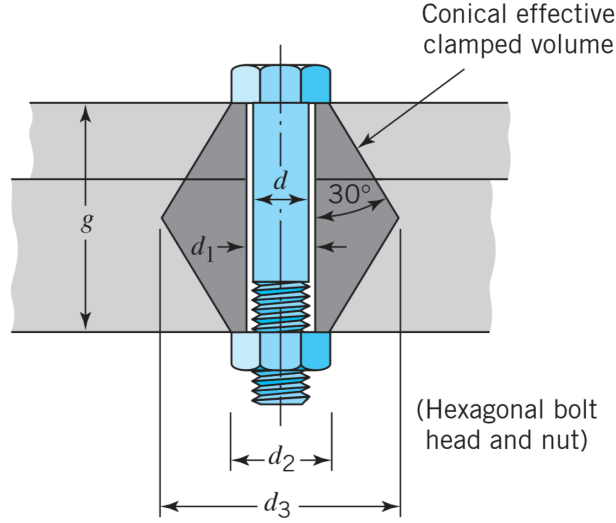


Figure 47: Determining spring constant of bolt and clamping member [14]

With an external tensile force F_t , the bolt tension and clamping force are given by

$$\begin{aligned}
 F_b &= F_i + \frac{k_b}{k_b + k_m} \frac{1}{n} \left(F_t + \frac{M_y}{(r_p + r_x)} \right) \\
 &= 6449.9N + \frac{618.42 \frac{N}{mm}}{618.42 \frac{N}{mm} + 2138.93 \frac{N}{mm}} \frac{1}{4\text{bolts}} \left(160N + \frac{62041Nmm}{(70mm) + (50mm)} \right) \quad (161) \\
 &= 6487.81N
 \end{aligned}$$

$$\begin{aligned}
 F_m &= F_i - \frac{k_m}{k_b + k_m} \frac{1}{n} \left(F_t + \frac{M_y}{(r_p + r_x)} \right) \\
 &= 6449.9N - \frac{618.42 \frac{N}{mm}}{618.42 \frac{N}{mm} + 2138.93 \frac{N}{mm}} \frac{1}{4\text{bolts}} \left(160N + \frac{62041Nmm}{(70mm) + (50mm)} \right) \quad (162) \\
 &= 6318.55N
 \end{aligned}$$

where F_t is the applied external force, k_b is the spring constant of the bolt, k_m is the spring constant of the clamping members, $\frac{M_y}{(r_p + r_x)}$ is the tension required to resist the moment M_y around the pivot point r_p (for the bolt the furthest from the pivot, and thus experiencing the highest stress), and n is the number of bolts. The applied force has little impact on the force felt by the member or bolt; the initial tension is still much larger. The safety factor in tension for the bolt is

$$\sigma_b = \frac{nF_b}{A_t} = \frac{4(6487.81N)}{\pi(5mm)^2} = 330.42MPa \quad (163)$$

$$SF_t = \frac{S_{yb}}{\sigma} = \frac{720MPa}{329.616MPa} = 2.17 \quad (164)$$

It was found that the safety factor sits around 2.2 regardless of the external load; this is likely because the initial tension of the bolt is significantly larger than the external forces, and thus they have little impact on the safety factor. A factor as low as two is allowed for tension. For cases where the bolts do not all have the same distance $r_p + r_x$, then only the number of bolts at distance $r_p + r_x$ should be considered.

4.8.7 Critical Review

Bolts that are likely to fail are found in two places; the bolts holding the hip motors and brackets to the chassis, and the bolts connecting the lower leg (tibia) to the pulley at the knee. The former was analyzed above. The safety factors for the fasteners at the hips are acceptable for all modes of failure for $d = 4mm$. The safety factor in tension is unlikely to dip under 2. Even with the normal force F_z increased by a factor of 100, the safety factor in tension is above 1.5; the majority of the loading in the bolts is still from the initial tightening, and thus the required safety factor has been lowered to 2. The safety factor in shear is more volatile, however, and given large loads or very small bolt diameters and r , it can pass below 2.5. Since the shear safety factor depends on the distance between the bolts and their centroid r and the bolt diameter d , but r and n are set by the part geometry independently of the fastener analysis, the bolt size is the only parameter influencing the shear safety factor. Crushing depends on the bolt diameter and thickness and edge shearing depends on thickness and distance ℓ . There are thus three parameters that can be modified to minimize the safety factors.

Some geometry was ignored. For example, when calculating the forces in tension, the load was evenly divided between the bolts. This is not correct, as the bolts furthest from the pivot point would take more force than those closer. Since the safety factor in tension does not vary until increasing the applied load by a couple orders of magnitude, this simplification is acceptable. For the given example, the height between the center of the hip bracket and the bolts shown in Figure 45 was forgotten. This would have reduced the moment impacting the tensile force, and so does not negatively impact the safety factor of the analysis. Finally, The bolts were not analyzed for fatigue either. Juvinal and Marshek note that fatigue occurs

only with repeated plastic yielding [14]. Since the bolts stay under their yield strength at all times, fatigue should not be a concern.

4.8.8 Parameterization

The distance P from the applied forces to the centroid, distance from the bolt to centroid r , and angles ρ and ϵ between P and x around z and y respectively will be given as inputs for parametrization. The values of d , t_m and ℓ are determined by first generating a range of values for all three, then creating 3D matrices with the following 2D principle extended to 3D:

$$\text{Matrix}_r = \begin{bmatrix} r_1 & r_1 & \dots & r_1 \\ r_2 & r_2 & \dots & r_2 \\ \dots & & & \dots \\ r_n & r_n & \dots & r_n \end{bmatrix} \quad (165)$$

$$\text{Matrix}_d = \begin{bmatrix} d_1 & d_2 & \dots & d_n \\ d_1 & d_2 & \dots & d_n \\ \dots & & & \dots \\ d_1 & d_2 & \dots & d_n \end{bmatrix} \quad (166)$$

The stress analysis functions are then applied to each combination of d , t_m and ℓ and the one that minimizes some measure of space occupied (such as minimizing the area occupied by the bolts) while maintaining the desired safety factors of 2 for tension and 2.5 for everything else will be selected.

4.9 Bellows

4.9.1 Inputs and Outputs

The bellow covering the hip and knee joints must be able to provide the required range of movement. The inputs include the available length for the bellow (nominal length), the required inner diameters of the conical bellow (chassis leg hole size and knee shaft size) and the required angular range of movement. The outputs are the number of folds required and their size.

4.9.2 Constants and Parameters

The chosen minimum safety factor for the bellow is 2.5 as to stretch the bellow to its maximum or minimum on a regular basis could cause it to fail prematurely. The bellow may also bend or stretch in unpredictable ways, and is subjected to the movement of two joints. The thickness of the bellow is chosen to be a constant value of 3 mm for a balance of flexibility and sturdiness. The inner diameter depends on the required size of the hole in the chassis for the leg. The hip will be positioned as close as possible to the side of the chassis to ensure a smaller hole is required.

4.9.3 Assumptions and Simplifications

For the calculations, it is assumed that the bellow is bent into a circular bend. The safety factor is added to make up for any behavior deviating from this assumption. As the bellow covers two joints, it will sometimes be bending in two opposing directions. However, as the distance between the joints is small, these bends will likely cancel each other to a certain extent: the bellow might come to rest on the thigh member inside it, which is considered acceptable as no sharp edges will be present to wear out the bellow, and it will not interfere with any moving components. Thus, the analysis is carried out for the maximum total angle provided by both joints in the same direction.

As the bellow is conical, the required extension and retraction are calculated using the largest diameter of the bellow, as this gives the more stringent requirements.

4.9.4 Material Selection

The chosen material for the bellows is silicone as it is a moldable flexible material which is uv-resistant, waterproof and operates on a large range of temperatures [22].

4.9.5 Free-Body Diagram

The bellow analysis is mainly geometric, thus the required dimensions are shown in Figure 48. The bellow at an angle is shown as being constant diameter, however the values with a conical bellow would be the same, but with using $d_{i,max}$ in calculations.

where n_{fold} is the number of folds in the bellow, L_{nom} is the nominal length of the bellow (straight un-extended), L_{fold} is the height (or width) of the folds when the bellow is at nominal length, d_i is the inner diameter of the bellow (max and min for conical bellow), ψ

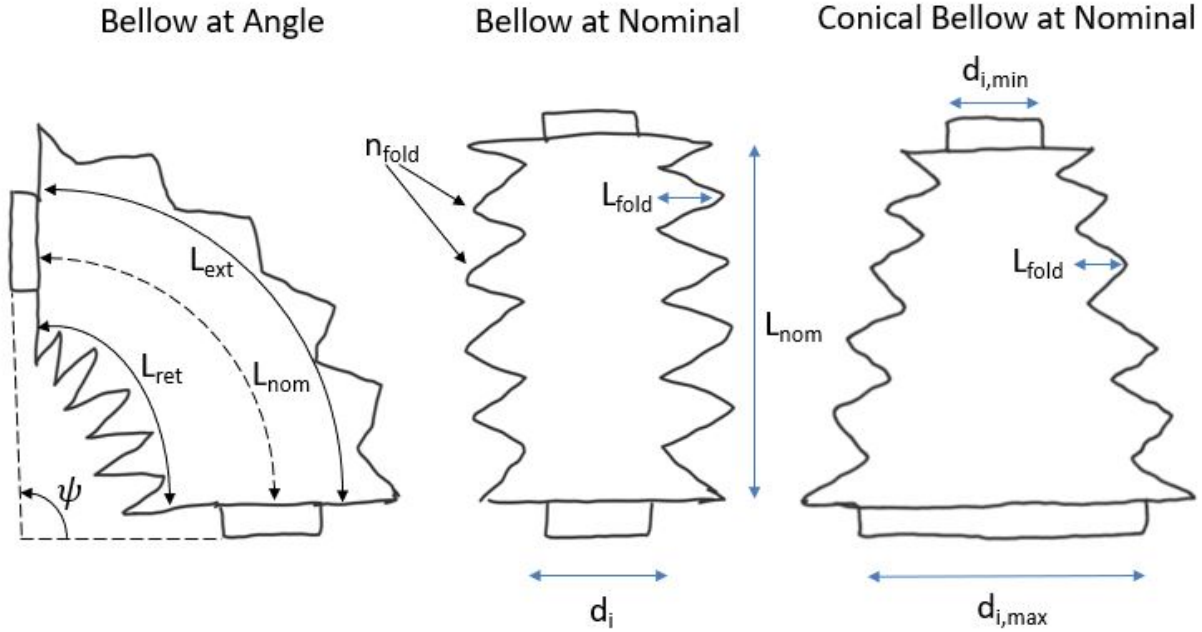


Figure 48: Bellow - Dimensions and Geometry

is the bend angle of the bellow in degrees, L_{ext} is the extended length of the bellow and L_{ret} is the retracted length of the bellow.

To determine the required inner diameter of the bellow at the chassis, the following diagram is used:

4.9.6 Analysis

First, the required inner diameter of the bellow is computed using the following equation, based on Figure 49. We use $L = 50mm$ based on harmonic drive diameter at the hip, $\theta = 45^\circ$ the maximum angle of the hip, $w = 70mm$ an approximation based on the pulley diameter and $t_{chassis} = 5mm$.

$$\begin{aligned}
 d_{i,max} &= h_{angle} + h_{thigh} + 2(t_{chassis}) = L \tan \theta + \frac{w}{\cos \theta} + 2t_{chassis} \\
 &= 50mm \tan 45^\circ + \frac{70mm}{\cos 45^\circ} + 2(5mm) = 159mm
 \end{aligned} \tag{167}$$

Next, the known geometrical values are used to find the required extended length and retracted length of the bellow. The nominal length and required angular range are used to get a nominal circumference $circ_{nom}$. The values used are $\psi = 40.2^\circ$ the total angle of the

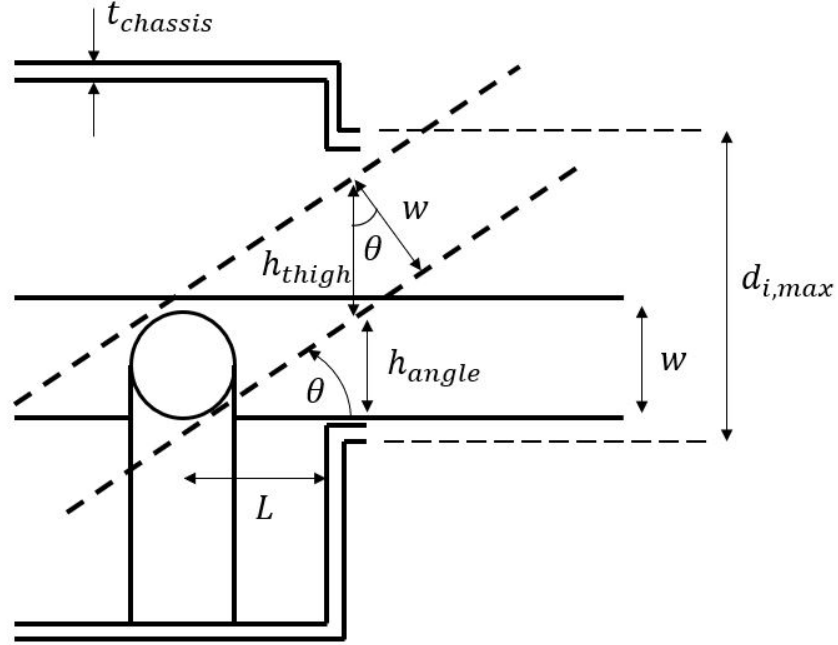


Figure 49: Bellow - Finding the required inner diameter based on chassis leg hole

hip and knee in the most extended position of the leg and $L_{nom} = 94mm$ the approximated nominal length of the bellow based on limb lengths and space for the bellow hose clamps.

$$circ_{nom} = \frac{360}{\psi} L_{nom} \frac{360}{40.2^\circ} 94mm = 841.5mm \quad (168)$$

This value makes it easy to get the retracted and extended length by subtracting or adding an internal diameter (using the maximum value for the conical bellow) to get the inner and outer circumferences of the bend ($circ_i$ and $circ_o$) and converting back to lengths:

$$circ_o = circ_{nom} + d_{i,max} = 841.5mm + 159mm = 1000.5mm \quad (169)$$

$$L_{ext} = circ_o \div \frac{360}{\psi} = 1000.5mm \div \frac{360}{40.2^\circ} = 111.8mm \quad (170)$$

$$circ_i = circ_{nom} - d_{i,max} = 841.5mm - 159mm = 682.5mm \quad (171)$$

$$L_{ret} = circ_i \div \frac{360}{\psi} = 682.5mm \div \frac{360}{40.2^\circ} = 76.2mm \quad (172)$$

Now for the design of an appropriate bellow to fill those length requirements, the following expressions are used. The first finds the minimum retracted length L_{min} of a bellow as a function of the number of folds n_{fold} and the thickness of the bellow wall t . The second finds the maximum extended length L_{max} of a bellow as a function of the number of folds and

their "height" at nominal length L_{fold} . t is a constant and is set to 3 mm and n_{fold} and L_{fold} are estimated until the proper safety factor is met.

$$L_{min} = 2n_{fold}t = 2(8)(3mm) = 48mm \quad (173)$$

$$L_{max} = 2n_{fold}L_{fold} = 2(8)(8.7mm) = 139.2mm \quad (174)$$

These values are then compared with the required values by calculating the extension/retraction value and finding the safety factor SF :

$$SF = \frac{L_{max} - L_{nom}}{L_{ext} - L_{nom}} = \frac{139.2mm - 94mm}{111.8mm - 94mm} = 2.5 \text{ Good!} \quad (175)$$

$$SF = \frac{L_{min} - L_{nom}}{L_{ret} - L_{nom}} = \frac{48mm - 94mm}{76.2mm - 94mm} = 2.6 \text{ Good!} \quad (176)$$

Thus the bellow has 8 folds of 8.7 mm in size. The value of $d_{i,min}$ is chosen based on the length of the exterior knee shaft, plus some clearance, giving a value of about 102 mm.

4.9.7 Critical Review

The analysis (with the added safety factor) gives a reasonable estimate of the dimensions of the bellow. However it is difficult to know to which extent it is being over designed, as its behavior in movement is difficult to predict and the equations use approximations (such as the fact that the bellow bends in a perfectly circular shape).

4.9.8 Parameterization

The goal for the parameterization of this component is to use known geometry (nominal length, required angle, required inner diameters) to find an appropriate combination of the number of folds and their height at nominal length.

4.10 Hip Bracket

4.10.1 Inputs and Outputs

This section is focused on the analysis of the hip bracket, which is the assembly holding the leg (at the hip control shaft) and attaching it to the chassis. Due to the required range of movement of the leg, this bracket may be quite high. Thus this analysis will take its height and all the forces applied to it and calculate the required thickness of the bracket to prevent failure.

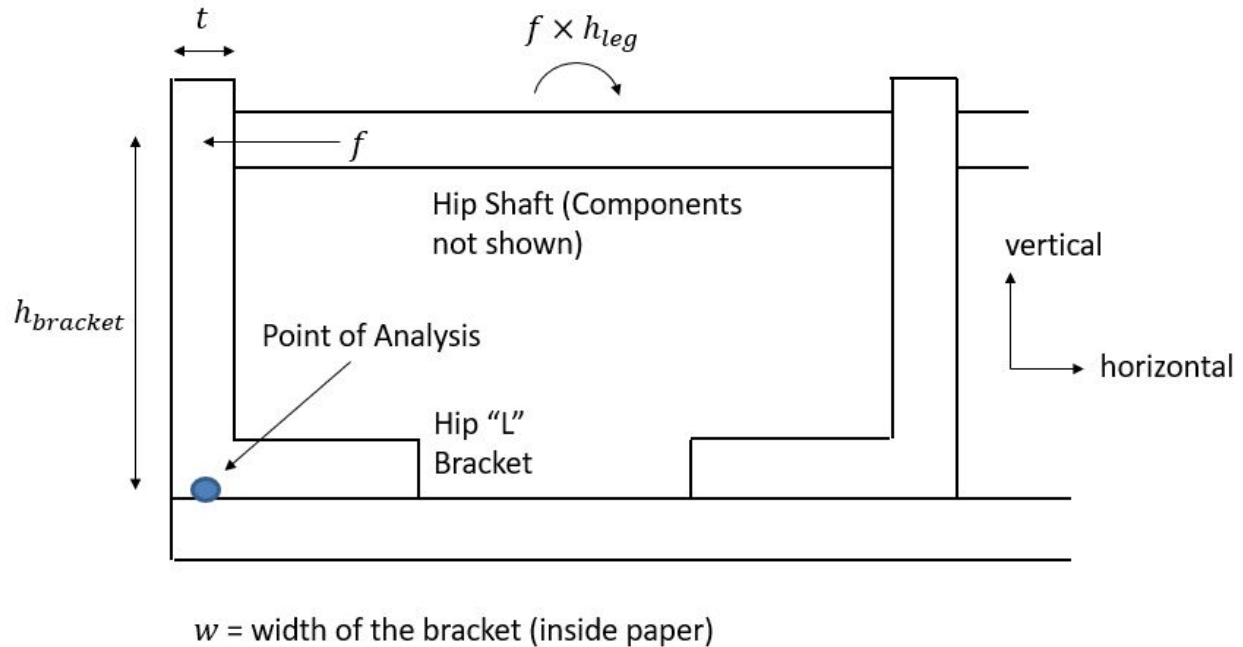


Figure 50: Hip Bracket - Bending Stress

4.10.2 Constants, Parameters and Assumptions

The safety factor chosen for this part is 2.0 as it is not moving and is merely a structural part. The biggest consideration for this bracket is bending at its lower corners in the direction of its thickness, as the bracket will be quite high. Thus, only this stress calculation is performed.

4.10.3 Material Selection

The chosen material is aluminum 6061-T6 as it is marine grade, strong and lightweight. Its yield strength is of about 276 MPa [9].

4.10.4 Free-Body Diagram

The following figure shows the various forces applied on the hip bracket and the point being analysed for bending.

where values of f and h_{leg} are as described in Figure 35, and their product is the moment created by friction at the foot.

4.10.5 Stress Analysis

The equation for the bending moment at the identified critical point (M_{crit}) is shown in the following equation. The values are $f = 51.7N$, $h_{leg} = 190mm$ and $h_{bracket} = 150mm$ based on required leg movement clearance.

$$\sum M : M_{crit} = f \times h_{leg} - f \times h_{bracket} = 51.7N(190mm - 150mm) = 2066.8Nmm \quad (177)$$

Now to find the required minimum thickness of the bracket, the stress equation (for a rectangular cross-section) [14] is used with the chosen safety factor. Values of $SF = 2$, $S_y = 276MPa$ and $w = 100mm$ are used.

$$t = \sqrt{\frac{6SF \times M_{crit}}{wS_y}} = \sqrt{\frac{6(2) \times 2066.8Nmm}{100mm(276MPa)}} = 0.9mm \quad (178)$$

4.10.6 Critical Review

The required value of thickness is quite small as the critical point is quite close to the ground, making the effect of the moment created by friction forces at the foot smaller.

4.10.7 Parameterization

This component will not be parameterized based on the previous analysis. Instead, the thickness value will be determined by the length of the sleeve bearings for the hip shaft, as they are supported by this bracket. The width of the bracket is based on the size of the harmonic drive and the height is ultimately based on harmonic drives as well, as they affect the required vertical space for the leg range.

5 Discussion and Future Work

The bolts holding the hip brackets to the chassis were analysed, but the bolts holding together the tibia and knee pulley, shown in Figure 7, were not. Since the bolts must fit through the pulley, space is limited, and so there is a risk of failure. Although not presented here, they will be parameterized alongside the bolts at the hips.

The hip plates in Figure 3 acting as the thigh and connecting the hip to the knee were not analyzed. They are made of Aluminium 6061 and have connecting pieces between them to carry compression and torsion loads. The remaining tensile and bending forces are likely not enough to damage the plates, and so it was decided that analyzing them was not necessary.

The bellows were analyzed to ensure they could compress and extend to the required lengths; no form of stress analysis was done to ensure that tearing does not occur.

The lower leg, or tibia, is press fit into a bracket at the knee. The foot is also press fit into the tibia. Neither were analyzed for safety factors, required heating temperature to press fit, or the required interference to ensure parts do not separate due to vibrations or regular loading.

The chassis itself was not analyzed. The robot itself is not too heavy, however if too thin a structural plate to mount all the components is used, then bending is a serious concern, as it could cause the structure of the chassis to pull away from the weatherproof polymer shell. The shell itself was also not analyzed, although the only loads that are applied on it are reactions to the bellows stretching, whatever stresses pass from the chassis to the shell via bending, and humans pushing on the outside of the shell.

The keys and bolts connecting the shaft collars to the Harmonic Drive and motor, and the bolts connecting the Harmonic Drive and motor to the hip brackets were not analyzed either, as it is highly likely that both Harmonic Drive and Maxon Motor selected bolt and key sizes that are sufficiently safe as long as operating within their design conditions.

The silicone sock covering the foot is held in place using a screw-on compression cap, shown in Figure 6. The sock was not analyzed to ensure it would not tear away while walking.

A tensioner in the form of a torsion spring was added to account for stretching in the belt over time and with temperature variations. The impact of the spring on the belt tension as a function of its various parameters could not accurately be modelled.

As an accurate method of determining the sleeve bearing (bushing) friction could not be found, this effect was neglected from the overall analysis.

6 References

- [1] A. Al-Jarrah, “MCG4134: Robot Design and Control,” Jan. 2019.
- [2] Harmonic Drive, “CSD-2a Component Set | Harmonic Drive,” 2019. [Online]. Available: <https://www.harmonicdrive.net/products/component-sets/cup-type/csd-2a>
- [3] maxon motor, “maxon DC motor and maxon EC motor Key information,” Nov. 2014. [Online]. Available: https://www.maxongroup.com/medias/sys_master/8815460712478.pdf?attachment=true
- [4] Environment and Climate Change Canada, “Solar Radiation - Hourly data for Ottawa (Kanata - Orléans).” [Online]. Available: https://ottawa.weatherstats.ca/charts/solar_radiation-hourly.html
- [5] SunPower, “Solar Panels,” Jan. 2018. [Online]. Available: <https://us.sunpower.com/products/solar-panels>
- [6] Voltaplex, “6s–16s (22.2v–74v, Adjustable) 100a max. BMS Battery Management System for Lithium-ion Battery Pack with Balancing and Communication.” [Online]. Available: <https://voltaplex.com/22-2v-59-2v-pcb-bms-battery-management-system-for-lithium-ion-battery-pack>
- [7] DigiKey Electronics, “Battery Life Calculator | DigiKey Electronics.” [Online]. Available: <https://www.digikey.com/en/resources/conversion-calculators/conversion-calculator-battery-life>
- [8] 18650batterystore, “18650 Batteries - Rechargeable Lithium Ion | 18650 Battery Store.” [Online]. Available: <https://www.18650batterystore.com/18650-Batteries-s/106.htm>
- [9] Matweb, “Aluminum 6061-T6; 6061-T651.” [Online]. Available: http://www.matweb.com/search/datasheet_print.aspx?matguid=1b8c06d0ca7c456694c7777d9e10be5b
- [10] R. G. Budynas and J. K. Nisbett, *Shigley’s Mechanical Engineering Design*, 10th ed. McGraw-Hill Education, 2015. [Online]. Available: <https://www.amazon.com/Shigleys-Mechanical-Engineering-Richard-Budynas/dp/0073398217>
- [11] listertube, “Tube Bending Design Guide | Listertube Tube Engineering Services.” [Online]. Available: <https://www.listertube.com/links/tube-bending-design-guide/>

- [12] G. Mectrol, “Timing Belt Theory,” 2006. [Online]. Available: http://www.gatesmectrol.com/mectrol/downloads/download_common.cfm?file=Belt_Theory06sm.pdf&folder=brochure
- [13] Gates Mectrol, “Urethane Belt Program,” 2018. [Online]. Available: http://www.gatesmectrol.com/common/downloads/files/mectrol/brochure/GatesMectrol_Belt_Pulley_Catalog.pdf
- [14] R. C. Juvinall and K. M. Marshek, *Fundamentals of Machine Component Design*, 5th ed. Wiley, 2012.
- [15] Metal Supermarkets, “Marine Grade Metals,” Apr. 2017. [Online]. Available: <https://www.metalsupermarkets.com/marine-grade-metals/>
- [16] Quality Bearings and Components, “FLANGED SLEEVE BEARINGS | Standard Series - Inch.” [Online]. Available: https://www.qbcbearings.com/BuyRFQ/SleeveB_StandardS_F_SB_I.php
- [17] Omnexus, “Polycarbonate (PC) Plastic: Properties, Uses, & Structure - Guide.” [Online]. Available: <https://omnexus.specialchem.com/selection-guide/polycarbonate-pc-plastic>
- [18] D. Inc, “Bushing PV Calculations,” Oct. 2013. [Online]. Available: <https://daemar.com/bushing-pv-calculations.html/>
- [19] Nord-Lock Group, “Should I choose fine or coarse threaded bolts?” Sep. 2010. [Online]. Available: <https://www.nord-lock.com/insights/bolting-tips/2010/choose-fine-or-coarse-thread-bolts/>
- [20] Azom, “AISI 1018 Mild/Low Carbon Steel,” Jul. 2012. [Online]. Available: <https://www.azom.com/article.aspx?ArticleID=6115>
- [21] A. Ahsan, “MCG3131: Machine Design,” University of Ottawa, 2018.
- [22] Custom Rubber Corp, “Rubber Molded Bellows.” [Online]. Available: <https://www.customrubbercorp.com/Applications/convoluted-boots-and-tubes>
- [23] NTN Bearing, “Deep Groove Ball Bearings | NTN Bearing.” [Online]. Available: <http://www.ntnamericas.com/en/products/ball-bearings/deep-groove>

A Equation Derivation

No additional equation derivation.

B Additional Analysis

B.1 Robot Coordinate System

For some calculations, the cartesian coordinates are used. Figure 51 shows the coordinate system used throughout the report.

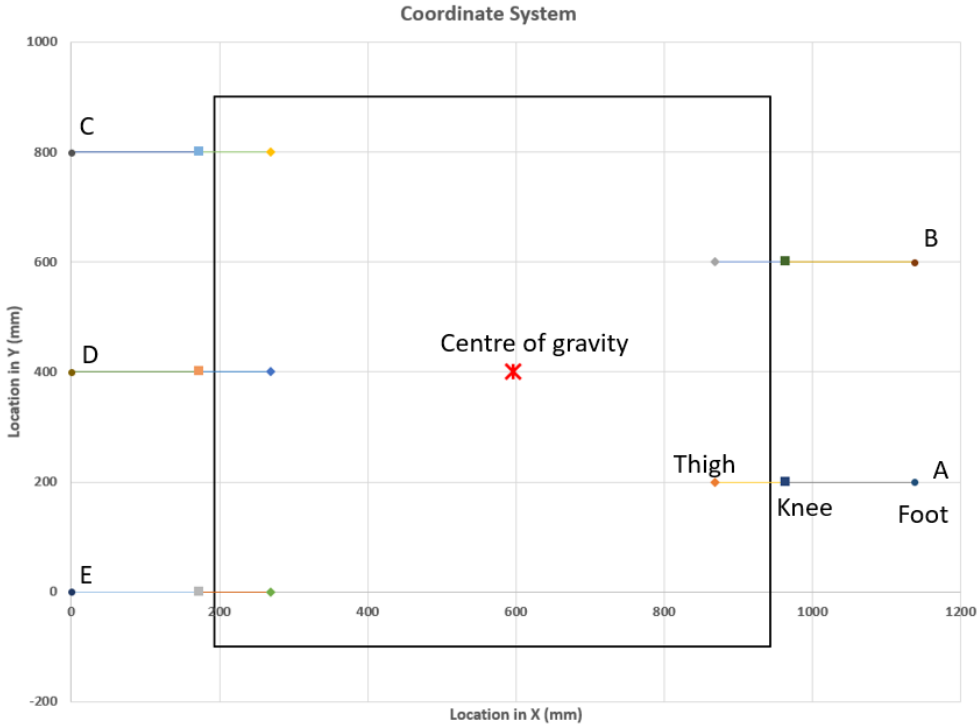


Figure 51: Coordinate System for the robot

B.2 Approximation Curved Beam

This is an alternative method to calculating the curved beam stresses due to the complex cross section.

The approximation is to calculate the distance from centroidal axis to neutral axis e .

The values are obtained from section 4.2

$$e = \frac{I}{r_c A} = \frac{\frac{\pi}{64}((17.175\text{mm})^4 - (14\text{mm})^4)}{(17.175\text{mm})(\frac{\pi}{4}((17.175\text{mm})^2 - (14\text{mm})^2))} = 1.79\text{mm} \quad (179)$$

$$c_i = r - e = 8.58\text{mm} - 1.79\text{mm} = 6.80\text{mm} \quad (180)$$

$$\sigma_i = \frac{M c_i}{A e r_i} = \frac{(20255.6\text{Nmm})(6.8\text{mm})}{(8.59\text{mm})(77.7\text{mm}^2)(1.8\text{mm})} = 115.5\text{MPa} \quad (181)$$

$$n = \frac{S_y}{\sigma_i + \sigma_x} = \frac{250\text{MPa}}{115.5\text{MPa} + 1.1\text{MPa}} = 2.2 \quad (182)$$

B.3 Limbs and Internal Stresses

Only the member BC stress diagram is shown in Section 4.2. All three links internal stresses are shown below.

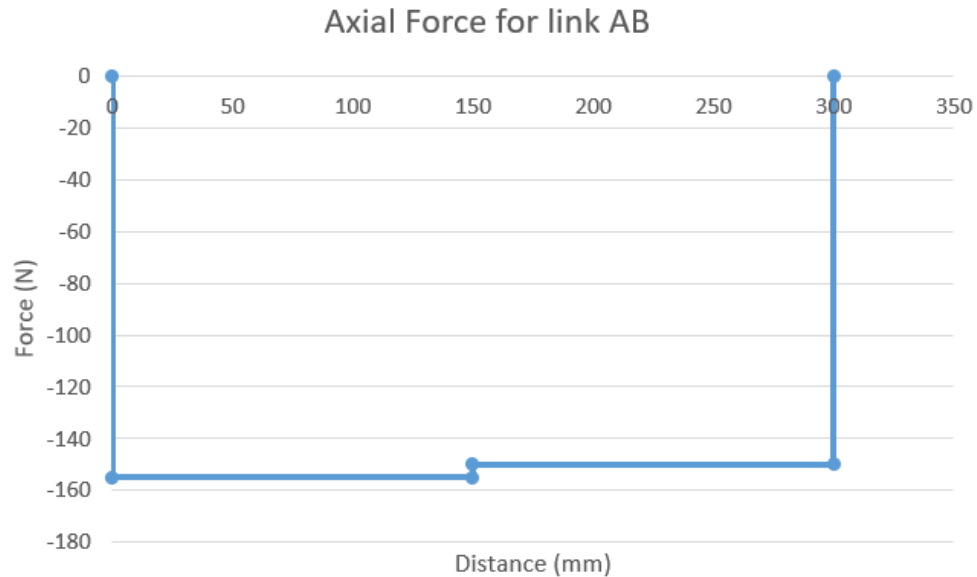


Figure 52: Axial Force Diagram for link AB

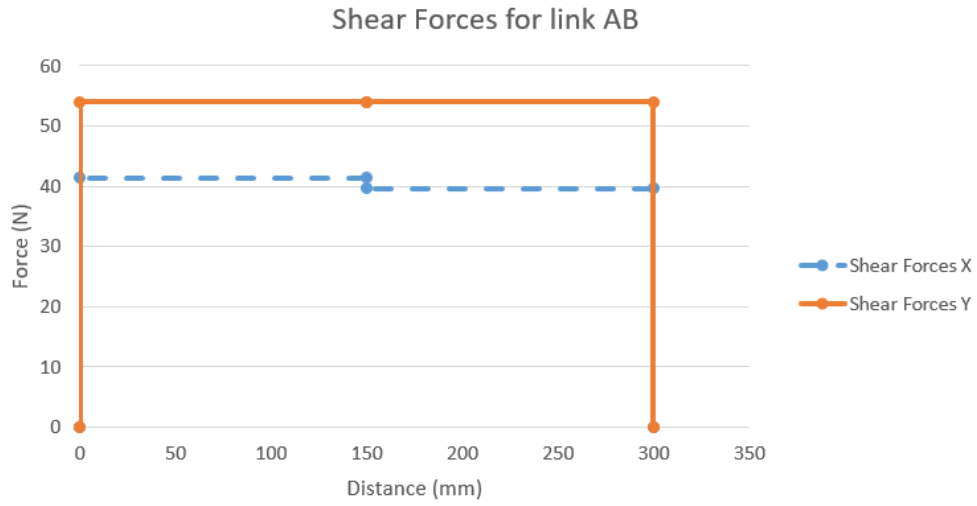


Figure 53: Shear Force Diagram for link AB

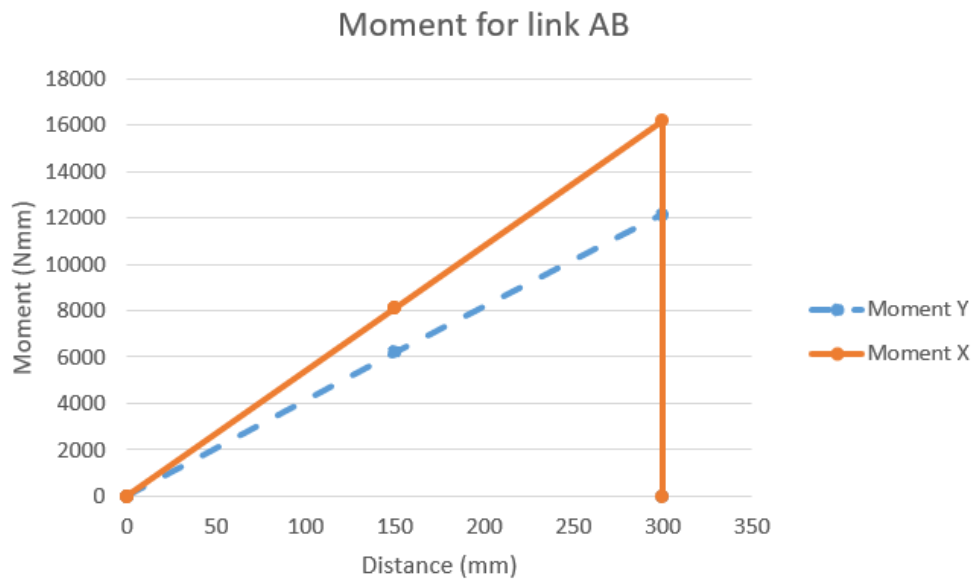


Figure 54: Moment Diagram for link AB

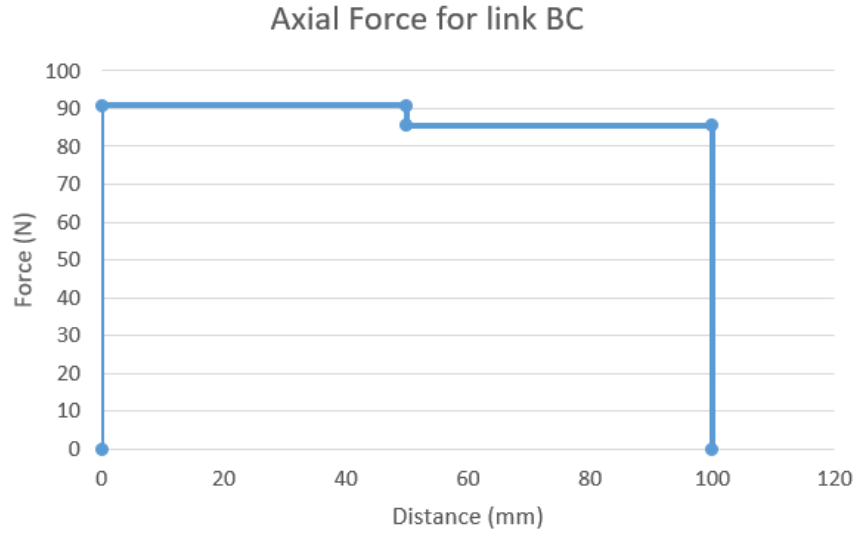


Figure 55: Axial Force Diagram for link BC

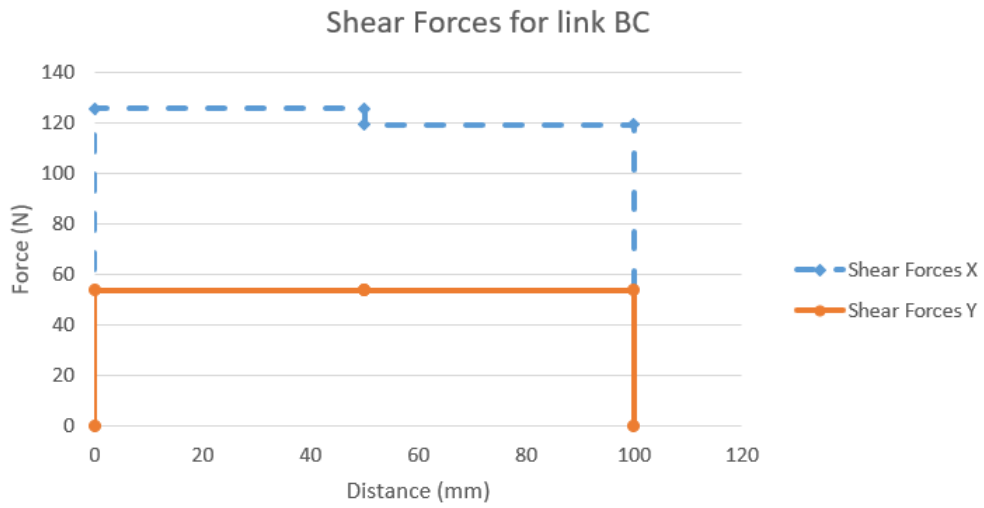


Figure 56: Shear Force Diagram for link BC

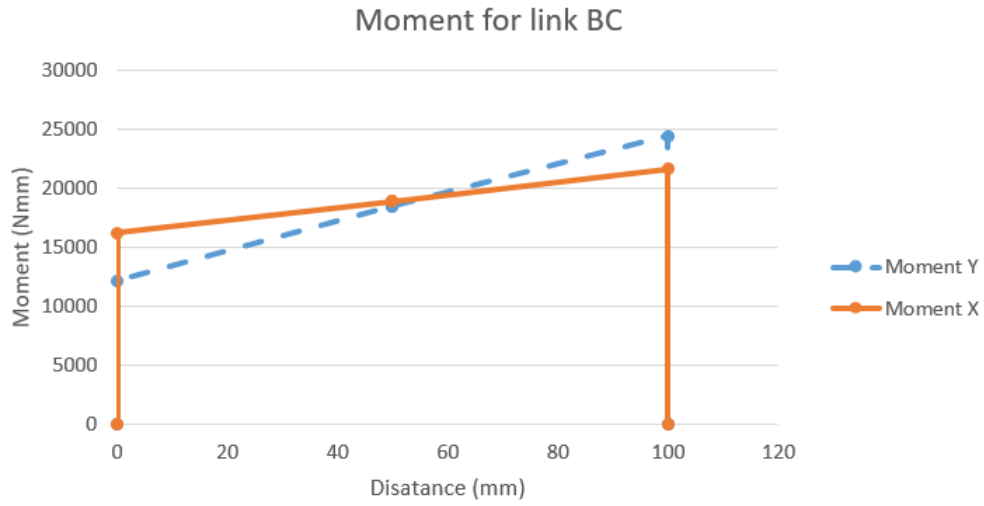


Figure 57: Moment Diagram for link BC

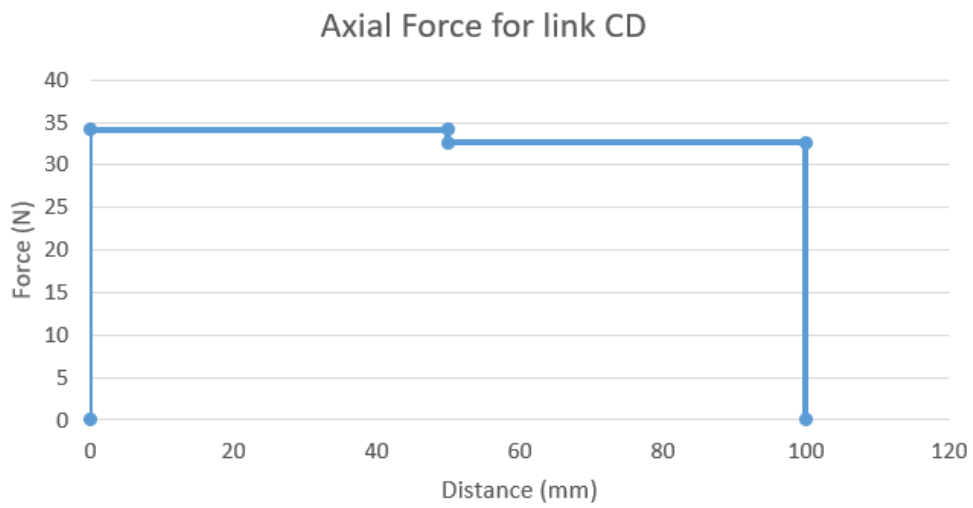


Figure 58: Axial Force Diagram for link CD

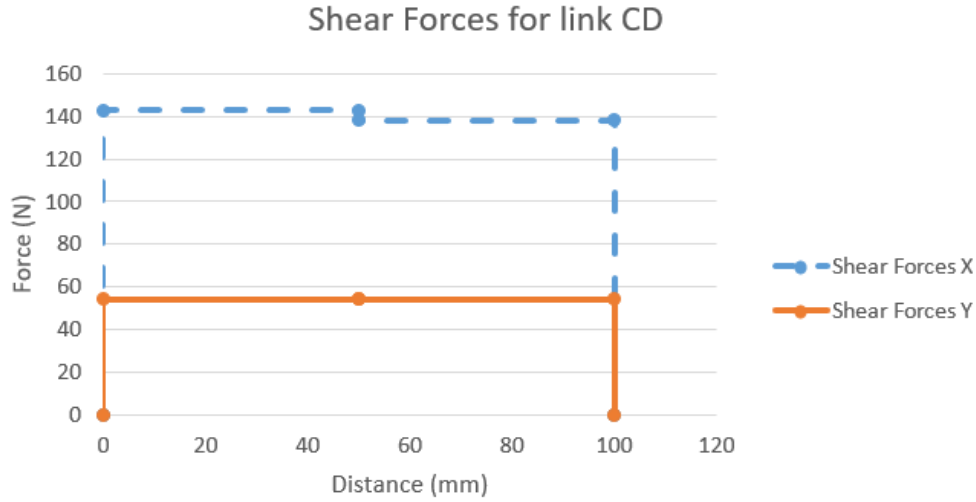


Figure 59: Shear Force Diagram for link CD

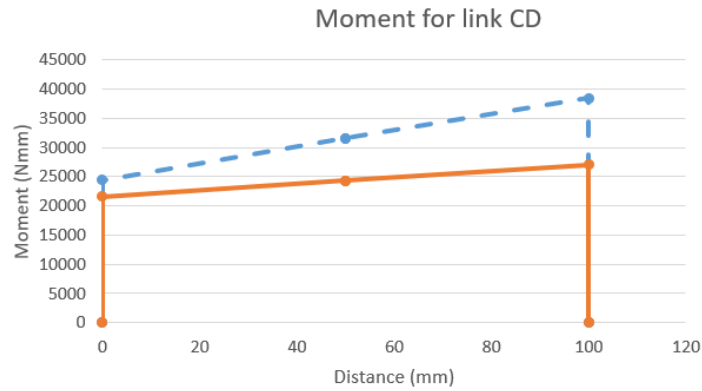


Figure 60: Moment Diagram for link CD

B.4 Ball Bearings

Originally it was decided to use ball or roller bearings for the shafts in order to limit friction. However, as this application is mostly static, reasonably sized bearings were unable to resist the static radial forces and thus sleeve bearings (bushings) were selected instead. The following equation was used to calculate the required rated capacity C_{req} of the ball bearings [14]:

$$C_{req} = F_e K_a \left(\frac{L}{K_r L_R} \right)^{0.3} \quad (183)$$

where K_a is the application factor, K_r is the reliability factor, L_R is the rated life in revolutions, L is the required life in rpm and F_e is the equivalent force, which is dependant on the ratio of axial to radial forces. As an example the value for required rated capacity is calculated for the exterior knee shaft. The values of $K_a = 1.4$ for light impact and $K_r = 1.0$ for 90% reliability are chosen based on the Juvinall textbook suggestions [14]. A life of 10000 hours is chosen as the application is used intermittently and requires good reliability. Using the maximum speed of 1.6 rpm, we can get the value of $L = 960000$ revolutions. The value of $L_R = 10^6$ revolutions is chosen to match the value used by the observed manufacturer (NTN Bearings) [23]. As the radial force on the bearings is much larger than the axial force, we get that $F_e = F_{radial} = 1124.1N$. We can now get the required rated capacity for the bearing:

$$C_{req} = 1124.1N(1.4)\left(\frac{960000rev}{(1.0)(10^6rev)}\right)^{0.3} = 12.3kN \quad (184)$$

From the NTN bearings catalogue [23], a medium load ball bearing of the appropriate size for this shaft (13 mm diameter) can only support about 10.3 kN dynamic and 4.6 kN static load. The dynamic rating could be achievable by increasing the size of the shaft slightly, but the static rating is extremely low and not feasible. This analysis is what led to the selection of sleeve bearings (or bushings).

B.5 Sleeve Bearing Friction

As this application is mostly static or at very low speeds, the bushing is submitted to boundary lubrication [14]. An approximation of the friction coefficient was attempted using Petroff's equation [14]:

$$f = \frac{2\pi^2\mu n(d/2)}{Pc} \quad (185)$$

where μ is the absolute viscosity in Pa s and c is the clearance between the shaft and bushing in mm. Absolute viscosity values were difficult to find. A conservative estimate was made, using the Temperature-Grade-Viscosity graph provided in the Juvinall textbook [14]. The highest viscosity grade (SAE 70) was chosen, and assumed to be operating at 30 degrees celsius. This temperature is selected as a reasonable temperature that might be found in the bushing on a cold day (with added friction and electronics heat). This gives an absolute viscosity of 1000 mPas, which is a relatively high value and will give a high estimate of the

friction. For the clearance in the bushing, it was found that the ratio of the shaft radius and clearance is generally between 500-1000, therefore a ratio of 1000 was selected as worst case scenario [14]. The value of the friction (drag) torque T_f is then found with the following equation [14], where F is the radial force applied on the bearing.

$$T_f = fF(d/2) \quad (186)$$

For a sample calculation on the exterior knee shaft bearings, the bearing friction coefficient is found using Equation 185, with $\mu = 1000mPas$, $c = \frac{d/2}{1000} = 0.0065mm$, $n = 1.60rpm$ and $d = 13.0mm$. The actual value of pressure P must be calculated first using Equation 123. Then, the drag torque is found using Equation 186.

$$P = \frac{F}{dL} = \frac{1124.1N}{13.0mm \times 4.0mm} \times = 21.6MPa \quad (187)$$

$$f = \frac{2\pi^2\mu n(d/2)}{Pc} = \frac{2\pi^2 \times 1Pas \times (1.60/60)rps \times (13.0mm/2)}{21.6 \times 10^6Pa \times 0.0065mm} = 2.4 \times 10^{-5} \quad (188)$$

$$T_f = fF(d/2) = 2.4 \times 10^{-5} \times 1125.1N \times (13.0mm/2) = 0.18Nmm \quad (189)$$

The friction does not make sense as it was found that friction coefficients for boundary lubrication should be about 0.05-0.20 [14]. The calculated value is extremely low. This might be due to the fact that the Petroff equation assumes no eccentricity, which would not be the case for boundary lubrication. The rotation speed in this application is also low, which causes the friction coefficient to be very low.

If the highest value of coefficient of friction in the range is chosen ($f = 0.20$), then a drag torque of 1463 Nmm is found, which is less than 5% of the applied torque. Thus, as our friction coefficient is likely lower, friction can be considered negligible.

C Data sheets

Ordering Code

CSD - 20 - 100 - 2A - GR - SP

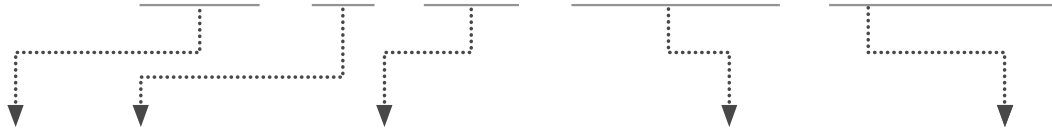


Table 063-1

Series	Size	Ratio*				Model	Special specification
CSD	14	50	80	100	—	2A-GR = component type (2A-R for Size 14, 17)	Blank= Standard product SP= Special specification code BB= Big Bore
	17	50	80	100	120		
	20	50	80	100	120		
	25	50	80	100	120		
	32	50	80	100	120		
	40	50	80	100	120		
	50	50	80	100	120		

* The reduction ratio value is based on the following configuration:
Input: wave generator, fixed: circular spline, output: flexspline

Technical Data

CSD-2A Component Set

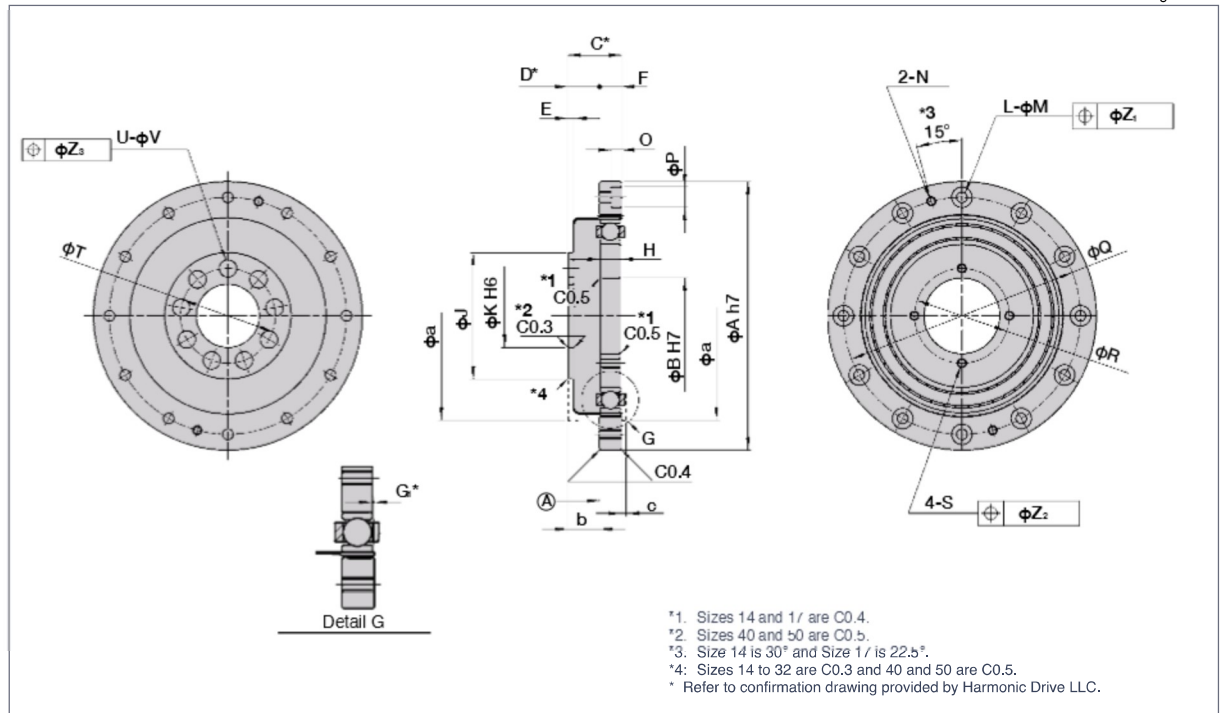
Size	Gear ratio	Rated torque at input speed 2000rpm		Limit for repeated peak torque		Limit for average torque		Limit for momentary peak torque		Maximum input speed (rpm)		Limit for average input speed (rpm)		Moment of inertia	
		Nm	kgfm	Nm	kgfm	Nm	kgfm	Nm	kgfm	Oil	Grease	Oil	Grease	$I \times 10^{-4} \text{kgm}^2$	$J \times 10^{-3} \text{kgfms}^2$
14	50	3.7	0.38	12	1.2	4.8	0.49	24	2.4	14000	8500	6500	3500	0.021	0.021
	80	5.4	0.55	16	1.6	7.7	0.79	31	3.2						
	100	5.4	0.55	19	1.9	7.7	0.79	31	3.2						
17	50	11	1.1	23	2.3	18	1.8	48	4.9	10000	7300	6500	3500	0.054	0.055
	80	15	1.5	29	3.0	19	1.9	55	5.6						
	100	16	1.6	37	3.8	27	2.8	55	5.6						
20	50	17	1.7	39	4.0	24	2.4	69	7.0	10000	6500	6500	3500	0.090	0.092
	80	24	2.4	51	5.2	33	3.4	76 (65)	7.7 (6.6)						
	100	28	2.9	57	5.8	34	3.5	76 (65)	7.7 (6.6)						
25	50	27	2.8	69	7.0	38	3.9	127	13	7500	5600	5600	3500	0.282	0.288
	80	44	4.5	96	9.8	60	6.1	152 (135)	15 (14)						
	100	47	4.8	110	11	75	7.6	152 (135)	15 (14)						
32	50	53	5.4	151	15	75	7.6	268	27	7000	4800	4600	3500	1.09	1.11
	80	83	8.5	213	22	117	12	359 (331)	37 (34)						
	100	96	9.8	233	24	151	15	359 (331)	37 (34)						
40	50	96	9.8	281	29	137	14	480	49	5600	4000	3600	3000	2.85	2.91
	80	144	15	364	37	198	20	685 (580)	70 (59)						
	100	185	19	398	41	260	27	694 (580)	71 (59)						
50	120	205	21	432	44	315	32	694 (580)	71 (59)	4500	3500	3000	2500	8.61	8.78
	50	172	18	500	51	247	25	1000	102						
	80	260	27	659	67	363	37	1300	133						
	100	329	34	686	70	466	48	1440 (1315)	147 (134)						
	120	370	38	756	77	569	58	1441	147 (134)						

- Moment of inertia: $I = \frac{1}{2} GD^2$
- *The maximum allowable momentary torque value marked by an asterisk(*) is restricted by the tightening torque of the flexspline.
- The parenthesized value indicates the value when the bore of the flexspline has the maximum value (BB type).
- See "Rating Table Definitions" on Page 12 for details of the terms.
- When the max allowable momentary torque is expected to be applied, see "Bolt tightening of the flexspline" on p. 75.

Outline Dimensions

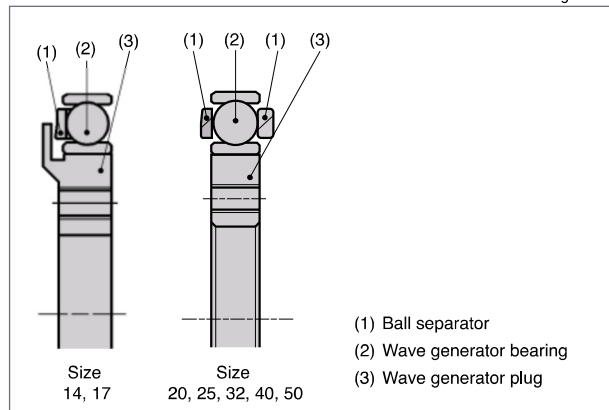
You can download the CAD files from our website: harmonicdrive.net

Fig. 064-1

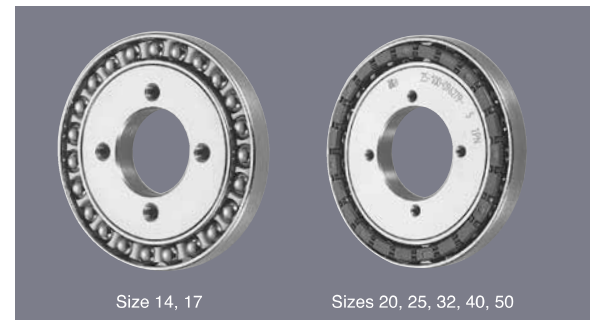


Structure and shape of the wave generator

Fig. 064-2



There is a difference in appearance of the ball separator depending on the size.



Dimensions

 Table 065-1
 Unit : mm

Symbol	Size	14	17	20	25	32	40	50
ϕA h7		50 ⁰ _{-0.025}	60 ⁰ _{-0.030}	70 ⁰ _{-0.030}	85 ⁰ _{-0.035}	110 ⁰ _{-0.035}	135 ⁰ _{-0.040}	170 ⁰ _{-0.040}
ϕB H7		11 ^{+0.018} ₀	15 ^{+0.018} ₀	20 ^{+0.021} ₀	24 ^{+0.021} ₀	32 ^{+0.025} ₀	40 ^{+0.025} ₀	50 ^{+0.025} ₀
C*		11	12.5	14	17	22	27	33
D*		6.5 ^{+0.2} ₀	7.5 ^{+0.2} ₀	8 ^{+0.3} ₀	10 ^{+0.3} ₀	13 ^{+0.3} ₀	16 ^{+0.3} ₀	19.5 ^{+0.3} ₀
E		1.4	1.7	2	2	2.5	3	3.5
F		4.5	5	6	7	9	11	13.5
G ₁ *		0.3 ^{+0.2} ₀	0.3 ^{+0.2} ₀	0.3 ^{+0.2} ₀	0.4 ^{+0.2} ₀	0.5 ^{+0.2} ₀	0.6 ^{+0.2} ₀	0.8 ^{+0.2} ₀
H		4 ⁰ _{-0.1}	5 ⁰ _{-0.1}	5.2 ⁰ _{-0.1}	6.3 ⁰ _{-0.1}	8.6 ⁰ _{-0.1}	10.3 ⁰ _{-0.1}	12.7 ⁰ _{-0.1}
ϕJ		23	27.2	32	40	52	64	80
ϕK H6	Standard	11 ^{+0.011} ₀	11 ^{+0.011} ₀	16 ^{+0.011} ₀	20 ^{+0.013} ₀	30 ^{+0.013} ₀	32 ^{+0.016} ₀	44 ^{+0.016} ₀
	BB spec.	11 ^{+0.011} ₀	11 ^{+0.011} ₀	20 ^{+0.013} ₀	24 ^{+0.013} ₀	32 ^{+0.016} ₀	40 ^{+0.016} ₀	50 ^{+0.016} ₀
L		6	8	12	12	12	12	12
ϕM		3.4	3.4	3.4	3.4	4.5	5.5	6.6
N		M3	M3	M3	M3	M4	M5	M6
O		—	—	3.3	3.3	4.4	5.4	6.5
ϕP		—	—	6.5	6.5	8	9.5	11
ϕQ		44	54	62	75	100	120	150
ϕR		17	21	26	30	40	50	60
S		M3	M3	M3	M3	M4	M5	M6
ϕT	Standard	17	19.5	24	30	41	48	62
	BB spec.	17	19.5	26	32	42	52	65
U	Standard	9	8	9	9	11	10	11
	BB spec.	9	8	12	12	14	14	14
ϕV	Standard	3.4	4.5	4.5	5.5	6.6	9	11
	BB spec.	3.4	4.5	3.4	4.5	5.5	6.6	9
ϕZ_1		0.2	0.2	0.2	0.2	0.25	0.25	0.3
ϕZ_2		0.25	0.25	0.2	0.2	0.25	0.25	0.3
ϕZ_3	Standard	0.2	0.25	0.25	0.25	0.3	0.5	0.5
	BB spec.	0.2	0.25	0.2	0.25	0.25	0.3	0.5
Minimum housing clearance	ϕa	38	45	53	66	86	106	133
	b	6.5	7.5	8	10	13	16	19.5
	c	1	1	1.5	1.5	2	2.5	3.5
Mass (kg)		0.06	0.10	0.13	0.24	0.51	0.92	1.9

(Note) Standard dimension for size 14 and 17 is the maximum bore.

- Surface A is the recommended mounting surface.
- The following dimensions can be modified to accommodate customer-specific requirements.

Wave Generator: B
 Flexspline: U and V
 Circular Spline: L and M

- *C, D and G₁ values indicate relative position of individual gearing components (wave generator, flexpline, circular spline). Please strictly adhere to these values when designing your housing and mating parts.
- Due to the deformation of the Flexspline during operation, it is necessary to provide a minimum housing clearance, dimensions ϕa , b, c

The wave generator, flexspline, and circular spline are not assembled when delivered.

Positional accuracy

See "Engineering data" for a description of terms.

Table 066-1

Ratio		14	17	20	25	32	40	50
Positional Accuracy	$\times 10^{-4}$ rad	4.4	4.4	2.9	2.9	2.9	2.9	2.9
	arc min	1.5	1.5	1.0	1.0	1.0	1.0	1.0

Hysteresis loss

See "Engineering data" for a description of terms.

Table 066-2

Ratio		Size	14	17	20	25	32	40	50
50	$\times 10^{-4}$ rad		7.3	5.8	5.8	5.8	5.8	5.8	5.8
	arc min		2.5	2.0	2.0	2.0	2.0	2.0	2.0
80 or more	$\times 10^{-4}$ rad		5.8	2.9	2.9	2.9	2.9	2.9	2.9
	arc min		2.0	1.0	1.0	1.0	1.0	1.0	1.0

Torsional stiffness

See "Engineering data" for a description of terms.

Table 066-3

Symbol		Size	14	17	20	25	32	40	50	
T_1	Nm		2.0	3.9	7.0	14	29	54	108	
	kgfm		0.2	0.4	0.7	1.4	3.0	5.5	11	
T_2	Nm		6.9	12	25	48	108	196	382	
	kgfm		0.7	1.2	2.5	4.9	11	20	39	
Reduction ratio 50	K_1	$\times 10^4$ Nm/rad	0.29	0.67	1.1	2.0	4.7	8.8	17	
		kgfm/arc min	0.085	0.2	0.32	0.6	1.4	2.6	5.0	
	K_2	$\times 10^4$ Nm/rad	0.37	0.88	1.3	2.7	6.1	11	21	
		kgfm/arc min	0.11	0.26	0.4	0.8	1.8	3.4	6.3	
	K_3	$\times 10^4$ Nm/rad	0.47	1.2	2.0	3.7	8.4	15	30	
		kgfm/arc min	0.14	0.34	0.6	1.1	2.5	4.5	9	
	θ	$\times 10^{-4}$ rad	6.9	5.8	6.4	7.0	6.2	6.1	6.4	
		arc min	2.4	2.0	2.2	2.4	2.1	2.1	2.2	
	θ	$\times 10^{-4}$ rad	19	14	19	18	18	18	18	
		arc min	6.4	4.6	6.6	6.1	6.1	5.9	6.2	
	Reduction ratio 80 or more	K_1	$\times 10^4$ Nm/rad	0.4	0.84	1.3	2.7	6.1	11	21
			kgfm/arc min	0.12	0.25	0.4	0.8	1.8	3.2	6.3
K_2		$\times 10^4$ Nm/rad	0.44	0.94	1.7	3.7	7.8	14	29	
		kgfm/arc min	0.13	0.28	0.5	1.1	2.3	4.2	8.5	
K_3		$\times 10^4$ Nm/rad	0.61	1.3	2.5	4.7	11	20	37	
		kgfm/arc min	0.18	0.39	0.75	1.4	3.3	5.8	11	
θ		$\times 10^{-4}$ rad	5.0	4.6	5.4	5.2	4.8	4.9	5.1	
		arc min	1.7	1.6	1.8	1.8	1.7	1.7	1.7	
θ		$\times 10^{-4}$ rad	16	13	15	13	14	14	13	
		arc min	5.4	4.3	5.0	4.5	4.8	4.8	4.6	

* The values in this table are reference values. The minimum value is approximately 80% of the displayed value.

Starting torque

See "Engineering data" for a description of terms. Please use as reference values; the values vary based on use conditions.

Table 067-1
Unit: Ncm

Ratio \ Size	14	17	20	25	32	40	50
50	3.7	5.7	7.3	14	28	50	94
80	2.7	3.8	4.8	8.8	19	32	63
100	2.4	3.3	4.3	7.9	18	29	56
120	—	3.1	3.8	7.2	16	27	53

Backdriving torque

See "Engineering data" for a description of terms. Please use as reference values; the values vary based on use conditions.

Table 067-2
Unit: Nm

Ratio \ Size	14	17	20	25	32	40	50
50	2.5	3.8	4.4	8.3	17	30	57
80	2.6	3.7	4.9	8.8	19	32	62
100	3.1	4.1	5.2	9.6	21	35	67
120	—	4.5	5.7	11	22	38	74

Ratcheting torque

See "Engineering data" for a description of terms.

Table 067-3
Unit: Nm

Ratio \ Size	14	17	20	25	32	40	50
50	60	105	150	315	685	1260	2590
80	75	140	245	475	980	1960	3780
100	55	110	180	350	700	1470	2870
120	—	80	165	325	685	1330	2660

Buckling torque

See "Engineering data" for a description of terms.

Table 067-4
Unit: Nm

Size	14	17	20	25	32	40	50
All ratios	190	330	560	1000	2200	4300	8000

No-load running torque

No-load running torque is the torque which is required to rotate the input side (high speed side), when there is no load on the output side (low speed side).

Measurement condition

Table 068-1

Ratio 100:1			
Lubricant	Grease lubrication	Name	Harmonic Grease SK-1A (size 20 or larger)
			Harmonic Grease SK-2 (size 14, 17)
		Quantity	Recommended quantity (See page 71)
Torque value is measured after 2 hours at 2000rpm input.			

* Contact us for oil lubrication.

■ Compensation value in each ratio

No load running torque of the gear varies with ratio. The graphs indicate a value for ratio 100. For other gear ratios, add the compensation values from table on the right.

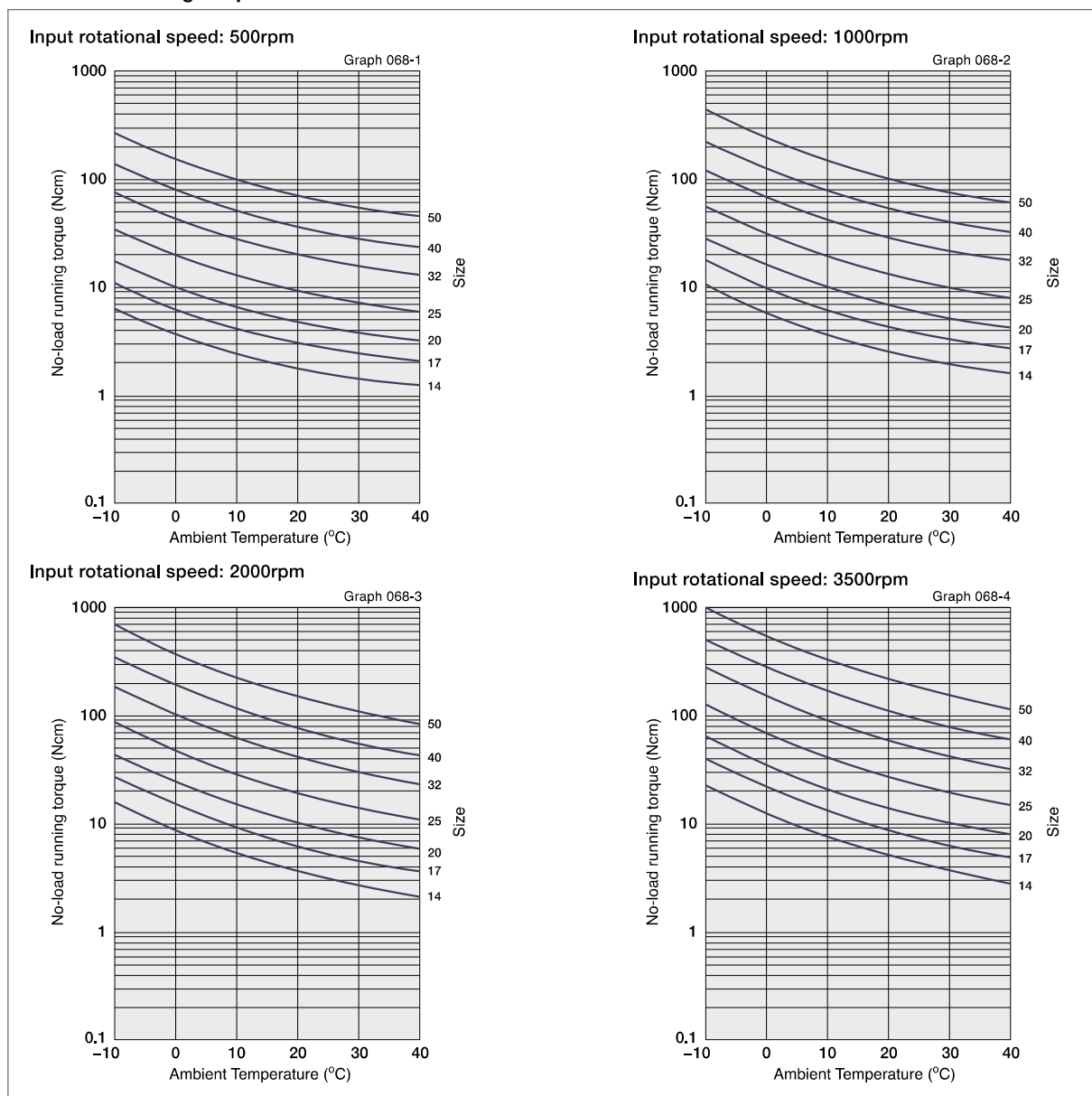
Compensation coefficient for no-load running torque

Table 068-2

Unit: Ncm

Size	Ratio	50
14		+0.56
17		+0.95
20		+1.4
25		+2.6
32		+5.4
40		+9.6
50		+18

■ No-load running torque for a reduction ratio of 100



* The values in this graph are average value "X".

Efficiency

The efficiency varies depending on the following conditions.

- Reduction ratio
- Input rotational speed
- Load torque
- Temperature
- Lubrication (Type and quantity)

■ Efficiency compensation coefficient

If the load torque is lower than the rated torque, the efficiency value decreases. Calculate the compensation coefficient K_e from Graph 069-1 to calculate the efficiency using the following calculation example.

* Efficiency Compensation coefficient $K_e=1$ holds when the load torque is greater than the rated torque.

Measurement condition

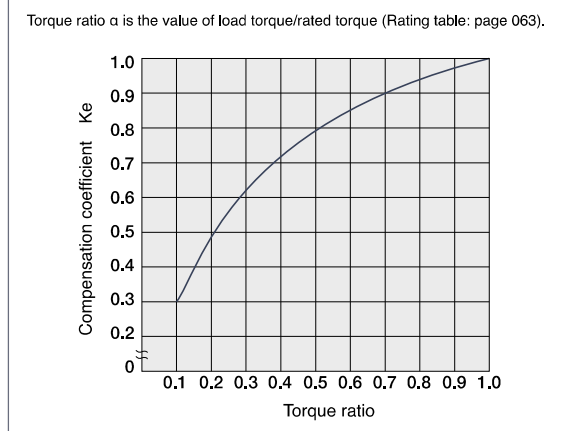
Table 069-1

Installation	Based on recommended tolerance		
Load torque	The rated torque shown in the rating table (see page 63)		
* When load torque is smaller than rated torque, the efficiency value is lowered. See efficiency compensation coefficient below.			
Lubricant	Grease lubrication	Name	Harmonic Grease SK-1A (size 20 or larger)
			Harmonic Grease SK-2 (size 14, 17)
		Quantity	Recommended quantity (see page 71)

* Contact us for oil lubrication.

Efficiency compensation coefficient

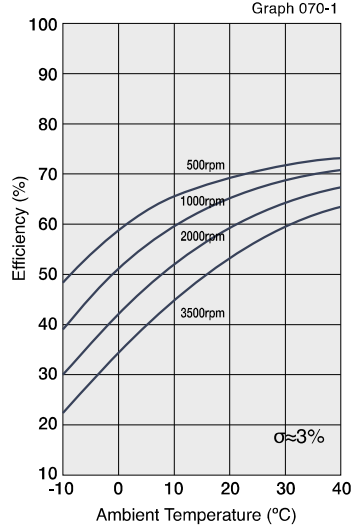
Graph 069-1



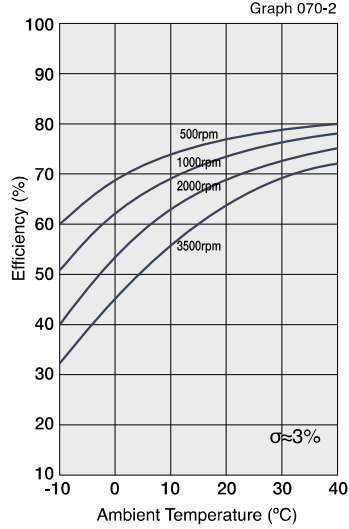
■ Efficiency at rated torque

Reduction ratio 50:1

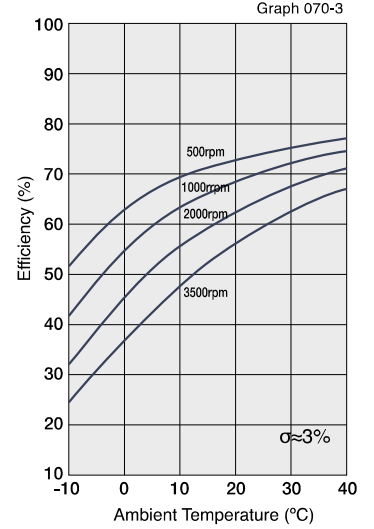
Size 14



Size 17, 20

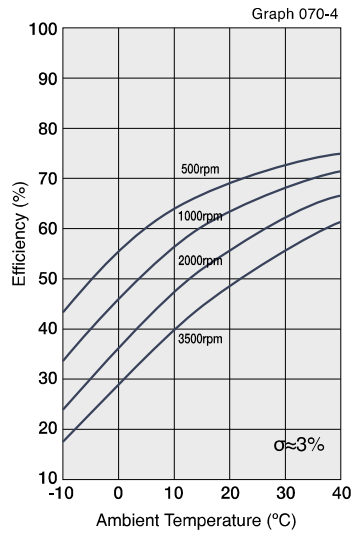


Size 25, 32, 40, 50

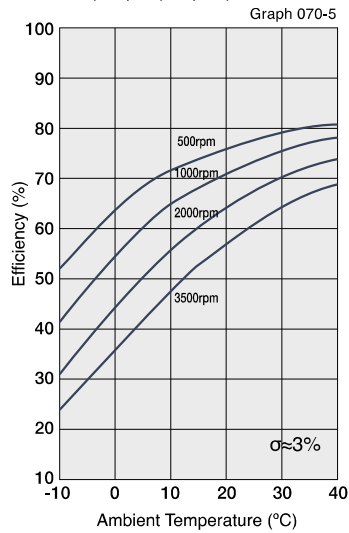


Reduction ratio 80, 100, 120:1

Size 14



Size 17, 20, 25, 32, 40, 50

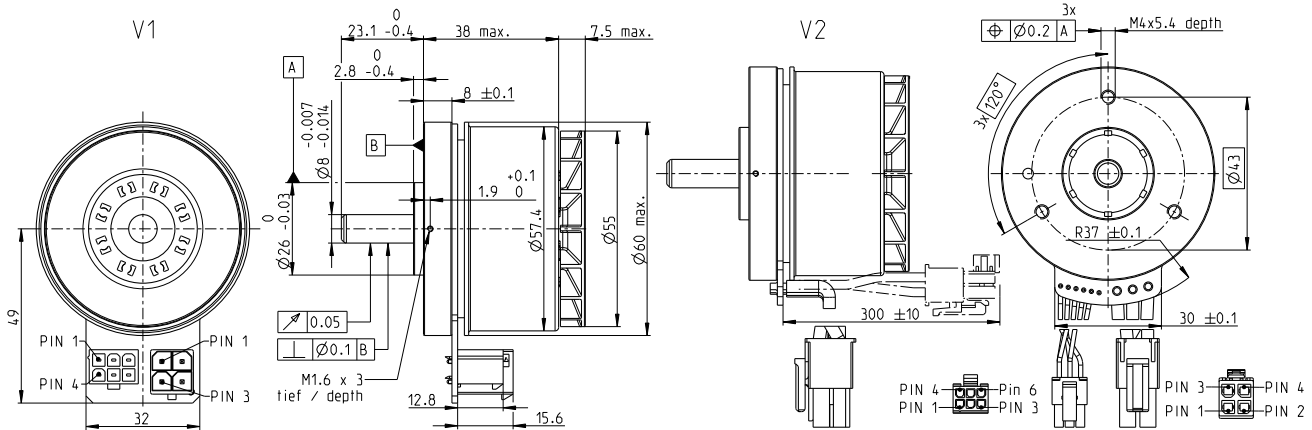


EC 60 flat Ø60 mm, brushless, 200 Watt

Ventilated

NEW

maxon flat motor



M 1:2

- Stock program
- Standard program
- Special program (on request)

Part Numbers

	V1 with Hall sensors	614949	625861
V2 with Hall sensors and cables	647696	642221	647697

Motor Data

Values at nominal voltage		12	24	48
1 Nominal voltage	V	12	24	48
2 No load speed	rpm	3760	4300	4020
3 No load current	mA	815	497	224
4 Nominal speed	rpm	2790	3240	3020
5 Nominal torque (max. continuous torque)	mNm	492	536	577
6 Nominal current (max. continuous current)	A	15.1	9.28	4.6
7 Stall torque ¹	mNm	3340	4300	4870
8 Stall current	A	111	81.9	43.2
9 Max. efficiency	%	83.8	85.2	86.3
Characteristics				
10 Terminal resistance phase to phase	Ω	0.108	0.293	1.11
11 Terminal inductance phase to phase	mH	0.0911	0.279	1.28
12 Torque constant	mNm/A	30	52.5	113
13 Speed constant	rpm/V	318	182	84.8
14 Speed/torque gradient	rpm/mNm	1.14	1.01	0.837
15 Mechanical time constant	ms	9.95	8.83	9.29
16 Rotor inertia	gcm ²	832	832	832

Specifications

Thermal data	
17 Thermal resistance housing-ambient	1.22 K/W
18 Thermal resistance winding-housing	0.843 K/W
19 Thermal time constant winding	9.19 s
20 Thermal time constant motor	44 s
21 Ambient temperature	-40...+100°C
22 Max. winding temperature	+125°C
Mechanical data (preloaded ball bearings)	
23 Max. speed	6000 rpm
24 Axial play at axial load < 12.0 N	0 mm
> 12.0 N	0.14 mm
25 Radial play	preloaded
26 Max. axial load (dynamic)	12 N
27 Max. force for press fits (static) (static, shaft supported)	170 N
28 Max. radial load, 5 mm from flange	8000 N
112 N	

Other specifications

29 Number of pole pairs	7
30 Number of phases	3
31 Weight of motor	360 g

Values listed in the table are nominal.

Connection V1

Pin	V1	V2 (sensors, AWG 24)
Pin 1	Hall sensor 1	Hall sensor 1
Pin 2	Hall sensor 2	Hall sensor 2
Pin 3	V _{Hall} 4.5...24 VDC	Hall sensor 3
Pin 4	Hall sensor 3	GND
Pin 5	GND	V _{Hall} 4.5...24 VDC
Pin 6	N.C.	N.C.

V2 (Motor, AWG 14)

Pin 1	Motor winding 1	Motor winding 1
Pin 2	Motor winding 3	Motor winding 2
Pin 3	Motor winding 2	Motor winding 3
Pin 4		N.C.

Wiring diagram for Hall sensors see p. 47

Connector Part number

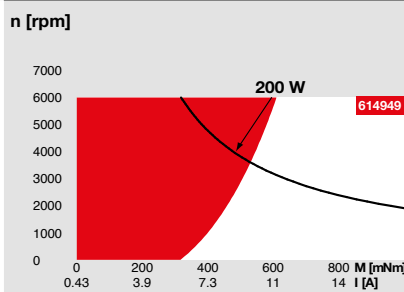
Molex 46015-0606	43025-0600
Molex 76829-0104	171692-0104

Connection cable for V1

Connection cable Universal, L = 500 mm **651900**

¹Calculation does not include saturation effect (p. 57/162)

Operating Range



Comments

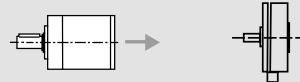
- Continuous operation**
In observation of above listed thermal resistance (lines 17 and 18) the maximum permissible winding temperature will be reached during continuous operation at 25°C ambient.
= Thermal limit.
- Short term operation**
The motor may be briefly overloaded (recurring).
- Assigned power rating**

maxon Modular System

Details on catalog page 36

Planetary Gearhead

Ø52 mm
4 - 30 Nm
Page 367



Recommended Electronics:

Notes	Page 36
ESCON Module 50/5	455
ESCON Mod. 50/8 (HE)	456
ESCON 50/5	457
ESCON 70/10	457
DEC Module 50/5	459

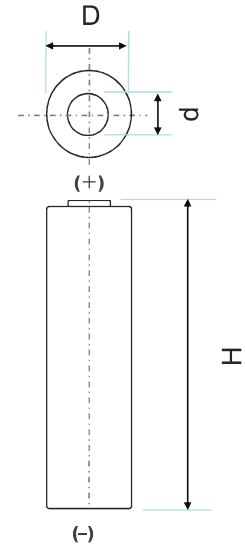
Specifications

Rated capacity ⁽¹⁾		2980mAh	2910mAh
Capacity ⁽²⁾	Minimum	3030mAh	2935mAh
	Typical	3180mAh	3080mAh
Nominal voltage		3.6V	
Charging	Method	CC-CV	
	Voltage	4.20V	4.15V
	Current	Std. 0.3CA	
Weight (max.) Without tube		49.5g	
Temperature	Charge	10 to +45° C	
	Discharge	-20 to +60° C	
	Storage	-20 to +50° C	
Energy density ⁽³⁾	Volumetric	630 Wh/l	615 Wh/l
	Gravimetric	217 Wh/kg	212 Wh/kg

⁽¹⁾ At 20° C ⁽²⁾ At 25° C

⁽³⁾ Energy density is calculated using bare cell dimensions (without tube).

Dimensions



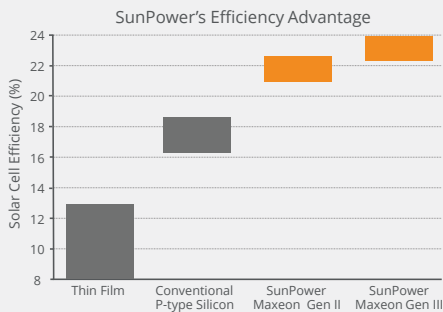
Without tube	H	Max. 65.10mm
	D	Max. 18.25mm
	d	Max. 6.6mm

When designing a pack, refer to the cell's mechanical drawing for precise dimensions.

MAXEON™ GEN III SOLAR CELLS

Power Advantage

SunPower designs, manufactures, and delivers high-performance solar electric technology worldwide. SunPower™ cells produce 25-35% more power compared to Conventional Cells¹ with outstanding aesthetics.



Energy Advantage

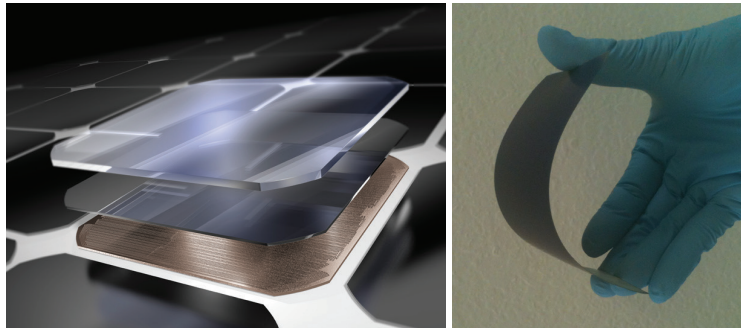
SunPower panels deliver the highest energy per rated watt compared to a Conventional Panel. (Photon International, Mar 2013, out of 151 panels tested).

- No Light-Induced Degradation = 2 - 3% more energy.
- No Temperature Coefficient = 1 - 2% more energy at 35-40°C ambient temperature.
- Low Light and Broad Spectral Response = up to 1% more energy in overcast and low-light conditions.

¹ As used throughout, "Conventional Cells" are silicon cells that have many thin metal lines on the front and 2 or 3 interconnect ribbons soldered along the front and back. "Conventional Panel" means a panel with 240W, 15% efficiency and approximately 1.6 m² made with Conventional Cells.

Durability Advantage

The Maxeon cell has strength and durability to survive extreme conditions year after year, enabling SunPower to provide superior, long-term performance in a broad range of applications.



- Corrosion Resistance: SunPower's tin-copper metal system is more corrosion resistant compared to the porous metal paste used in Conventional Cells, which can crack more easily and corrode.
- Crack Resistance: SunPower's cells are thinner and more flexible than Conventional Cells. When a SunPower cell does crack, the backside copper metal foundation keeps the cell intact and maintains a high power output. When Conventional Cells crack, the cell breaks apart with typically a significant loss of power.
- Eco-Friendly: SunPower cells solder to lead-free components and are RoHS compliant. Conventional Cells often require components with lead.



Photo courtesy of Hans-Peter van Velthoven

Optifuel Lab 2 Renault Trucks laboratory vehicle

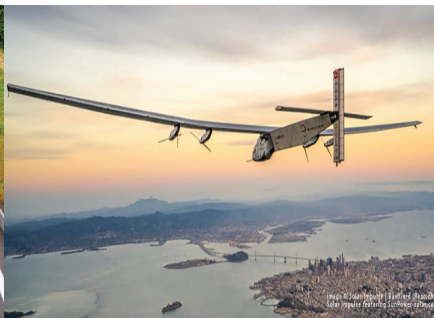


Photo courtesy of Phil Shar Racing



Photo courtesy of philsharacing.com

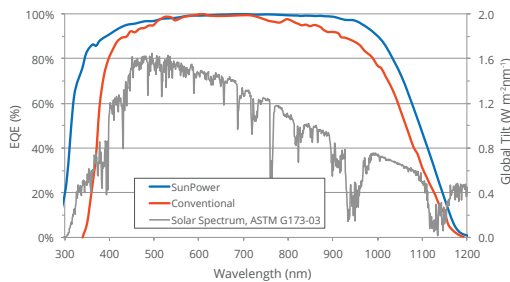
MAXEON™ GEN III SOLAR CELLS

Electrical Characteristics of a typical Maxeon Gen III Cell At Standard Test Conditions (STC) STC: 1000W/m², AM 1.5G and cell temp 25°C

	Cell Bin	P _{mp} (Wp)	Eff. (%)	V _{mp} (V)	I _{mp} (A)	V _{oc} (V)	I _{sc} (A)
Ultra Peak Performance	Me1	3.72	24.3	0.632	5.89	0.730	6.18
Ultra Premium Performance	Le1	3.62	23.7	0.621	5.84	0.721	6.15
Ultra High Performance	Ke1	3.54	23.1	0.612	5.79	0.713	6.11

Electrical parameters are nominal values.
Temp. Coefficients in SunPower Panels: Voltage: -1.74mV/°C, Current: 2.9mA/°C, Power: -0.29%/°C

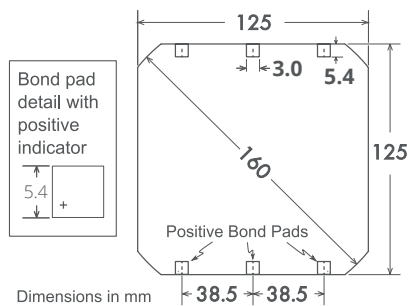
Spectral Response



References
SunPower: NREL data, commissioned by SPWR
Conventional: Progress in Photovoltaics: Research and Applications, Solar cell efficiency tables, version 36 18(5), (2010) 46–352

Cell Physical Characteristics

Wafer: Monocrystalline silicon
Design: All back contact
Front: Uniform, black antireflection coating
Back: Tin-coated, copper metal grid
Cell Area: Approximately 153cm²
Cell Weight: Approximately 6.5grams
Cell Thickness: 150µm +/- 30µm



Bond pad area dimensions are 5.4mm x 3.0mm
Metal finger pitch between positive and negative fingers is 471µm.
Positive/Negative pole bond pad sides have "+/-" indicators on leftmost and rightmost bond pads

Positive Electrical Grounding

If cell voltage is below frame ground the cell power output will be reduced. Therefore, modules and systems produced using these cells should be configured as "positive ground systems." If this creates a problem, please consult with SunPower.

Interconnect Tab and Process Recommendations



SunPower recommends customers use SunPower's patented tin-plated copper strain-relieved interconnect tabs, which can be purchased from SunPower. These interconnects are easily solderable and compatible with lead free processing. Tabs weigh approximately 0.3 grams.

Our patented interconnect tabs are packaged in boxes of 3600 or 36,000 each.

<http://us.sunpower.com/about/sunpower-technology/patents/>

Production Quality

ISO 9001:2015 certified

Soft handling procedures to reduce breakage and crack formation

100% cell performance testing and visual inspection

Packaging

Cells are packed in boxes of 1500 each; grouped in 10 shrink-wrapped stacks of 150 with interleaving. 24 boxes are packed in a water-resistant "Master Carton" containing 36,000 cells suitable for air transport.

Purchase Terms

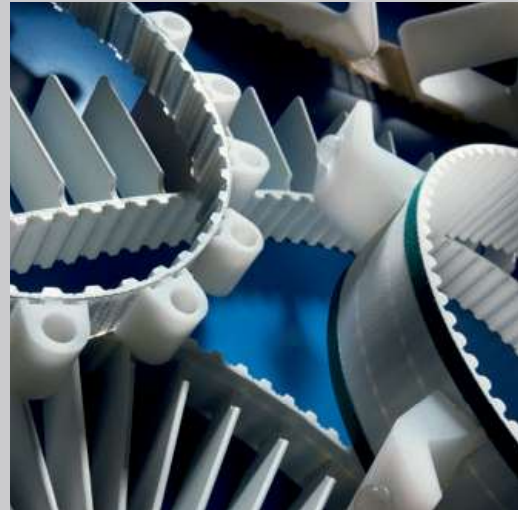
Customers shall not reverse engineer, disassemble or analyze the Solar Cells or any prototype, process, product, or other item that embodies Confidential Information of SunPower. Customers shall not cause or allow any inspection, analysis, or characterization of any properties (whether mechanical, structural, chemical, electrical, or otherwise) of the Solar Cells, whether by itself or by a third party.

Customer agrees that it will not transfer (whether by sale, loan, gift, or other conveyance) the Solar Cells from its possession.

SunPower solar cells are provided "AS IS" without warranty.

Full terms and conditions are in the Cell Purchase Agreement

Urethane Belt Program



Urethane Timing Belts and Pulleys

Table of Contents

Tooth Pitch Comparison 4

Linear Belts

Linear Belt Overview 5

Linear Belt Applications 6

Linear Belt Specifications 7

 Imperial Pitch Belts 10

 T Pitch Belts 11

 AT Pitch Belts 12

 HTD® and STD Pitch Belts 13

Self Tracking Belts 14

 Integral V-Guide Specifications 16

Sealed Belting 19

Wide Belt Overview 21

 Wide Belt Specifications 22

Truly Endless Belts

Truly Endless Belt Overview 23

Flex Belts 24

Gates Synchro-Power® (Cast) Belts 25

Flat Belts

Flat Belt Overview 29

Flat Belt Specifications 30

Design Recommendations 32

Profiled Belts

Profiled Belts Overview 33

Design Recommendations 34

QuickShip Profile Program 37

Backings

Backings Overview 39

Backings Specifications 42

Fabrication

Fabrication Capabilities 44

Special Processing

Custom Finishing Capabilities 45

Timing Pulleys and Clamps

Pulley Overview 46

Custom Pulley Program 47

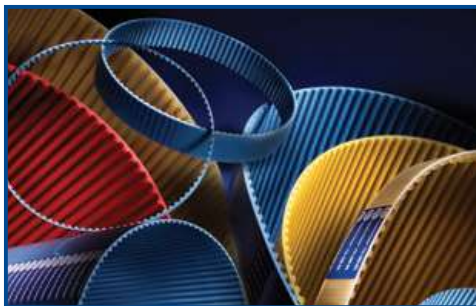
Clamp Plates 49

Tools and Reference

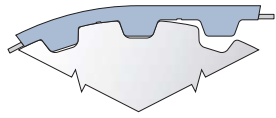
Notes 51

Contact Information 52

Broadest Range Available

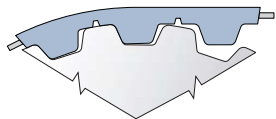


Industrial Tooth Pitch Comparison



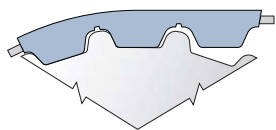
Imperial Pitch Belts - XL, L, H, XH

This classic trapezoidal pitch is the original timing belt tooth design. This tooth pitch is commonly used for **conveying applications**. The tooth profile is fairly low and has a large surface area at the tip of the tooth providing good support on sliding conveyor surfaces.



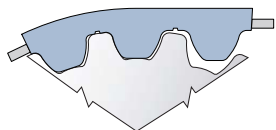
T Pitch Belts - T2.5, T5, T10, T20

These metric trapezoidal pitches are similar to imperial pitches, also commonly used for **conveying applications**, yet have a slightly deeper tooth engagement than imperial profiles. The tooth meshing is more reliable. However, backlash can be slightly greater.



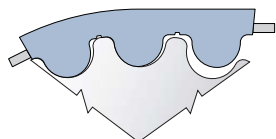
AT Pitch Belts - AT5, AT10, AT20

This pitch was developed to enable higher load carrying capacity combined with low backlash. The stronger and stiffer tooth makes these belts ideal for **linear positioning and motion control**, but may require larger pulley diameters.



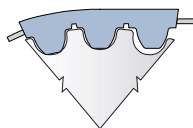
STD Pitch Belts - STD5, STD8

This tooth pitch provides superior load distribution, low backlash, and **reduced wear and noise** characteristics. It is an excellent profile for **linear positioning and power transmission** applications.



HTD Pitch Belts - HTD5, HTD8, HTD14

This rounded tooth pitch is similar to STD, and is also an excellent profile for **linear and rotary positioning and power transmission** applications, yet has deeper tooth engagement. Note that the HTD pitch may exhibit slight increases in noise and wear.



GMT3

This modified profile is available in widths 10" to 18". It is appropriate for non "knife edge" applications as the minimum pulley diameter is 0.75".

Linear Belt Specifications

Refer to these product notes in reviewing the Linear Belt Specifications pages that follow

Calculating Belt Weight

Imperial Units

Belt Weight = (Specific Belt Wt, lbf/ft/in) x (Belt Length, ft) x (Belt Width, in)

e.g. 200 ft of H600, Steel Cord

Belt Weight = 79 lbs = (0.066 lbf/ft/in) x (200 ft) x (6 in)

Metric Units

Belt Weight = (Specific Belt Wt, kgf/m/cm) x (Belt Length, m) x (Belt Width, cm)

e.g. 100 meters of 150T10, Steel Cord

Belt Weight = 111 kg = (0.074kgf/m/cm) x (100 m) x (15 cm)

Service Temperature Range

-5° C to 70° C (23° F to 158° F)

Hardness

92 Shore A - Standard PU, 85 Shore A - FDA Compliant PU

Coefficient of Friction

Urethane vs. UHMWPE (dry)

Urethane vs. Steel (dry)	0.5 to 0.7
Urethane vs. Aluminum (dry)	0.5 to 0.6
Urethane vs. UHMWPE (dry)	0.2 to 0.4
Nylon vs. Steel (dry)	0.2 to 0.4
Nylon vs. UHMWPE (dry)	0.1 to 0.3

- Most belts are available with Nylon Fabric on either or both sides.
For Nylon on the tooth side, specify "NT"
For Nylon on the back side, specify "NB"
For Nylon on both sides, specify "NTB"
Note: Nylon on tooth side is NOT available on HTD5 Steel or Kevlar in widths greater than 50 mm.
- Belting produced to specific length tolerance is available upon request.
- Many linear positioning applications require belts of a specific length tolerance, or a "minus pitch tolerance." Gates Mectrol can produce belts to specific minus tolerances. Consult a Gates Mectrol Applications Engineer to determine the proper length tolerance calculation.

Linear Belt Specifications

			XL	L	H	XH	T5	AT5	ATL5	T10	
Pitch (Imperial and Metric)			.200"	.375"	.500"	.875"	5 mm	5 mm	5 mm	10 mm	
Ultimate Tensile Strength per Inch or 25 mm Belt Width	Steel	lbf/in	759	1474	1605	3204	759	1602	2369	1605	
		N/25 mm	3375	6555	7140	14250	3375	7125	10540	7140	
	Kevlar	lbf/in	1882	1727	1818	3639	1200	1877	N/A	1818	
		N/25 mm	8370	7682	8085	16185	5332	8350	N/A	8085	
	Stainless Steel	lbf/in	N/A	N/A	N/A	N/A	N/A	N/A	N/A	N/A	
		N/25 mm	N/A	N/A	N/A	N/A	N/A	N/A	N/A	N/A	
	High Flex	lbf/in	N/A	N/A	2369	N/A	N/A	N/A	N/A	N/A	2369
		N/25 mm	N/A	N/A	10540	N/A	N/A	N/A	N/A	N/A	10540
Max. Allowable Belt Tension per Inch or 25 mm Belt Width	Steel	Open Ended	lbf/in	192	371	436	854	189	396	526	429
			N/25 mm	853	1652	1939	3801	840	1761	2340	1909
		Welded	lbf/in	96	186	218	427	94	198	198	214
			N/25 mm	427	826	970	1900	420	880	880	954
	Kevlar	Open Ended	lbf/in	209	276	243	400	180	272	N/A	239
			N/25 mm	930	1229	1081	1778	801	1210	N/A	1064
		Welded	lbf/in	157	207	182	300	140	204	N/A	179
			N/25 mm	698	922	810	1334	687	908	N/A	798
	Stainless Steel	Open Ended	lbf/in	N/A	N/A	N/A	N/A	N/A	N/A	N/A	N/A
			N/25 mm	N/A	N/A	N/A	N/A	N/A	N/A	N/A	N/A
		Welded	lbf/in	N/A	N/A	N/A	N/A	N/A	N/A	N/A	N/A
			N/25 mm	N/A	N/A	N/A	N/A	N/A	N/A	N/A	N/A
	High Flex	Open Ended	lbf/in	N/A	N/A	534	N/A	N/A	N/A	N/A	526
			N/25 mm	N/A	N/A	2377	N/A	N/A	N/A	N/A	2340
		Welded	lbf/in	N/A	N/A	267	N/A	N/A	N/A	N/A	263
			N/25 mm	N/A	N/A	1189	N/A	N/A	N/A	N/A	1170
Allowable Effective Tension for Belt Teeth (15 and more teeth in mesh)			lbf/in	180	360	441	879	200	290	290	380
			N/25 mm	800	1600	1960	3910	890	1290	1290	1690
Specific Belt Weight	Steel	lbf/ft/in	0.036	0.059	0.066	0.180	0.037	0.055	0.062	0.074	
		kgf/m/cm	0.021	0.035	0.039	0.105	0.022	0.032	0.036	0.043	
	Kevlar	lbf/ft/in	0.033	0.052	0.055	0.155	0.033	0.046	N/A	0.062	
		kgf/m/cm	0.019	0.030	0.032	0.091	0.020	0.027	N/A	0.036	
	Stainless Steel	lbf/ft/in	N/A	N/A	N/A	N/A	N/A	N/A	N/A	N/A	
		kgf/m/cm	N/A	N/A	N/A	N/A	N/A	N/A	N/A	N/A	
	High Flex	lbf/ft/in	N/A	N/A	0.072	N/A	N/A	N/A	N/A	N/A	0.079
		kgf/m/cm	N/A	N/A	0.042	N/A	N/A	N/A	N/A	N/A	0.046
Specific Belt Stiffness (Open Ended)	Steel	lbf/in	47950	92800	109000	213600	47950	100500	133600	109000	
		N/mm	8400	16255	19085	37410	8400	17605	23400	19085	
	Kevlar	lbf/in	52250	69100	60700	100000	52250	69100	N/A	60700	
		N/mm	9155	12100	10635	17500	9155	12100	N/A	10635	
	Stainless Steel	lbf/in	N/A	N/A	N/A	N/A	N/A	N/A	N/A	N/A	
		N/mm	N/A	N/A	N/A	N/A	N/A	N/A	N/A	N/A	
	High Flex	lbf/in	N/A	N/A	133600	N/A	N/A	N/A	N/A	N/A	133600
		N/mm	N/A	N/A	23400	N/A	N/A	N/A	N/A	N/A	23400
Min. No. of Pulley Teeth	Steel and Kevlar		10	10	14	18	10	15	15	14	
	Stainless Steel		N/A	N/A	N/A	N/A	N/A	N/A	N/A	N/A	
	High Flex		N/A	N/A	12	N/A	N/A	N/A	N/A	12	
Min. Pitch Diameter (Inch or mm)	Steel and Kevlar	inch or mm	.64"	1.19"	2.23"	5.01"	16 mm	24 mm	24 mm	45 mm	
		mm	N/A	N/A	N/A	N/A	N/A	N/A	N/A	N/A	
	High Flex	inch or mm	N/A	N/A	1.91"	N/A	N/A	N/A	N/A	38 mm	
Min. Diameter of Tensioning Idler Running on Back of Belt	Steel and Kevlar	in/mm	1.125"/30mm	2.375"/60mm	3.125"/80mm	5.875"/150mm	1.125"/30mm	2.375"/60mm	2.375"/60mm	3.125"/80mm	
		in/mm	N/A	N/A	N/A	N/A	N/A	N/A	N/A	N/A	
	High Flex	in/mm	N/A	N/A	2.375"/60mm	N/A	N/A	N/A	N/A	2.375"/60mm	
Available in FDA Compliant Construction (85 Shore A Urethane)			Yes	Yes	Yes		Yes			Yes	
Standard Colors (N=Natural, W=White)			N	N	N,W	N	N,W	W	W	N,W	

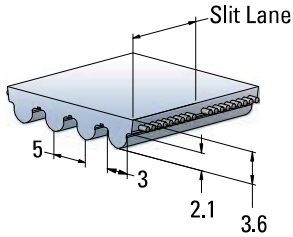
The specifications listed are based on Gates Mectrol's experience. However, our specifications and data do NOT cover all possible belt drive conditions. It is the responsibility of the belt drive system designer to ensure Gates Mectrol's belts are appropriate for a given system and application. The provided data is representative of our in-house experience and does not necessarily match product performance in industrial use.

AT10	ATL10	T20	AT20	ATL20	HTD5	HTD8	HTDL8	HTD14	HTDL14	STD5	STD8
10 mm	10 mm	20 mm	20 mm	20 mm	5 mm	8 mm	8 mm	14 mm	14 mm	5 mm	8 mm
3204	5445	3204	5445	7913	2369	3204	5445	4667	7848	2369	3204
14250	24220	14250	24220	35200	10540	14250	24220	20760	34909	10540	14250
3639	N/A	3639	4900	N/A	1818	3639	4900	4200	N/A	1818	3639
16185	N/A	16185	21798	N/A	8085	16185	21798	18684	N/A	8085	16185
2403	N/A	2403	N/A	N/A	N/A	2403	N/A	N/A	N/A	N/A	N/A
10687	N/A	10687	N/A	N/A	N/A	10687	N/A	N/A	N/A	N/A	N/A
N/A	6059	N/A	N/A	N/A	N/A	2917	6059	5193	N/A	N/A	2917
N/A	26950	N/A	N/A	N/A	N/A	12975	26950	23100	N/A	N/A	12975
841	1317	841	1317	1732	526	841	1317	1159	1718	526	841
3741	5860	3741	5860	7705	2340	3741	5860	5156	7641	2340	3741
421	421	421	659	N/A	263	421	N/A	580	N/A	263	421
1870	1870	1870	2930	N/A	1170	1870	N/A	2578	N/A	1170	1870
393	N/A	393	393	N/A	239	393	393	341	N/A	239	393
1750	N/A	1750	1750	N/A	1063	1750	1750	1515	N/A	1063	1750
295	N/A	295	295	N/A	179	295	N/A	255	N/A	179	295
1312	N/A	1312	1312	N/A	797	1312	N/A	1136	N/A	797	1312
631	N/A	631	N/A	N/A	N/A	631	N/A	N/A	N/A	N/A	N/A
2805	N/A	2805	N/A	N/A	N/A	2805	N/A	N/A	N/A	N/A	N/A
315	N/A	315	N/A	N/A	N/A	315	N/A	N/A	N/A	N/A	N/A
1402	N/A	1402	N/A	N/A	N/A	1402	N/A	N/A	N/A	N/A	N/A
N/A	11420	N/A	N/A	N/A	N/A	777	1142	1005	N/A	N/A	777
N/A	5079	N/A	N/A	N/A	N/A	3456	5079	4470	N/A	N/A	3456
N/A	421	N/A	N/A	N/A	N/A	388	N/A	502	N/A	N/A	164
N/A	1871	N/A	N/A	N/A	N/A	1728	N/A	2235	N/A	N/A	728
580	580	710	1221	1221	229	420	420	771	771	220	409
2580	2580	3160	5430	5430	1020	1870	1870	3430	3430	980	1820
0,096	0,114	0,125	0,169	0,185	0,07	0,101	0,135	0,182	0,21	0,067	0,087
0,056	0,067	0,073	0,099	0,108	0,041	0,059	0,079	0,107	0,123	0,039	0,051
0,071	N/A	0,101	0,124	N/A	0,05	0,08	0,077	0,143	N/A	0,05	0,074
0,042	N/A	0,059	0,073	N/A	0,029	0,047	0,045	0,084	N/A	0,029	0,043
0,096	N/A	0,125	N/A	N/A	N/A	0,101	N/A	N/A	N/A	N/A	N/A
0,056	N/A	0,073	N/A	N/A	N/A	0,059	N/A	N/A	N/A	N/A	N/A
N/A	0,118	N/A	N/A	N/A	N/A	0,113	0,141	0,191	N/A	N/A	0,956
N/A	0,069	N/A	N/A	N/A	N/A	0,066	0,083	0,112	N/A	N/A	0,056
213600	334600	213600	334600	440000	133600	213600	334588	294400	440000	133600	213600
37410	58600	37410	58600	77050	23400	37410	58600	51560	77050	23400	37410
100000	N/A	100000	100000	N/A	60700	100000	99920	86500	N/A	60700	100000
17500	N/A	17500	17500	N/A	10635	17500	17500	15150	N/A	10635	17500
160212	N/A	160212	N/A	N/A	N/A	160212	N/A	N/A	N/A	N/A	N/A
28057	N/A	28057	N/A	N/A	N/A	28057	N/A	N/A	N/A	N/A	N/A
N/A	290000	N/A	N/A	N/A	N/A	197327	289996	255199	N/A	N/A	197330
N/A	50790	N/A	N/A	N/A	N/A	34560	50790	44695	N/A	N/A	34560
15	25	15	18	30	14	20	32	28	43	14	20
20	N/A	20	N/A	N/A	N/A	25	N/A	N/A	N/A	N/A	N/A
N/A	20	N/A	N/A	N/A	N/A	16	25	23	N/A	N/A	16
48 mm	80 mm	96 mm	115 mm	191 mm	22 mm	51 mm	81 mm	125 mm	191 mm	22 mm	51 mm
64 mm	N/A	127 mm	N/A	N/A	N/A	64 mm	N/A	N/A	N/A	N/A	N/A
N/A	64 mm	N/A	N/A	N/A	N/A	41 mm	64 mm	102 mm	N/A	N/A	41 mm
4,75"/120 mm	5,875"/150 mm	4,75"/120 mm	7,125"/180 mm	9,875"/250 mm	2,375"/60 mm	4,75"/120 mm	6,00"/150 mm	7,875"/200 mm	9,875"/250 mm	2,375"/60 mm	4,75"/120 mm
6,25"/160 mm	N/A	6,25"/160 mm	N/A	N/A	N/A	6,00"/150 mm	N/A	N/A	N/A	N/A	N/A
N/A	5,125"/130 mm	N/A	N/A	N/A	N/A	4,00"/100 mm	5,125"/130 mm	6,25"/160 mm	N/A	N/A	4,00"/100 mm
W	W	N,W	W	W	W	W	W	W	W	W	W

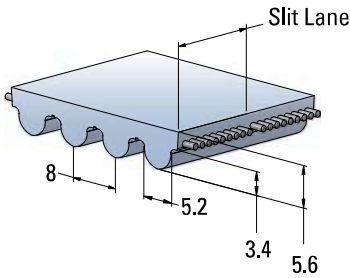
Gates Mectrol cannot assume any liability concerning the suitability and process ability of our products. We also cannot assume liability for process results, damages or consequential damages associated with the use of our products. Note, ultimate tensile strengths are listed for references purposes only. Ultimate tensile strength values listed above are a theoretical calculation based on average cord strength and may not represent actual tensile test results.

HTD® and STD Pitch Belts

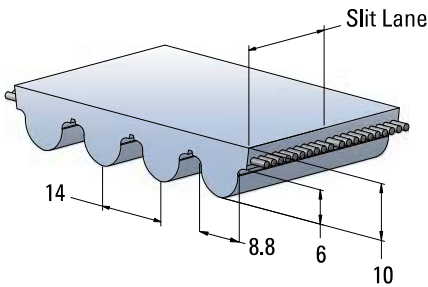
HTD5 5 mm Pitch



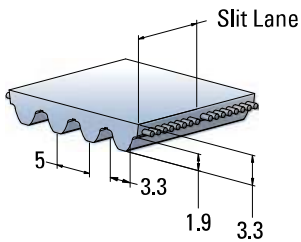
HTD8 8 mm Pitch



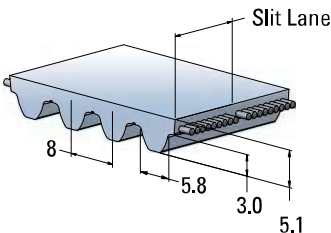
HTD14, HTDL14 14 mm Pitch



STD5 5 mm Pitch



STD8 8 mm Pitch



		HTD5	HTD8, HTDL8, HTD8-HF	HTD14, HTD14-HF	HTDL14	STD5	STD8, STD8-HF
Min. Welded Belt Length	mm	450	456	1000	N/A	450	456
Standard Roll Lengths	meters	100	100	50	50	100	100
Standard Slitting Lanes	mm	25	25	55	N/A	25	20, 30
Available Slitting Lanes	mm	10, 12, 15, 16	10, 20	85	N/A	10, 15	25

All roll lengths are ±1%.

Standard Widths

mm	HTD5	HTD8, HTDL8, HTD8-HF	HTD14, HTDL14, HTD14-HF	STD5	STD8
5	X			X	
10	X	X		X	X
15	X	X		X	X
20		X			X
25	X	X	X	X	X
30		X			X
40			X		
50	X	X		X	X
55			X		
85	X	X	X		X
100	X	X	X		X
115			X		
150	X	X			X
170		X*	X		
200		X*			

All belts are available in any width between the minimum and maximum listed width.

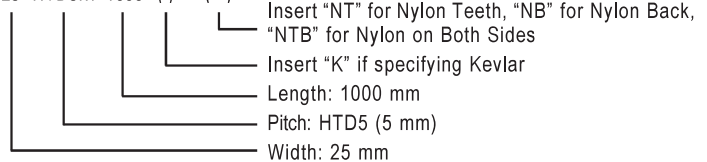
* This width is available in Kevlar only.

Width Tolerances

Width	HTD5	HTD8, HTDL8, HTD8-HF	HTD14, HTDL14, HTD14-HF	STD5	STD8
Up to 50 mm	±0.5 mm	±0.75 mm	±1.0 mm	±0.5 mm	±0.75 mm
> 50-100 mm	±0.75 mm	± 1.0 mm	±1.5 mm	N/A	± 1.0 mm
> 100-150 mm	±0.75 mm	± 1.0 mm	±2.0 mm	N/A	N/A
> 150-170 mm	N/A	±2.0 mm	±2.0 mm	N/A	N/A
> 170 mm	N/A	±2.0 mm	N/A	N/A	N/A

To Order HTD and STD Pitch Belts

25 HTD5M 1000 () ()



Pulley Overview

Gates Mectrol manufactures a complementary line of timing pulleys. While industry standards do exist for most pulley groove geometries, each manufacturer has its own interpretation of those standards. For the longest belt life and quietest operation, it is recommended that the timing belts and pulleys be single-sourced so that the components are matched. Recognizing that any project may have different pulley style requirements, Gates Mectrol offers a Custom Pulley Program, which allows for additional features as needed.

In addition to pulley alternatives, Gates Mectrol offers a Clamp Plate Program to match any project needs.

Custom Pulley Program

This program is designed to meet your made-to-print custom pulley requirements.

- Unlimited design freedom
- Three raw material choices:
aluminum, steel or stainless steel

Clamp Plates

Gates Mectrol offers a clamp plate program for standard and custom requirements.



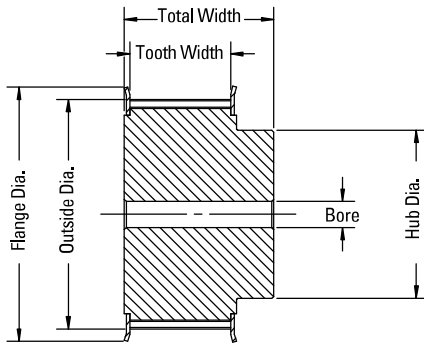
Custom Pulley Program

Pulleys can be customized to fit specific applications. Below are the options available:

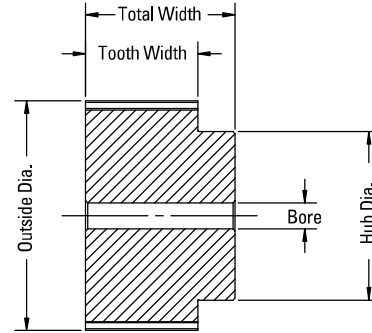
Material	Flanges	Coatings	Optional Pitches
<ul style="list-style-type: none"> Aluminum Steel Stainless steel 	<ul style="list-style-type: none"> Zinc plated steel Stainless steel (for stainless steel pulleys) 	<ul style="list-style-type: none"> Clear anodize Black anodize Clear hardcoat Black oxide Electroless nickel 	<p>Most pitches can be supplied as zero backlash</p> <ul style="list-style-type: none"> Typically used for precise positioning applications only

Pulley Types

2F – Two Flanges



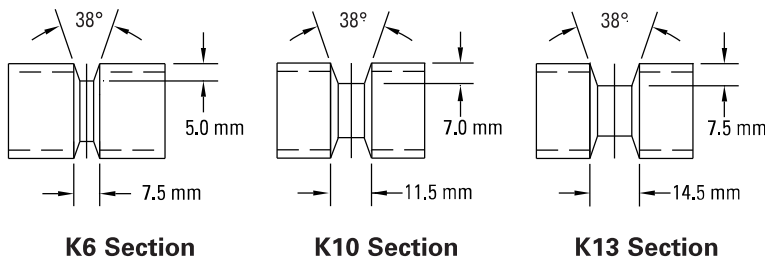
0F – No Flanges



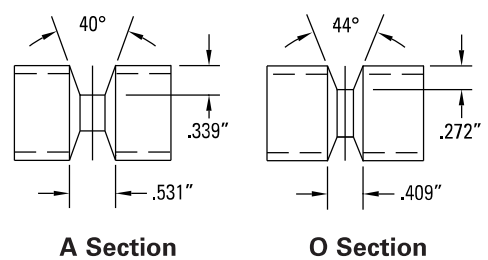
V-Guides

For wider belts, and larger pulleys without flanges, one of the following V-guides is recommended for improved tracking:

For Metric Pitch Belts

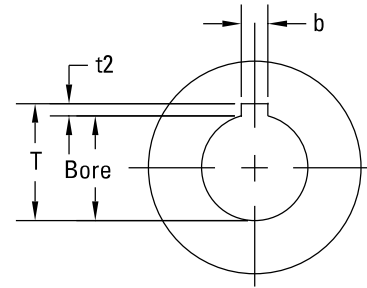
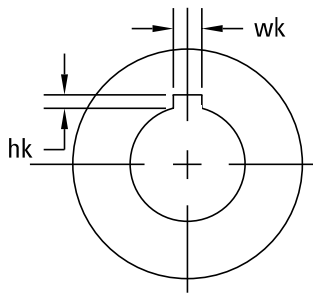


For Imperial Pitch Belts



Custom Pulley Program

Standard Keyway Dimensions and Tolerances



Imperial Shaft Diameter

Over	Up to and Including	Width wk	Tolerance wk	Depth hk	Tolerance hk
	0.438	0.094		0.047	
0.438	0.563	0.125	+0.0030	0.063	
0.563	0.875	0.188	-0.0000	0.094	
0.875	1.250	0.250		0.125	
1.250	1.375	0.313	+0.0035	0.156	+0.015 -0.000
1.375	1.750	0.375	-0.0000	0.188	
1.750	2.250	0.500		0.250	
2.250	2.750	0.625		0.313	
2.750	3.250	0.750	+0.0040	0.375	
3.250	3.750	0.875	-0.0000	0.438	
3.750	4.500	1.000		0.500	
4.500	5.500	1.125	+0.0050	0.625	
5.500	6.500	1.500	-0.0000	0.750	

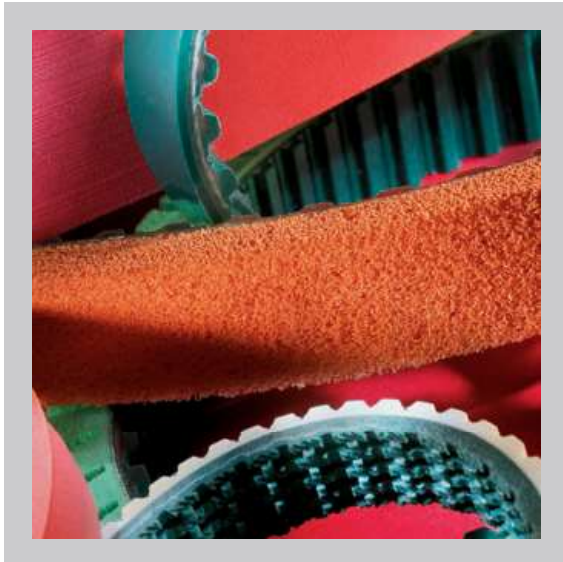
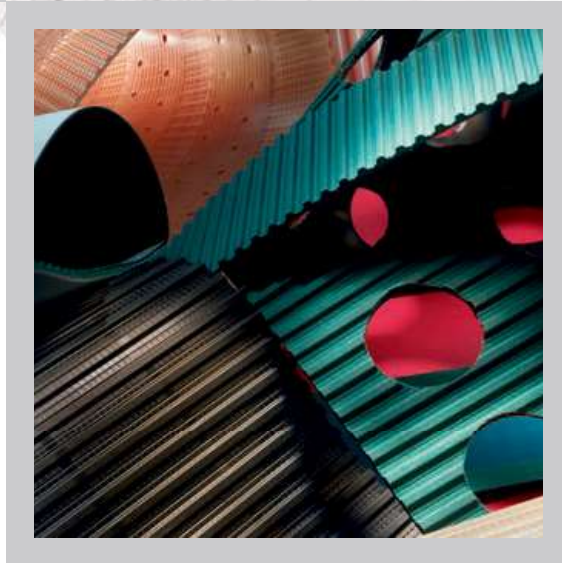
Metric Shaft Diameter

Over	Up to and Including	Width b	Tolerance on b	*Depth t ₂	Tolerance t ₂
6	8	2	+0.060	1.0	
8	10	3	+0.020	1.4	
10	12	4	+0.078	1.8	+0.1
12	17	5	+0.030	2.3	-0
17	22	6		2.8	
22	30	8	+0.098	3.3	
30	38	10	+0.040	3.3	
38	44	12		3.3	
44	50	14	+0.120	3.8	
50	58	16	+0.050	4.3	
58	65	18		4.4	+0.2
65	75	20		4.9	-0
75	85	22	+0.149	5.4	
85	95	25	+0.065	5.4	
95	110	28		6.4	
110	130	32		7.4	
130	150	36	+0.180	8.4	+0.3
150	170	40	+0.080	9.4	-0

* Metric keyway depths are specified from the bottom of the keyway to a line tangent to the bore at the keyway centerline.
 $T = \text{Bore Diameter} + t_2$

USA
CORPORATE HEADQUARTERS

Gates Mectrol, Inc.
9 Northwestern Drive
Salem, NH 03079, U.S.A.
Tel. +1 (603) 890-1515
Tel. +1 (800) 394-4844
Fax +1 (603) 890-1616
Email: contact@gatesmectrol.com



Gates Mectrol and GMT3™ are registered trademarks of Gates Mectrol Incorporated. Synchro-Power is a registered trademark of Gates Corporation. All other trademarks used herein are the property of their respective owners.

© Copyright 2018 Gates Mectrol Incorporated.
All rights reserved. 8/18

GM_UTB_18_US

D Code

D.1 Power Consumption

The power consumption is more accurately calculated using the MATLAB script below.

D.1.1 Power Consumption Script

```
%% Variables
clc; clear;
m1 = 0.836;
m2 = 0.532;
N = 160;
f = 10;
r1 = 100;
r2 = 50;
r3 = 300;
ed = 50;
dd = 0;
ddd = 0;
edd = 0;
alpha = 68.58;
length_begin = 124;
length_end = 241; % taken from get_max_extension.m
precision = 0.001;
e = length_begin : precision : length_end;
array_size = (length_end-length_begin)/precision + 1;
d = 210;
gearRatio=100;

Torque1 = zeros(3, array_size);
Torque2 = zeros(3, array_size);
Torque1_spring = zeros(3, array_size);
Torque2_spring = zeros(3, array_size);
spring1 = zeros(3, array_size);
spring2 = zeros(3, array_size);
```

```

theta = zeros(array_size,1);
thetad = zeros(array_size,1);
thetadd =zeros(array_size,1);
phi = zeros(array_size,1);
phid = zeros(array_size,1);
phidd = zeros(array_size,1);
psy = zeros(array_size,1);

```

```

%% Get Torque Phase 1

```

```

for i = 1:1:array_size
    [theta(i), phi(i), psy(i), R] = leg_angles(r1,r2,r3,alpha,d,e(
        i));
    [thetad(i), phid(i)] = leg_angles_dot(r1,R,theta(i),phi(i),dd,
        ed);
    [thetadd(i), phidd(i)] = leg_angular_acceleration(r1,R,theta(i)
        ),thetad(i),phi(i),phid(i),ddd,edd);
    [Torque1(1,i),Torque2(1,i)] = Dynamic_Equation(m1,m2,R/1000,r1
        /1000, theta(i), phi(i),thetadd(i), phidd(i), N,f);
    [Torque1_spring(1,i),Torque2_spring(1,i)] =
        Dynamic_Equation_Springs(m1,m2,R/1000,r1/1000, theta(i),
        phi(i),thetadd(i), phidd(i), N,f);
    [spring1(1,i),spring2(1,i)] = Spring(theta(i), phi(i));
end

```

```

%% Get Torque Phase 2 – Phi increases

```

```

for i = 1:1:array_size
    [Torque1(2,i),Torque2(2,i)] = Dynamic_Equation(m1,m2,R/1000,r1
        /1000, theta(1), phi(i),0, 0, 0,0);
    [Torque1_spring(2,i),Torque2_spring(2,i)] =
        Dynamic_Equation_Springs(m1,m2,R/1000,r1/1000, theta(1),
        phi(i),0, 0, 0,0);
    [spring1(2,i),spring2(2,i)] = Spring(theta(1), phi(i));

```

end

%% Get Torque Phase 3 – Theta Decreases

for i = 1:1:array_size

[Torque1(3,i),Torque2(3,i)] = Dynamic_Equation(m1,m2,R/1000,r1
/1000, theta(i), phi(array_size),0, 0, 0,0);

[Torque1_spring(3,i),Torque2_spring(3,i)] =
Dynamic_Equation_Springs(m1,m2,R/1000,r1/1000, theta(i),
phi(array_size),0, 0, 0,0);

[spring1(3,i),spring2(3,i)] = Spring(theta(i), phi(array_size)
);

end

%% Get Harmonic Drive and Motor Specs

Max_Torque1 = **max**([**max**(**abs**(Torque1(1,:))),**max**(**abs**(Torque1(2,:))),
max(**abs**(Torque1(3,:)))]);

Max_Torque2 = **max**([**max**(**abs**(Torque2(1,:))),**max**(**abs**(Torque2(2,:))),
max(**abs**(Torque2(3,:)))]);

Max_Torque1_spring = **max**([**max**(**abs**(Torque1_spring(1,:))),**max**(**abs**(
Torque1_spring(2,:))), **max**(**abs**(Torque1_spring(3,:)))]);

Max_Torque2_spring = **max**([**max**(**abs**(Torque2_spring(1,:))),**max**(**abs**(
Torque2_spring(2,:))),**max**(**abs**(Torque2_spring(3,:)))]);

Min_Torque1_spring = **min**([**min**(**abs**(Torque1_spring(1,:))),**min**(**abs**(
Torque1_spring(2,:))), **min**(**abs**(Torque1_spring(3,:)))]);

Min_Torque2_spring = **min**([**min**(**abs**(Torque2_spring(1,:))),**min**(**abs**(
Torque2_spring(2,:))),**min**(**abs**(Torque2_spring(3,:)))]);

Min_thetad = **min**(**abs**(thetad));

Min_phid = **min**(**abs**(phid));

HdSpecs_theta = get_hd_specs(Max_Torque1_spring);

HdSpecs_phi = get_hd_specs(Max_Torque2_spring);

```

% get_hd_inputs() gives results in mNm and rpm
[Max_Torque1_motor, Min_thetad_motor] = get_hd_inputs(Min_thetad,
    Max_Torque1_spring, HdSpecs_theta(3), gearRatio);
[Max_Torque2_motor, Min_phid_motor] = get_hd_inputs(Min_phid,
    Max_Torque2_spring, HdSpecs_phi(3), gearRatio);
MotorSpecs_theta = get_motor_specs(Max_Torque1_motor); %
    get_motor_specs takes input in mNm
MotorSpecs_phi = get_motor_specs(Max_Torque2_motor);

%% Phase Time
Phase_Time = [(length_end-length_begin)/ed, (max(phi)-min(phi))/(
    mean(abs(phid))*180/pi), (max(theta)-min(theta))/(mean(abs(
    thetad))*180/pi)];
Step_Time = Phase_Time./array_size;

%% Joules Consumed
Joules_Consumed = [0,0,0];
Coulombs_Consumed = [0,0,0];
thetad_mean = mean(abs(thetad));
phid_mean = mean(abs(phid));

for i = 1:1:array_size
    %% Get Joules Phase 1
    [torque_motor_theta, rpm_motor_theta] = get_hd_inputs(abs(
        thetad(i)), abs(Torque1_spring(1,i)), HdSpecs_theta(3),
        gearRatio);
    [torque_motor_phi, rpm_motor_phi] = get_hd_inputs(abs(phid(i)),
        abs(Torque2_spring(1,i)), HdSpecs_phi(3), gearRatio);
    [joulestheta, coulombstheta] = get_motor_inputs(
        torque_motor_theta, rpm_motor_theta, MotorSpecs_theta(6),
        MotorSpecs_theta(7), MotorSpecs_theta(5));
    [joulesphi, coulombsphi] = get_motor_inputs(torque_motor_phi,
        rpm_motor_phi, MotorSpecs_phi(6), MotorSpecs_phi(7),

```

```

    MotorSpecs_phi(5));
Coulombs_Consumed(1) = Coulombs_Consumed(1) + (coulombstheta+
    coulombsphi)*Step_Time(1);
Joules_Consumed(1) = Joules_Consumed(1) + (joulestheta+
    joulesphi)*Step_Time(1);

```

```

%% Get Joules Phase 2

```

```

[torque_motor_theta ,rpm_motor_theta] = get_hd_inputs(0,abs(
    Torque1_spring(2,i)),HdSpecs_theta(3),gearRatio);
[torque_motor_phi ,rpm_motor_phi] = get_hd_inputs(abs(phid_mean
    ),abs(Torque2_spring(2,i)),HdSpecs_phi(3),gearRatio);
[joulestheta ,coulombstheta] = get_motor_inputs(
    torque_motor_theta ,rpm_motor_theta ,MotorSpecs_theta(6) ,
    MotorSpecs_theta(7) ,MotorSpecs_theta(5));
[joulesphi ,coulombsphi] = get_motor_inputs(torque_motor_phi ,
    rpm_motor_phi ,MotorSpecs_phi(6) ,MotorSpecs_phi(7) ,
    MotorSpecs_phi(5));
Coulombs_Consumed(2) = Coulombs_Consumed(2) + (coulombstheta+
    coulombsphi)*Step_Time(2);
Joules_Consumed(2) = Joules_Consumed(2) + (joulestheta+
    joulesphi)*Step_Time(2);

```

```

%% Get Joules Phase 3

```

```

[torque_motor_theta ,rpm_motor_theta] = get_hd_inputs(abs(
    thetad_mean),abs(Torque1_spring(3,i)),HdSpecs_theta(3) ,
    gearRatio);
[torque_motor_phi ,rpm_motor_phi] = get_hd_inputs(0,abs(
    Torque2_spring(3,i)),HdSpecs_phi(3),gearRatio);
[joulestheta ,coulombstheta] = get_motor_inputs(
    torque_motor_theta ,rpm_motor_theta ,MotorSpecs_theta(6) ,
    MotorSpecs_theta(7) ,MotorSpecs_theta(5));
[joulesphi ,coulombsphi] = get_motor_inputs(torque_motor_phi ,
    rpm_motor_phi ,MotorSpecs_phi(6) ,MotorSpecs_phi(7) ,
    MotorSpecs_phi(5));

```



```

    Coulombs_Consumed(3) = Coulombs_Consumed(3) + (coulombstheta+
        coulombsphi)*Step_Time(3);
    Joules_Consumed(3) = Joules_Consumed(3) + (joulestheta+
        joulesphi)*Step_Time(3);
end

%% Amps and Watts
Amps_phase = [Coulombs_Consumed(1)/Phase_Time(1),Coulombs_Consumed
    (2)/Phase_Time(2),Coulombs_Consumed(3)/Phase_Time(3)];
Amps_Consumed = (sum(Coulombs_Consumed)*5)/(Phase_Time(1) +
    Phase_Time(2)*5 + Phase_Time(3)*5);
Watts_Consumed_Phase = [Joules_Consumed(1)/Phase_Time(1),
    Joules_Consumed(2)/Phase_Time(2),Joules_Consumed(3)/Phase_Time
    (3)];
Watts_Consumed = (sum(Joules_Consumed)*5)/(Phase_Time(1) +
    Phase_Time(2)*5+Phase_Time(3)*5);
fprintf('Average_Current_(no_other_electronics):_%.1fA\n',
    Amps_Consumed);

current_other_components = 2.133;
Amps_Consumed = Amps_Consumed + current_other_components;
fprintf('Average_Current_(with_other_electronics):_%.1fA\n',
    Amps_Consumed);

ah_per_cell = 3.4;
v_per_cell = 3.6;
kg_per_cell = 0.05;
hours = 2;
voltage = 48;
cells_series = ceil(voltage/v_per_cell);
cells_parallel = ceil(Amps_Consumed*hours/ah_per_cell);
cells_total = cells_parallel*cells_series;
kg_total = cells_total*kg_per_cell;

```

```
fprintf('Number_of_Cells: %f\n', cells_total);
fprintf('Weight_of_battery: %fkg\n', kg_total);
```

D.1.2 Harmonic Drive Inputs Script

```
function [torque_motor, rpm_motor] = get_hd_inputs(speed_output,
torque_output, torque_rated, gear_ratio)
    %% INPUTS
    % speed at output of harmonic drive (rad/s)
    % torque at output of harmonic drive (Nm)
    % rated torque of harmonic drive (Nm)
    % gear ratio of harmonic drive (100:1)
    %% OUTPUTS
    % torque at output of motor/input of harmonic drive (mNm)
    % speed at output of motor/input of harmonic drive (rpm)

    rpm_output = speed_output*30/pi;
    rpm_motor = rpm_output*gear_ratio;

    %% SPEED EFFICIENCY
    eta_r = (4.848*(10^(-9)))*(rpm_motor^2) + (-5.879*(10^(-5))
    )*(rpm_motor) + 0.8367;
    if eta_r > 0.81
        eta_r = 0.81;
    elseif eta_r < 0.69
        eta_r = 0.69;
    end

    %% TORQUE EFFICIENCY
    alpha = torque_output/torque_rated;
    if alpha > 1
        alpha = 1;
    end
    k_e = (-1.481*(alpha^4))+(4.312*(alpha^3))-(5.013*(alpha^2))
    +(3.159*alpha)-0.02076;
```

```

if k_e < 0.3
    k_e = 0.3;
end

    %% MOTOR TORQUE
    eta_HD = eta_r*k_e;
    torque_motor = torque_output*1000/(gear_ratio*eta_HD);
end

```

D.1.3 Motor Inputs Script

```

function [power_motor_in , current_motor] = get_motor_inputs(
    torque_motor , rpm_motor , torque_constant , speed_constant ,
    resistance_motor)
    %% INPUTS:
    % speed at output of motor (rpm)
    % torque at output of motor (mNm)
    % torque constant of motor (mNm/A)
    % speed constant of motor (rpm/V)
    % resistance of the motor (Ohms)
    %% OUTPUTS:
    % electrical power into motor (W)
    % current into motor (A)

    U = (1/speed_constant)*(((30000*resistance_motor*
        torque_motor)/(pi*torque_constant^2))+rpm_motor);
    a = resistance_motor;
    b = -U;
    c = (pi*rpm_motor*torque_motor)/(30000);
    I_upper = (-b+sqrt((b^2)-(4*a*c)))/(2*a);
    I_lower = (-b-sqrt((b^2)-(4*a*c)))/(2*a);
    % When speed is 0, I_lower = 0
    if I_lower <= 0
        current_motor = I_upper;
    else

```

```
        current_motor = I_lower;  
end  
power_motor_in = U * current_motor;  
  
end
```